Doctoral Dissertation

Optimization of Monitoring System using Plastic Scintillator for Beta nuclide including Tritium in Water

UkJae Lee

Department of Nuclear Engineering

Graduate School of UNIST

2020

Optimization of Monitoring System using Plastic Scintillator for Beta nuclide including Tritium in Water

UkJae Lee

Department of Nuclear Engineering

Graduate School of UNIST

Optimization of Monitoring System using Plastic Scintillator for Beta nuclide including Tritium in Water

A dissertation
submitted to the Graduate School of UNIST
in partial fulfillment of the
requirements for the degree of
Doctor of Philosophy

UkJae Lee

12/27/2020
Approved by

_____

Advisor
Hee Reyoung Kim

Optimization of Monitoring System using Plastic scintillator for Beta nuclide including Tritium in Water

UkJae Lee

This certifies that the dissertation of UkJae Lee is approved.
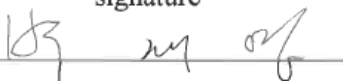
12/27/2020

signature

Advisor: Hee Reyoung Kim

signature

Seung Jun Lee: Thesis Committee Member #1

signature

Jaeyoung Park: Thesis Committee Member #2

signature

Kune Woo Lee: Thesis Committee Member #3

signature

Sang-bum Hong: Thesis Committee Member #4;

ABSTRACT

Various radionuclides can be generated from decommissioning sites and nuclear facilities. Radionuclides can move through water, so monitoring is essential. A monitoring system has been established to detect beta-nuclides in water samples around nuclear facilities. Beta-nuclides, including tritium, have a short range and difficulty in detecting in water samples. In order to solve this problem, the detection chamber of the structure in which the scintillator and the water sample directly contact is designed and constructed. The system is constructed using a plastic scintillator that does not react with water and has a low background level because of its low atomic number.

In order to increase detection efficiency, the area of reaction between the water sample and the scintillator is increased by using the multi-layer scintillators structure. Thirteen scintillators are used for low energy beta, such as ^{3}H, and seven scintillators were used for the relatively high energy ^{90}Sr.

Using the manufactured detection chamber, an electronics of monitoring system for each nuclide is set. The change of the detection efficiency is confirmed by changing the amplification degree of the main amplifier. The amplification degree of the main amplifier is selected for each case of ^{3}H and ^{90}Sr.

The major beta nuclides, ^{90}Sr and ^{3}H nuclides are considered, and the performance of the system is evaluated by the time required to derive the MDA to satisfy regulatory standards for each nuclide. The liquid radioactive effluent level is used for ^{90}Sr and ^{3}H. In case of ^{90}Sr, it takes 18 seconds to satisfy 0.02 Bq/g of effluent level. In the case of ^{3}H, it takes 2,300 seconds to satisfy the standard for effluent level of 40 Bq/g.

It is considered that scintillation-based radiation monitoring systems for beta nuclide in water can be used to evaluate effluent level for ^{3}H and ^{90}Sr. The system is expected to be used to ensure the radiological safety of the operating nuclear facilities and decommissioning sites of nuclear power plants.

CONTENTS

FIGURE CONTENTS

TABLE CONTENTS

1. Introduction

  Periodic groundwater monitoring is required before and after decommissioning of nuclear facilities, especially under long-term radioactivity monitoring, for limited release of regulation after restoration of decommissioning sites. There is a need to develop an integrated site-monitoring technology that can monitor beta radiation, including tritium, in decommissioned groundwater.

  With the ending design life of nuclear power plants, the world's decommissioning market has been expanding. Of the total 443 nuclear power plants in the world, 150 are in the stage of end of operation. Moreover, older nuclear plants are on the rise. The global nuclear decommissioning market is ~350 trillion won for except countries having decommissioning technologies (US, UK, Japan, France, Germany, and Russia) and 73 trillion won for developing countries (India and China). In Korea, as the Kori Nuclear Power Plant 1, which started its first commercial operation in 1978, is scheduled to end operation in 2017, a technology for actual dismantling of nuclear power plants needs to be urgently developed. At 633.3 billion won decommissioning cost per unit (24 nuclear power plants in operation), the total decommissioning market in Korea is estimated at ~14 trillion won. To enter the global market and prevent the erosion of the domestic market, it is necessary to secure core technologies at an appropriate time.

  As beta-emitting nuclides from decontamination activities or decommissioning sites of nuclear facilities are radionuclides that must be managed from a health physics perspective, technologies that can rapidly and accurately determine the degree of contamination are required. Tritium (^{3}H) has the same chemical properties as hydrogen, and thus, normally exists in the form of water. Therefore, inhalation due to breathing, ingestion, and injury can result in high levels of internal exposure to the human body in the form of moisture or organic matter in the body. Tritium is an element that rarely exists in nature, and is generated much higher during nuclear power generation than that in nature. Therefore, it must be managed.

  The low-energy beta nuclide has a short range; thus, radioactivity analysis is conducted using a measuring instrument, such as a liquid scintillation counter (LSC), after pretreatment with specific sampling methods. This process, however, consumes much time and labor. Moreover, there is a problem of generation of organic and second radioactive wastes. Therefore, field measurement techniques for beta-emitting radionuclides, including tritium, generated during nuclear dismantling are required.

  Pure beta radiation monitoring using low-energy beta detectors, such as LSCs, is not available on site because it needs much time for sampling, pretreatment, and analysis, including long measurement times. The technology that enables real-time monitoring of beta-emitting nuclide contamination in the site by

continuously measuring the radioactivity concentration of beta nuclides, including tritium, is not sufficiently developed at home and abroad. Thus, it is necessary to accumulate technology related to decommissioning of nuclear power plants.

As a technology for monitoring beta rays in Korea, the research project of "Radiation Instrument Design and Manufacturing Technology Development" was conducted from March 2002 to February 2005 [1]. In this project, the development of a scintillator as a radiation detector was studied. In particular, the development of a beta-ray detector using a scintillator was studied, and a measurement technology using the phoswich structure was developed for the simultaneous beta-gamma detection. In 2014, a study on the development of a system capable of real-time monitoring of radiation at a long distance at Myongji University was published in the Journal of Radiation Protection [2]. In this study, a radiation monitoring system was constructed through a photomultiplier device using CsI:Tl inorganic scintillators, which are highly reactive to gamma, beta, and X-ray detection. The monitoring system was filed with Korean patent application No. 10-2014-0049603 for "on-site water radioactivity monitoring method and apparatus." This technique can measure gamma rays and X-rays by submerging gas ionizers and GM(Geiger-Mullier) counters in water, using vertical controllers and waterproofing. However, it cannot measure underwater beta rays.

Overseas, there are monitoring systems and in situ beta nuclide detection technologies that detect beta nuclides in water samples and those in air samples. In the case of an air tritium monitor, there are portable monitoring instruments using ion chambers. The sensitivity of tritium is several kBq/m^3, and its optimum available range is several tens of kBq/m^3 [3]. A tritium monitor using ion chambers is limited to tritium in air and cannot be used for tritium monitoring in water.

As a technology for beta monitoring in air, the iCAM™-HD model from MIRION Technologies is a high-flow alpha/beta gas monitor. In this technology, air is sucked in through the instrument via an external pump or vacuum system and particulate matter in the air gets attached to the removable filter for detection. The filter is monitored with a CANBERRA CAM1700 PIPS® (passivated ion-implanted planar silicon) radiation detector, which allows simultaneous measurement of alpha and beta radiations in the material deposited on the filter. CAM1700 also provides gamma correction of beta measurements.

The LIQ-X- (H3) series from TECHNICAL Associates is a continuous real-time underwater tritium measurement instrument. The system comprises a small, lightweight detector assembly that interfaces with the sample via a 1/4" pipe fitting with a reader and processor assembly, through two BNC connectors. The sample for radioactivity is then deionized and filtered. The system's tabletop or rack-mounted processor and display parts analyze the output of the optical magnification tube by using the pulse height and matching, to eliminate most background (noise) counts in the system. This instrument

is a portable, on-site beta-nuclide analysis module that is highly sensitive to beta rays and can be measured below the EPA Protective Action Guide level and the Military Drinking Water Limits guidelines. This monitoring system is an underwater tritium monitoring instrument with a sensitivity of ~74,000 Bq/L for 2 min measurement time [4], which is much above the domestic tritium drainage management standard (40,000 Bq/L) [5]. To increase the sensitivity, the measurement time must be set to 24 h or more, which is not suitable for field application.

Currently, there are several measurement techniques that perform alpha, beta, and gamma analyses in water. In particular, in the case of beta, measurement of specific nuclides (^{40}K, ^{137}Cs, ^{90}Sr, etc.), including tritium, is being performed. Tritium, with very low beta energy, takes a long time to measure. It is anticipated that a special pretreatment is required to reduce the attenuation effect in the water sample. Through this study, the development of a tritium monitoring technology that improves the detection efficiency of tritium using beta analysis technology and pretreatment of water samples in the decommissioning site is suggested.

The final goal of this study is to construct a monitoring system that can be used to simultaneously detect high-energy beta and low-energy nuclides in water samples. A detection system that can be applied for analyzing strontium and tritium is constructed using a scintillator. The time required for deriving an MDA that satisfies the effluent concentration limit is considered as the major factor in the evaluation of system performance. The standard for the effluent concentration limit of tritium is 4E+07 Bq/m^3 (4E+01Bq/g) and that for strontium is 2E+04 Bq/m^3 (2E-02Bq/g). A commercialized in situ monitoring system for tritium in water requires much more than one hour for satisfying the effluent level. Therefore, the final goal of the proposed system is to achieve a time of less than an hour for deriving an MDA that satisfies the effluent concentration limit.

2. Literature survey

There are many methods for monitoring beta nuclides. Normally, an LSC is widely used for this purpose. It uses an organic scintillant with appropriate solvents dissolved (e.g., toluene), and is suitable for low-energy β emitters and α-ray measurements (4π count possible). An LSC is widely used for analyzing beta nuclides, such as high-energy ($E_{max} > 200$ keV) beta particles or mono-energy (>50 keV) electrons, under low quenched conditions. However, it requires much time and labor for the pretreatment and sampling. Furthermore, it generates second radioactive waste, and is only applicable at laboratories.

Another method for beta radiation monitoring is the use of a proportional counter. It operates in higher-voltage regions than the ion chamber and has an electronic amplification of $\sim 10^6$ times. Therefore, its performance depends on parameters such as gas type, pressure, applied voltage, and counter structure. A proportional counter is suitable for measuring α, β, and low-energy X-rays with shorter range. Its output signal magnitude is proportional to the incident radiation energy. Normally, a proportional counter uses P-10 gas as the filled gas and has a dead time of several microseconds.
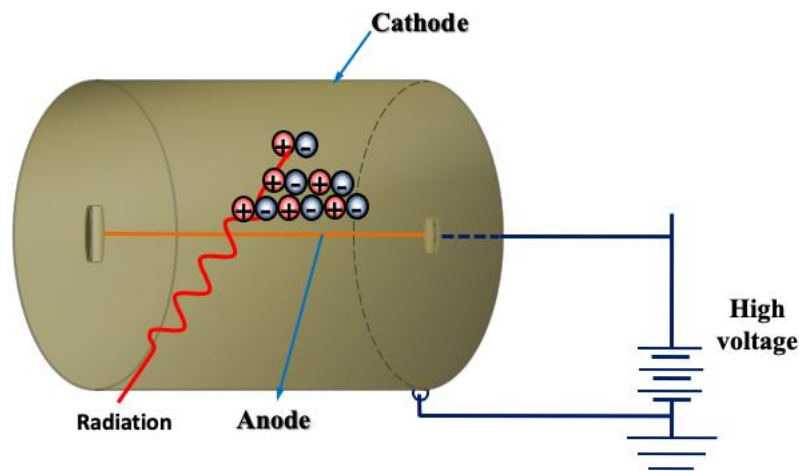
Figure 1 Diagram for detection mechanism of proportional counter

Another method for beta nuclide monitoring is the use of an ionization chamber. It collects all charges generated by direct ionization, and is divided into direct current and pulse types. The direct current type directly measures currents collected in the electrode pair. The pulse type counts the charged particles incident on the count value of the current pulse. Ionization chamber can measure the dose rate

(especially exposure dose), and exhibits poor sensitivity, because of the weak output current. The current is measured by primary ionization, and its amplitude is 1.
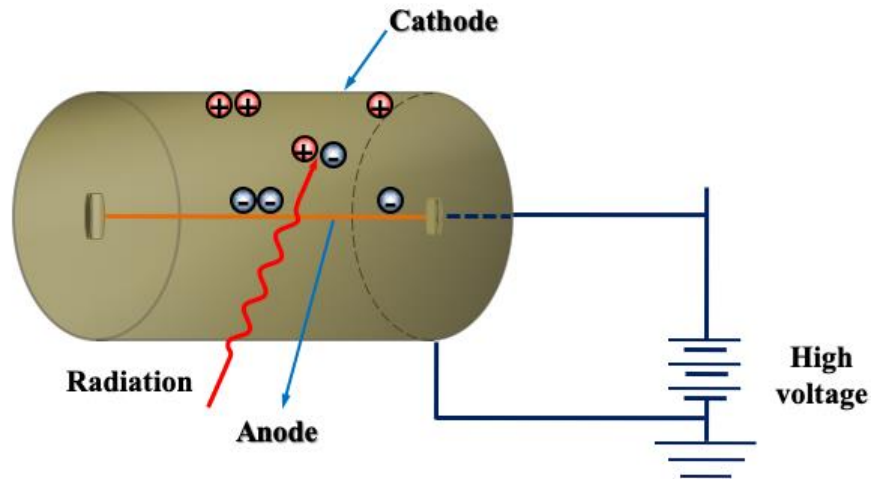
Figure 2 Diagram for detection mechanism of ionization chamber

Another monitoring method for beta nuclide is the use of a scintillator counter. When the energy of the radiation is absorbed by the scintillator, the electrons in the full band are excited by the conduction band, which then transition within 10^{-8} s to emit visible light. The scintillator counter has a short luminescence time (10^{-9} to 10^{-5} s) and its detection characteristics depend on the type of scintillator used. Luminous intensity is proportional to the incident radiation energy. As compared to other detectors, it has shorter resolution time and higher counting efficiency.

The application of a scintillator to the beta monitoring system has been extensively studied [6-8]. The new detection system is equipped with a twin-type NaI(Tl) X-ray detector, which operates as a detector of the low-energy X-rays induced by beta rays from tritiated water. Figure 3 and Figure 4 show the detection system.
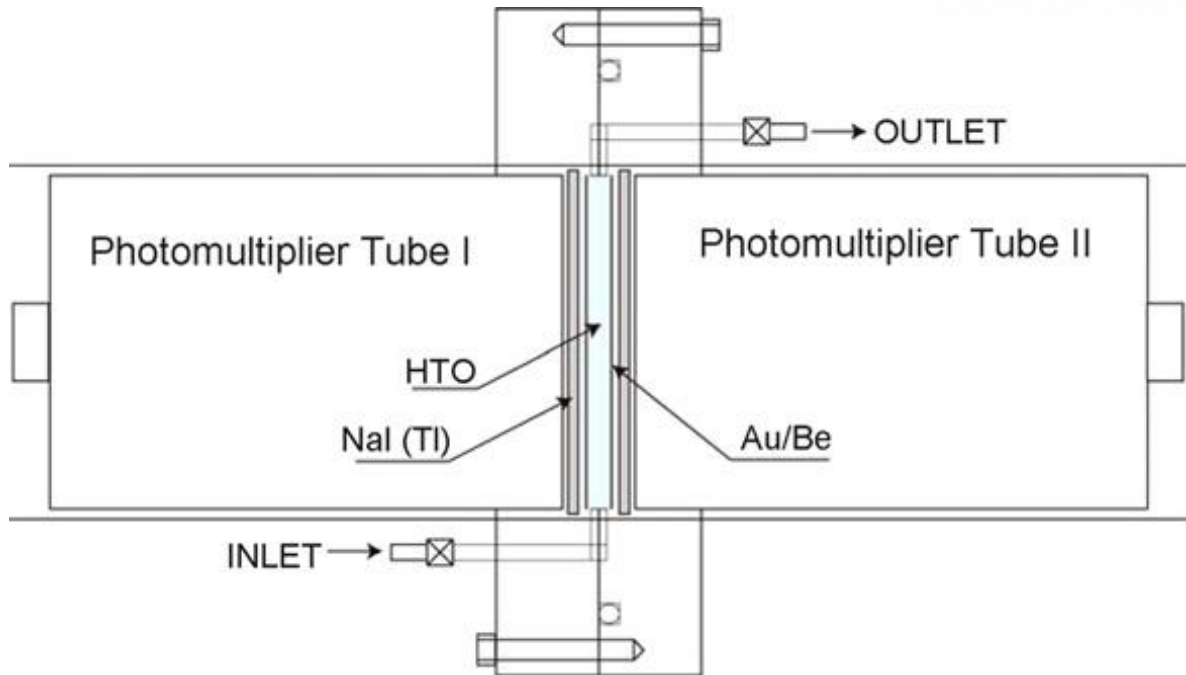
Figure 3 Detector of a new detection system for monitoring high-level tritiated water

Figure 4 (A)Detection part and (B)electronics for detection system

Only high-level tritiated water has been researched, and this system needs a more quantitative analysis because the previous studies have only conducted experiments for the count rate. A prototype system with a CaF$_2$ scintillator has been suggested, and an unknown concentration of the tritium water sample has been analyzed by the system. Granular grain-type scintillators are filled in the flow-cell detector. The overall system is shown in Figure 5. However, this system is applied only for a measurement time of 10,000 s.
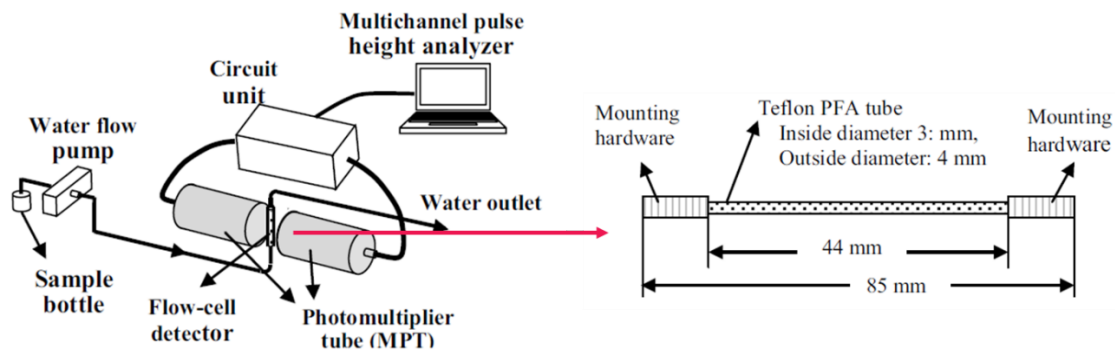
Figure 5 Tritium water monitoring system based on CaF$_2$ flow-cell detector

A previous study has suggested the replacement of a liquid scintillator with a plastic scintillator [9]. This study used ^{90}Sr, ^{13}C, and ^{3}H for the measurement. However, as this study used a Quantulus liquid scintillation detector (EG&G Wallac), it was only applicable for laboratory circumstances.

The selection of the detector type, as well as the method for analyzing radioactivity, such as in the laboratory or in situ, are the main factors to be considered for detection method. The laboratory measurement method involves radioactivity analysis after sampling and pretreatment. It exhibits an advantage that it can analyze very low levels of radioactivity depending on the concentration method used. However, it requires considerable time for sampling, pretreatment, and nuclide analysis. Furthermore, secondary radioactive wastes are generated after the analysis. The field measurement method is a direct method of measuring radioactivity on site without any sampling or pretreatment; thus, it can save time and money. Moreover, it does not generate secondary radioactive wastes. However, it cannot be applied to very low levels of radiation.

The ionization chamber, proportional counter, LSC, and scintillator counter are compared for selecting the best method of monitoring beta radiation in a water sample. The detector type that can be applied to beta detection and tritium analysis in water and does not need sampling and field monitoring

application is chosen. Among these, only the scintillator detector can be applied to the field monitoring of beta nuclides, including tritium, in water.

Scintillators can be divided into different types depending on the phase and material. Solid scintillator-based detectors are designed to react directly with beta nuclides in water samples. Therefore, a scintillator that does not react with water is required. Nonhygroscopic inorganic scintillators, such as BaF_2, CeF_3, bismuth germinate (BGO), and lutetium yttrium orthosilicate (LYSO), are considered as a detector for field monitoring of beta nuclides, including tritium, in water.

Table 1 Classification of scintillators by phases and materials

Solid	Inorganic	NaI(Tl), LiI(Eu), ZnS(Ag), BGO, CWO, GSO, LSO
	Organic	Anthracene, Stilbene
	Plastic	Dissolving organic scintillator in solvent and polymerizing it into solid solution
Liquid		Use organic scintillant to dissolve appropriate solvents (toluene, etc.)
Gas		He, Ar, Xr, Xe

The BGO ($Bi_4Ge_3O_{12}$) scintillator, with a high atomic number of Bi, exhibits high detection efficiency and density and low energy resolution. It is a stable crystal due to its excellent mechanical strength and chemical properties. It is used for detecting X-ray CT and PET because of its short decay time of luminescence. Unlike other inorganic scintillators, no active agent (impurity; Tl) is used. An LYSO scintillator exhibits a high scintillation efficiency and good light output with very fast decay time. Its low refractive index is advantageous for light transmission. A plastic scintillator is mainly used for α and β detection due to its low atomic number, because C, H, and O are its main components. It is difficult to use the crystal form due to its low mechanical strength, but it exhibits excellent fabrication.

The nonhygroscopic inorganic scintillators considered as detectors for monitoring beta nuclides in a water sample include BGO, LYSO, and a plastic scintillator. The detection characteristics of BGO, LYSO, and plastic scintillators are confirmed with standard sources of ^{14}C and ^{90}Sr.

9

Scintillators are considered for monitoring beta radionuclides, including tritium, in water samples. Table 2 lists a comparison of each scintillator for applying the monitoring system. Liquid, inorganic, and plastic scintillators can be applied to beta monitoring systems in water samples, but the liquid scintillator can only be applied in laboratory. Therefore, inorganic scintillators of BGO and LYSO and plastic scintillators are selected as the candidate scintillator for the monitoring system.

Table 2 Selection table for scintillator to applying beta monitoring system including tritium in water

	Organic scintillator	Gas scintillator	Liquid scintillator	Inorganic scintillator	Plastic scintillator
Applicable to beta detection	O	O	O	O	O
Non-hygroscopic	X	O	O	O	O
Detector housing is not needed	X	X	O	O	O
Tritium in water analysis	X	X	O	O	O

A basic experiment is conducted to check the detection characteristics of each scintillator with a standard radioactive source. BGO, LYSO, and plastics are used as scintillators and ^{14}C (10 μCi) and ^{90}Sr (0.1 μCi) are used as the standard radioactive sources. Figure 6 shows the used scintillator.
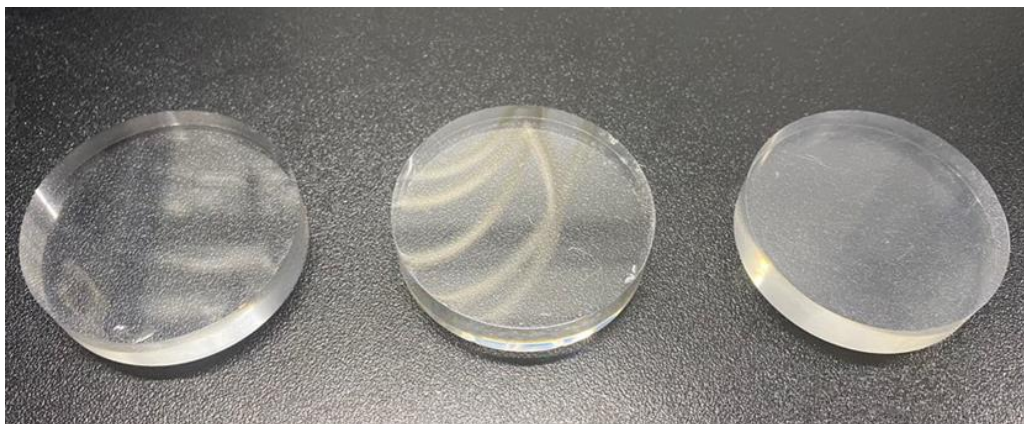
Figure 6 (left) BGO, (middle) LYSO and (right) plastic scintillator

The count rates for the background and standard sources of ^{14}C and ^{90}Sr are checked. Tables 3 and 4 list the detection results with coarse gains of 40 and 100, respectively. The background value of BGO is hardly affected by the coarse gain. In the case of BGO and LYSO, as the coarse gain increases, the count rate of ^{14}C also increases. However, in the case of ^{90}Sr, the count rate decreases. In the case of plastic scintillators, when the coarse gain increases, the background increases, but the value measured by the source decreases.

Table 3 Count rate measurement for each scintillator and radioactive source with coarse gain 40

		Count rate (cps)	
	Scintillator	Target	**Average**
Coarse gain 40	BGO	Bkg	1.73E+01
		^{14}C	1.38E+04
		^{90}Sr	9.22E+02
	LYSO	Bkg	1.22E+03
		^{14}C	2.41E+03
		^{90}Sr	3.08E+03
	PS	Bkg	**4.59E+00**
		^{14}C	2.55E+04
		^{90}Sr	9.41E+02

11

Table 4 Count rate measurement for each scintillator and radioactive source with coarse gain 100

		Count rate (cps)	
	Scintillator	Target	**Average**
Coarse gain 100	BGO	Bkg	1.61E+01
		^{14}C	1.52E+04
		^{90}Sr	6.98E+02
	LYSO	Bkg	2.52E+03
		^{14}C	6.50E+03
		^{90}Sr	2.86E+03
	PS	Bkg	7.59E+00
		^{14}C	2.12E+04
		^{90}Sr	8.12E+02

The detection efficiency is calculated as the difference between the count rate of the standard source and background divided by the radioactivity of the standard source. The detection efficiency of each scintillator is listed in Table 5, where the highest efficiency of each measurement is indicated in bold.

Table 5 The detection efficiency of each scintillator

Coarse gain	40		100	
Target	^{14}C	^{90}Sr	^{14}C	^{90}Sr
BGO	3.73E-02	2.45E-01	4.10E-02	1.84E-01
LYSO	3.22E-03	**5.03E-01**	1.08E-02	**9.19E-02**
PS	**6.89E-02**	2.53E-01	**5.73E-02**	2.17E-01

The measured experimental values are considered in terms of MDA. The equation for MDA is expressed below, and the measurement time and sample volume are obtained under the same conditions with different scintillators. Changes in scintillation affect the background radiation level and detection efficiency.

$$MDA = \frac{2.71 + 4.65 \times \sqrt{N_b}}{T \times \frac{\varepsilon}{100} \times V_c}$$

MDA: Minimum detectable activity (Bq/g)

N_b: Background count

T: Measurement time

: Detection efficiency

V_c: Volume of sample

The detected count rate for the background and radioactive source values of BGO and LYSO are divided by the plastic scintillator and relative ratios are obtained. The relative MDA of BGO and LYSO is obtained and the results are presented in Table 6.

Table 6 Relative ratio of measured count rate with plastic scintillator in coarse gain 40

Coarse gain 40	Detection object	Relative ratio with Plastic Scintillator	Relative change rate of MDA
BGO	Bkg	3.78E+00	-
	^{14}C	5.39E-01	7.00E+00
	^{90}Sr	9.79E-01	3.86E+00
LYSO	Bkg	2.66E+02	-
	^{14}C	9.43E-02	2.82E+03
	^{90}Sr	3.27E+00	8.13E+01

Table 7 Relative ratio of measured count rate with plastic scintillator in coarse gain 100

Coarse gain 100	Detection object	Relative ratio with Plastic Scintillator	Relative change rate of MDA
BGO	Bkg	2.12E+00	-
	^{14}C	7.17E-01	2.96E+00
	^{90}Sr	8.59E-01	2.47E+00
LYSO	Bkg	3.32E+02	-
	^{14}C	3.07E-01	1.08E+03
	^{90}Sr	3.52E+00	9.44E+01

The background radiation levels for BGO and LYSO are higher than that for PS. This means that a higher MDA is obtained in cases of BGO and LYSO. In case of ^{14}C, both BGO and LYSO show lower

14

efficiency than the plastic scintillator. In case of ^{90}Sr, the efficiency of LYSO is found to be much higher than that of the plastic scintillator. However, as the background radiation of LYSO is much higher than that of the plastic scintillator, LYSO is not advantageous in terms of MDA. In conclusion, the optimal scintillator for detecting beta nuclides in terms of MDA is the plastic scintillator.

Plastic scintillators are obtained by the polymerization of a liquid monomer in which scintillating additives are dissolved. In effect, a block of homogeneous scintillators can be obtained. Benzene, toluene, and xylene form the most widely used matrix for a plastic scintillator base because of their best scintillating properties. Polymers cannot be an effective scintillator because of the weak fluorescence efficiency and short mean free path for scintillating light. There are several chemical compounds that can be used as primary flours in plastic scintillators (e.g., PTP, PPO, PPD, BBD, PBD, and BPBD). However, they have different maxima of emission wavelength, so one can adjust the substance to the particular application. There are also several substances that can be used as wavelength shifters in plastic scintillators (e.g., POPOP, DM-POPOP, Bis-MSB, BBO, DPS, and DPA). Electrons in the tritium beta energy range mainly cause excitation and ionization in plastic scintillators.

$$\frac{dE}{dx} = \left(\frac{dE}{dx}\right)_{co} + \left(\frac{dE}{dx}\right)_{br}$$

The ratio of the two specific energy losses is approximately

$$\frac{\left(\frac{dE}{dx}\right)_{br}}{\left(\frac{dE}{dx}\right)_{co}} \approx \frac{EZ}{7 \cdot 10^5}$$

where E is an electron's energy (in keV) and Z is the atomic number of the absorbing material.

For an electron with an energy of 5.7 keV (average energy of tritium betas) in a low-Z material (e.g., carbon, Z = 6, which is present in the molecules of organic scintillators), the collisional losses are $2 \cdot 10^4$ times higher than those caused by the Bremsstrahlung equation. Virtually, the entire electron energy is deposited in the scintillator, causing scintillation. Therefore, a plastic scintillator is suitable for beta detection in water samples.

3. Methods

3.1 Design of detection part

 The detection part is designed to detect short-range beta nuclides in the aquatic environment of the decommissioning site. The main contents reflected in the detection part design are as follows.

- Design of a detector where the scintillator reacts directly with the radiation source for short-range beta measurement.

- On-site monitoring system resulting from the reduction of measurement time due to increased detection efficiency.

- Software design for on-site error factor analysis and noise minimization.

3.1.1 Considerations for beta detection in water

 Beta nuclides are nuclides that release charged particles. The distance that a charged particle travels until it loses its kinetic energy in the material is defined as its range. When the charged particle proceeds a certain distance while progressing through the material, its ionization action is drastically reduced. Thus, beta rays have a specific range with energy in water. The characteristics of the range according to the type of charged particles in water are shown in Figure 7. Beta nuclides are electron-emitting nuclides, following the below equation [10]:

$$\log(range\ in\ mm) = 0.0419(logE)^3 - 0.172(logE)^2 + 1.20(logE) + 0.572$$

Equation 1. Equation for calculating range to charged particle

 In particular, the beta ray of tritium, which has a very low energy, has a range of 0.005797 mm when the maximum energy is 0.0186 MeV, according to the formula for the range according to the energy of charged particles. It is necessary to design the distance minimization between the source and the scintillator to detect the short-range beta ray. Therefore, a detector that can directly detect water samples containing beta nuclides is designed.

17
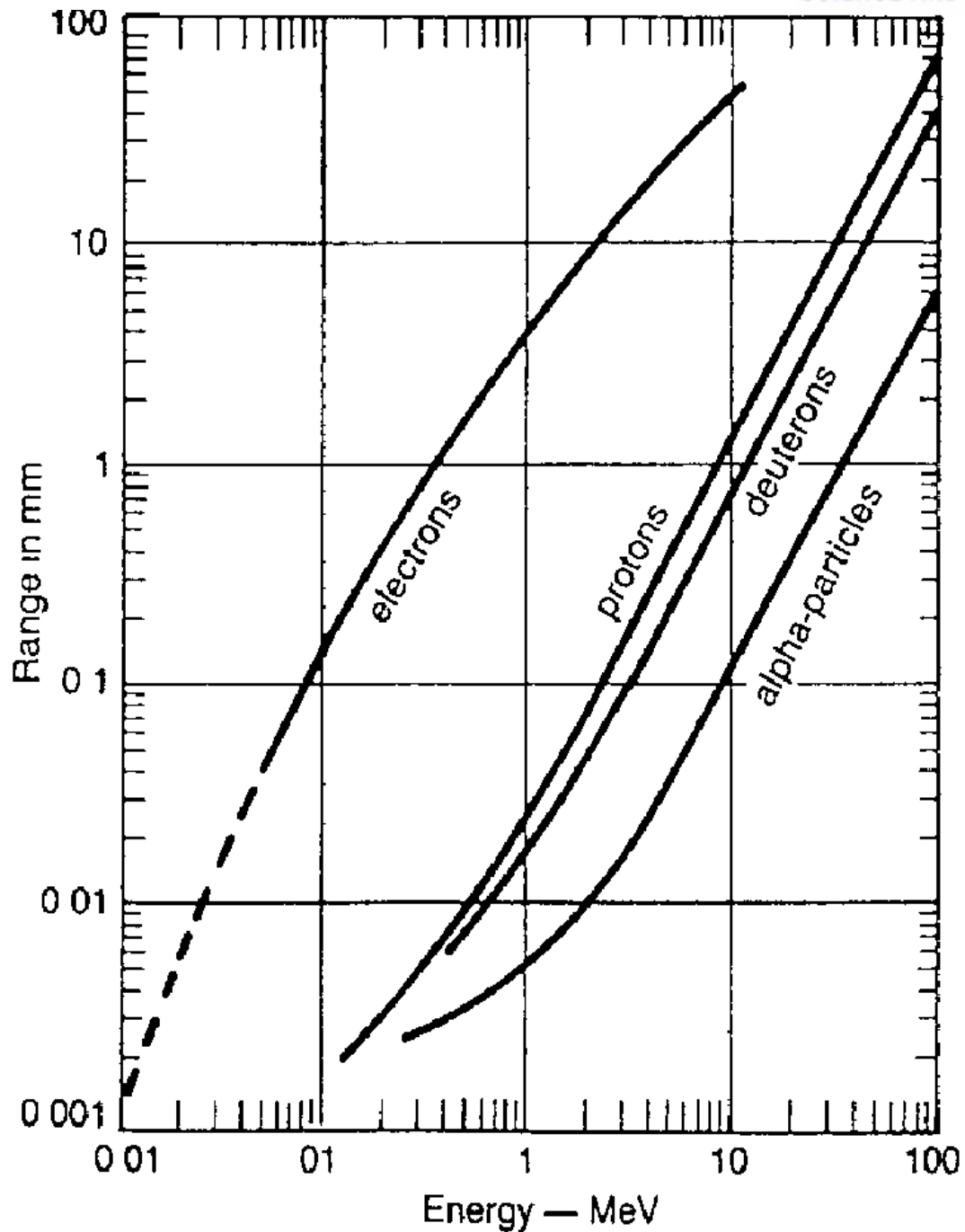
Figure 7 Range in water according to the type of charged particles

The spectral characterization of ^{90}Sr and ^{14}C using plastic scintillators and tritium measurement characteristics using disc-shaped plastic scintillators have been reported. To directly measure low-energy beta nuclides in the field, a detection module is designed to direct the source flow to the scintillator material considering the short range, as shown in Figure 8.
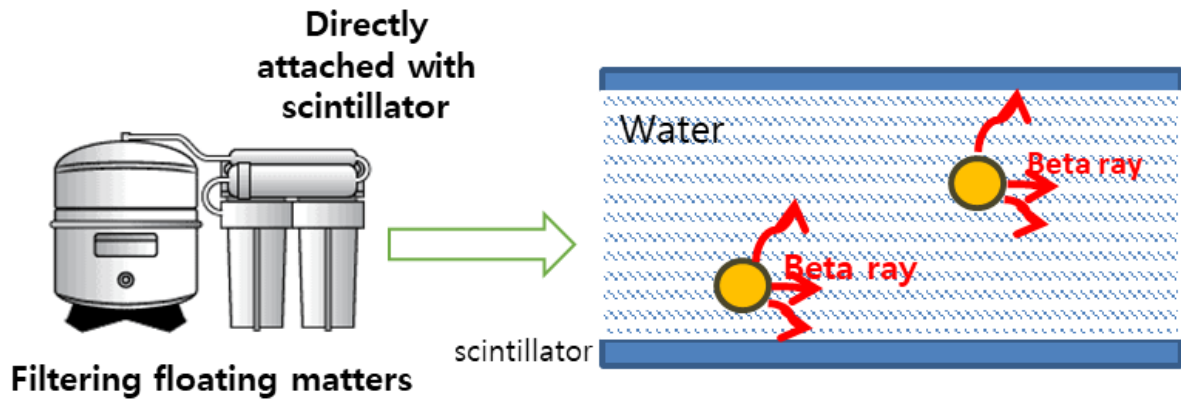
Figure 8 Design for detection module based on direct the flow of source to the scintillator

Some basic detection modules have been designed to analyze the reaction characteristics of beta nuclides and plastic scintillators. The flow path and a scintillator acrylic support structure of $60 \times 60 \times 50$ mm^3 are fabricated through acrylic processing, as shown in the Figure 9, so that the liquid including the source can flow. The upper and lower parts are manufactured to a diameter of 52 mm, so that PMT can be inserted, and the depth is set to ~15 mm. In addition, after descending to a depth of 15 mm, a projection part of 5 mm is developed to create a space for bonding the plastic scintillator. On both sides, the protruding part is processed to ~15 mm, and the silicon tube is inserted to process the water. The inner diameter of the used tube is 6 mm and the diameter of the protruding portion is 8 mm; thus, the tube can be firmly fixed to the scintillator acrylic support structure. The developed plastic scintillator acrylic support structure for the water flow is shown in Figure 9.
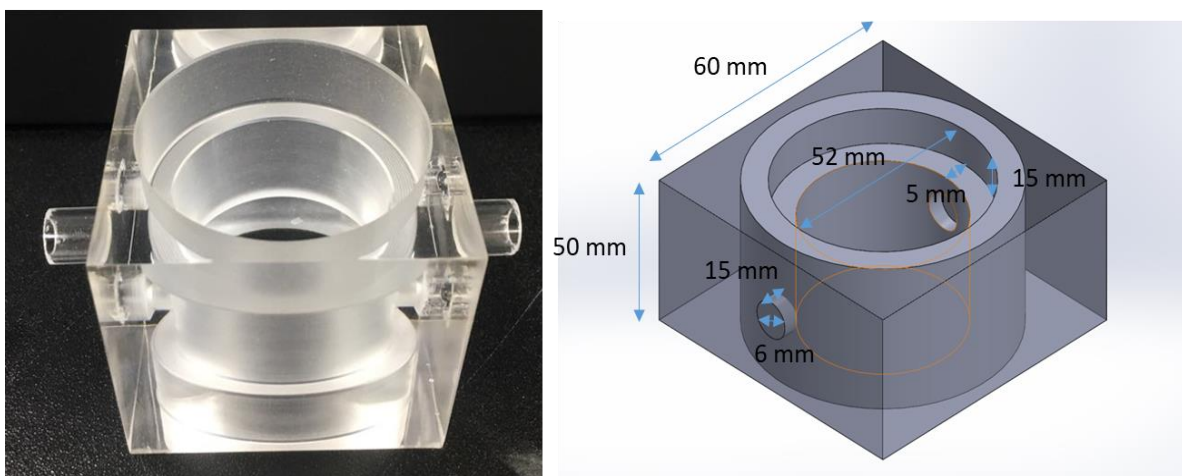
Figure 9 Plastic scintillator acrylic support structure for water flow

3.1.2 Considerations for detection part

If the detector is composed of a high-atomic-number material, such as metal, the Bremsstrahlung reaction may occur, so the detector is made of acrylic material. Tritium has very low energy and a short range, and therefore, it shows low detection efficiency in water. The detection chamber optimization is needed to enhance the detection efficiency, which can be achieved by increasing the reaction cross-section area, rather than increasing the amount of the sample. There are several approaches for increasing the area, such as the use of a large detector or the pellet form. This study uses a plastic scintillator of dimensions 16 cm × 35 cm for ^{90}Sr detection in water [11].
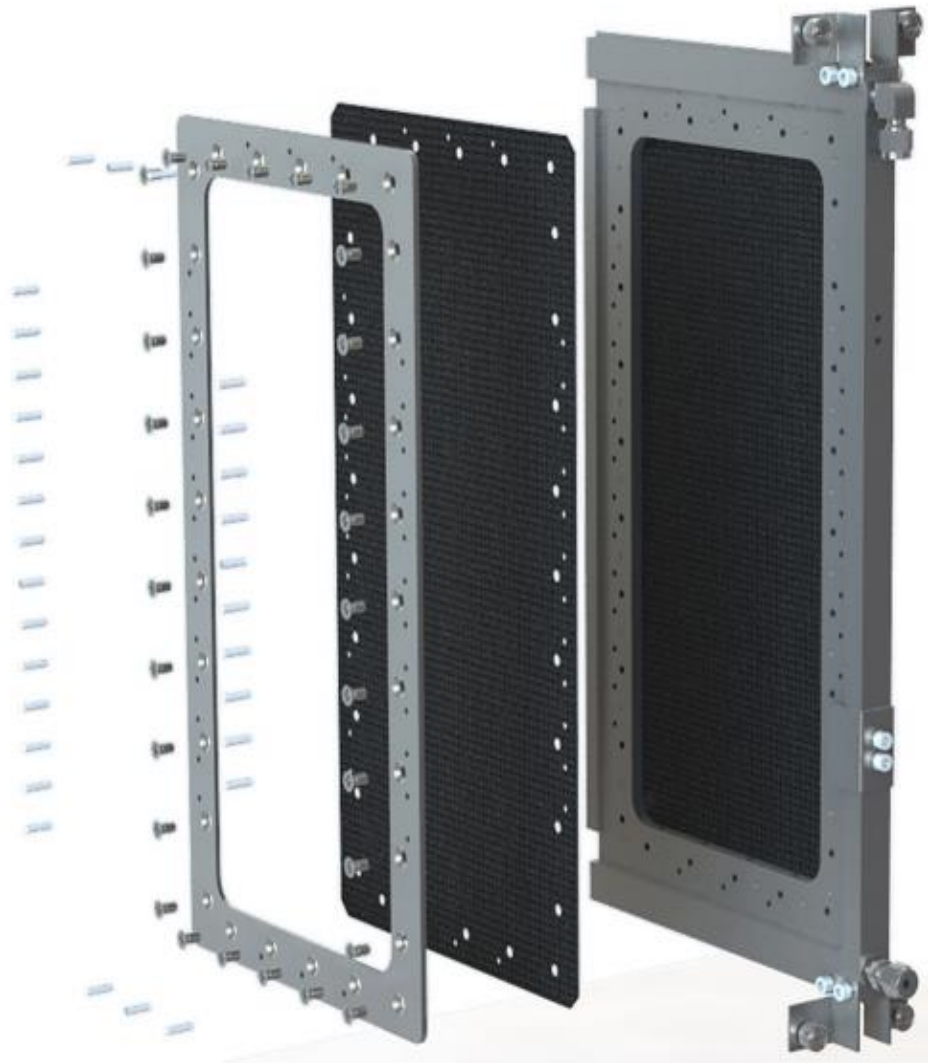
Figure 10 Detector design for performance of a low activity beta-sensitive ^{90}Sr water monitor

However, the large size of plastic scintillator has limit for applying field monitoring because scale for shielding system also enlarged like Figure 11.

Figure 11 Entire system for performance of a low activity beta-sensitive ^{90}Sr water monitor

The pellet-type plastic scintillator also increases the cross-sectional area. These scintillators are put into specific geometric structures with radioactive samples, as shown in Figure 12 [12]. In case of pellet-type scintillators, the amount of loaded radioactive sample in the detection part is relatively small. This is not advantageous in decrement in MDA.
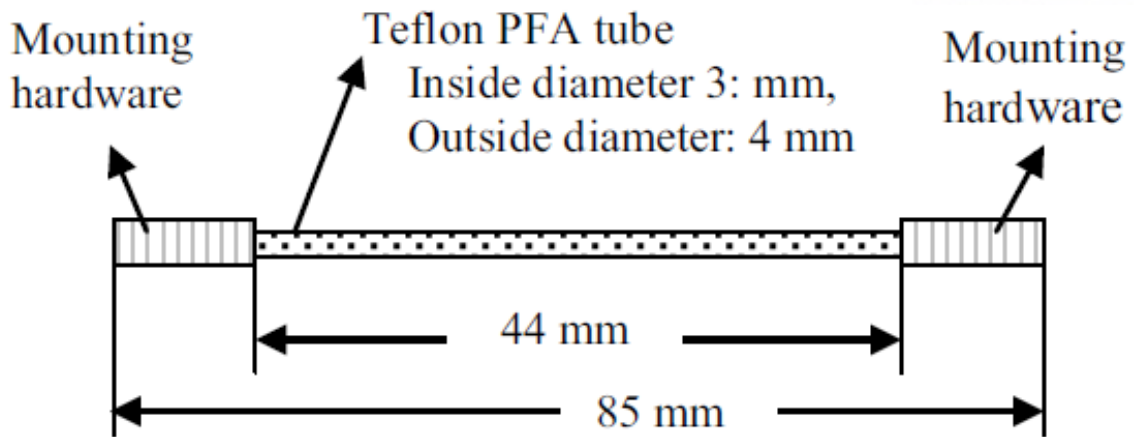
Figure 12 Pellet type scintillator-based radiation monitoring

In this study, a multilayer thin plastic scintillator is used to increase the cross-sectional area with a large amount of loaded water sample. Optimization of the detection part is conducted based on the number of plastic scintillators used. Figure 13 shows example cases of small and large numbers of plastic scintillators used. The red part indicates the acrylic support for the detection part, the green lines indicates thin-plate-type plastic scintillators, and blue sections indicate the water samples.
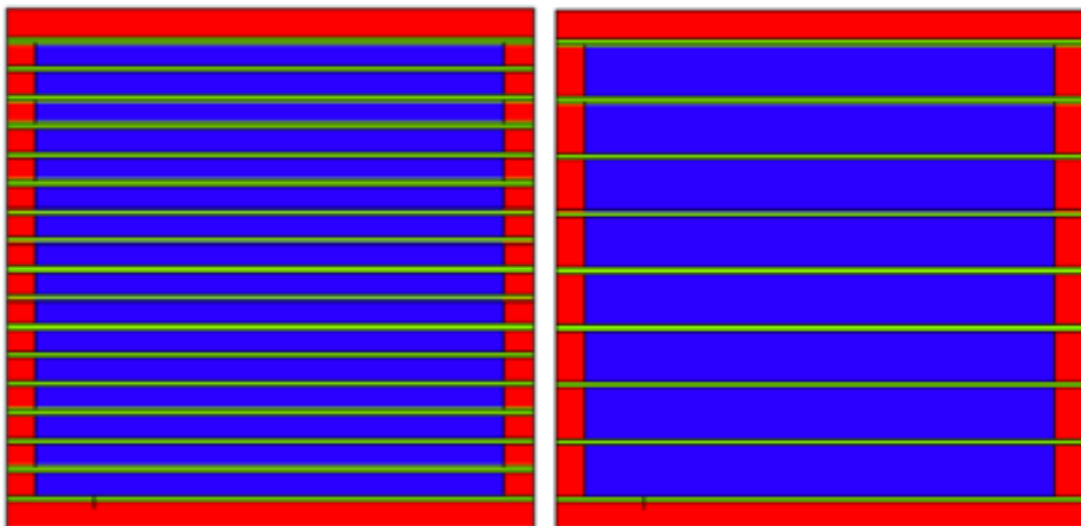
Figure 13 Schematic diagram for multi-layer scintillator detection chamber for (left) 13 scintillator and (right) 7 scintillator

Based on the number of scintillators and target radionuclides, the detection geometry is evaluated by MCNP simulation and experiment. In this study, the detection conditions for low- and high-energy beta are suggested with the optimization process.

Detector modules are designed and fabricated for quantitative analysis of the detection of beta nuclides, including tritium, in water. To improve the detection efficiency, a detection module is designed with increasing reaction cross-sectional area of radionuclides and plastic scintillators in the water samples. Seven and 13 plastic scintillators with thickness of 1 mm are inserted into the detection modules to maximize the reaction cross section.

The seven scintillator-based detection part is designed to detect high-energy beta nuclides, to set the distance between the scintillators based on the range corresponding to the maximum energy of yttrium. The details about detection part design are shown in Figure 14-Figure 17.
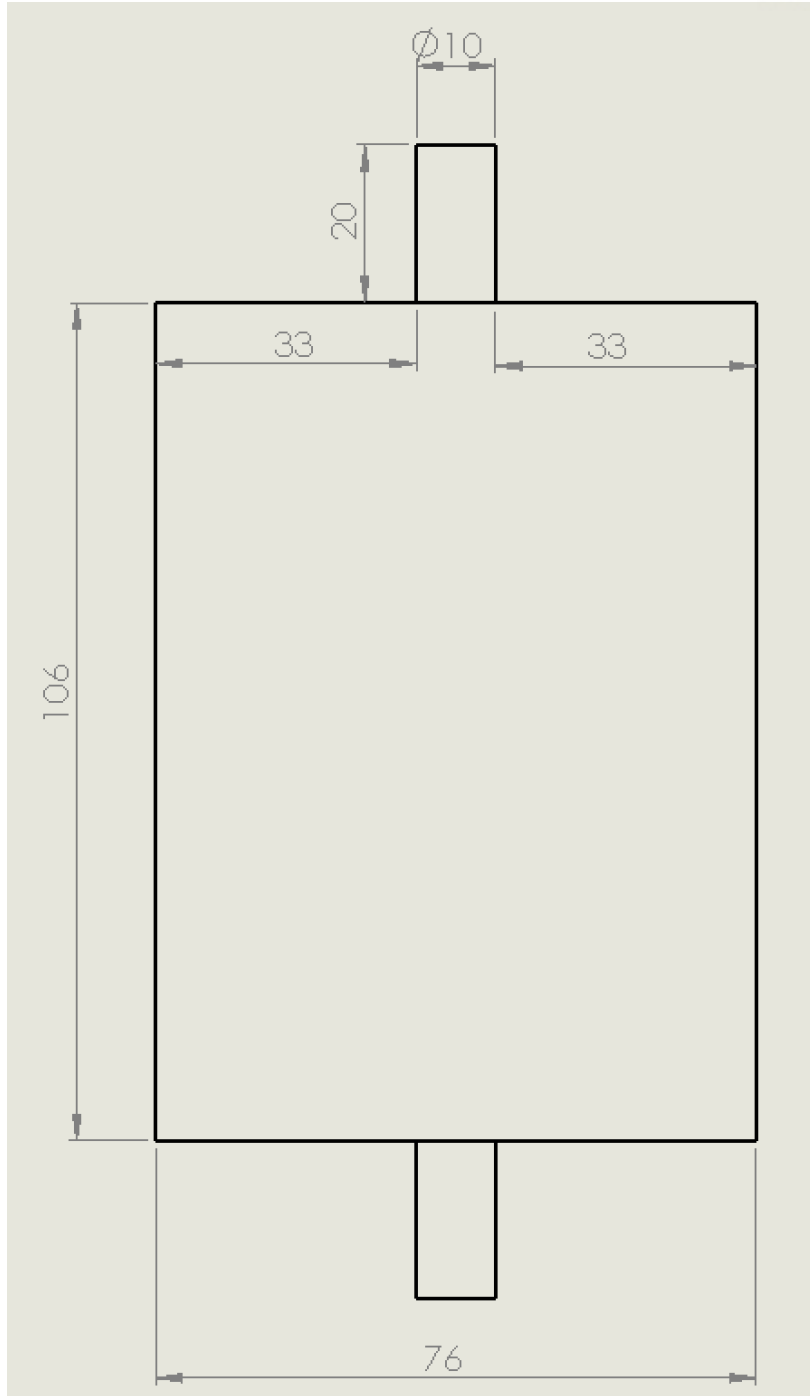
Figure 14 Top view of acrylic support module for detection part
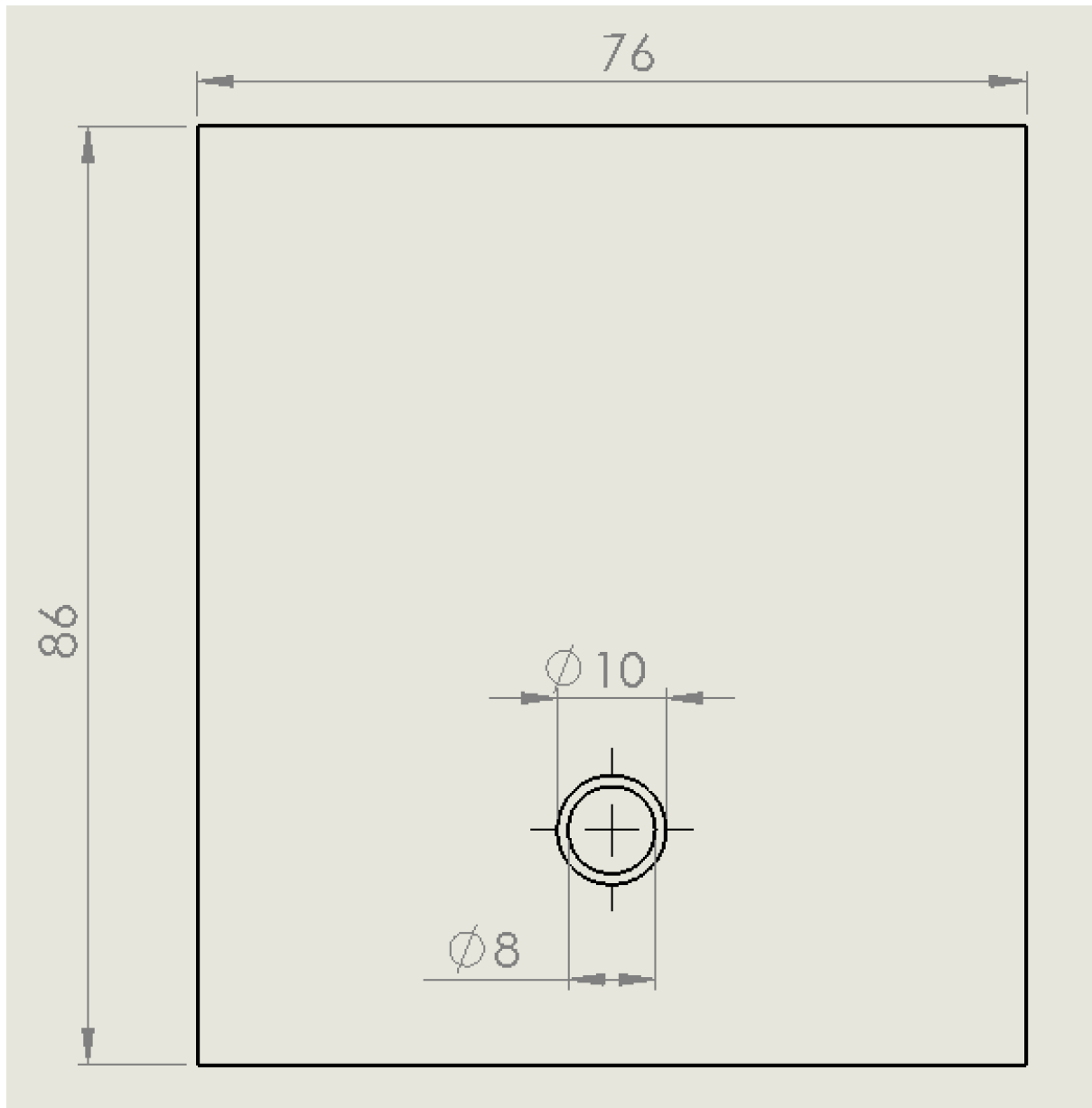
Figure 15 Front view of acrylic support module for detection part
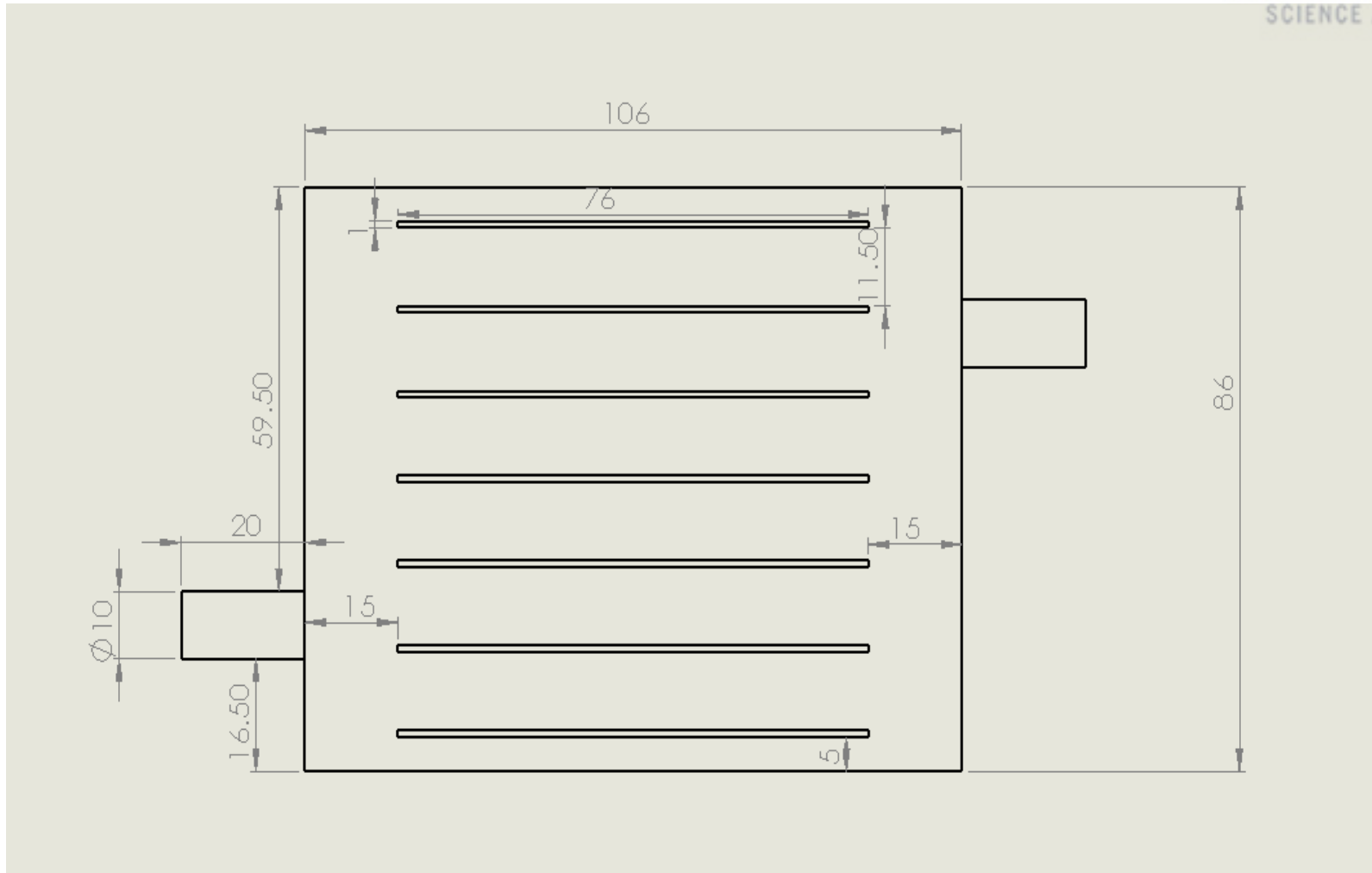
Figure 16 Side view of 7 scintillator-based acrylic support module for detection part
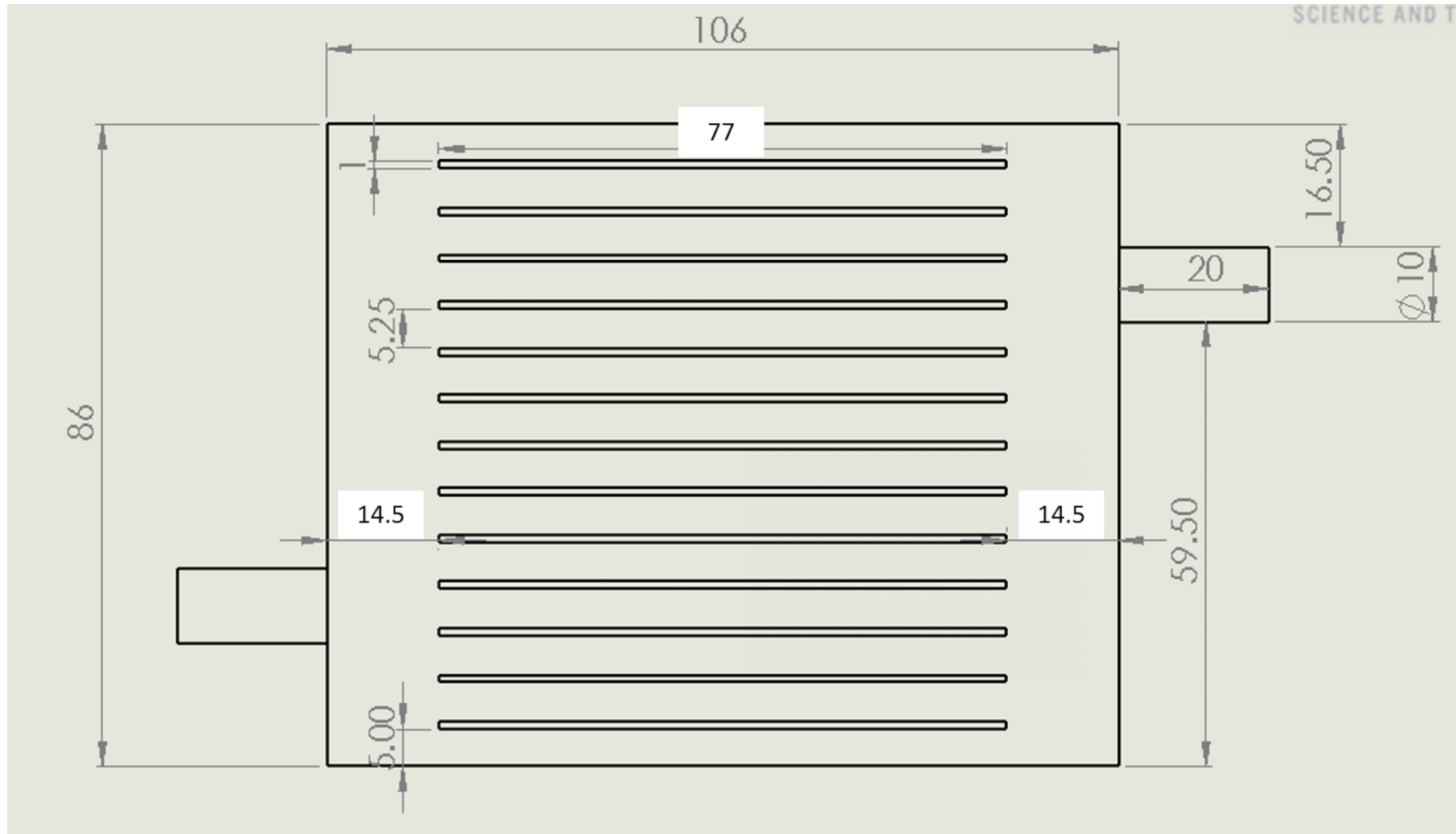
Figure 17 Side view of 13 scintillator-based acrylic support module for detection part

Increasing the number of scintillators reduces the amount of water sample by the volume of scintillators. The volume of water samples in 7 and 13 scintillators, according to the number of scintillators, is derived and used for MDA calculation. The geometric information of the 7 and 13 scintillation-based detection parts is shown in Table 8–10.

Table 8 Geometric information of detection chamber

Volume of detection part			
Outer wall		Inner wall	
Width	7.6 cm	Width	6.6 cm
Length	10.6 cm	Length	9.6 cm
Height	8.6 cm	Height	7.6 cm
Volume	692.816 cm^3	Volume	481.536 cm^3

Table 9 Geometric information of plastic scintillator

Volume of scintillator			
Outer wall		Inner wall	
Width	7.6 cm	Width	6.6 cm
Length	7.6 cm	Length	7.6 cm
Height	0.1 cm	Height	0.1 cm
Volume	5.776 cm^3	Volume	5.016 cm^3

Table 10 Volume of water sample considering detection chamber and plastic scintillator

	13 scintillators	7 scintillators
Volume of scintillator	$6.52E+01$ cm^3	$3.51E+01$ cm^3
Volume of water sample	$4.16E+02$ cm^3	$4.46E+02$ cm^3
Cross-sectional areas	$1.30E+03$ cm^2	$7.02E+02$ cm^2
Ratio between volume and cross-sectional area	$3.13E+00$ cm^{-1}	$1.57E+00$ cm^{-1}
Ratio of two scintillators	$1.99E+00$	

3.1.3 Radiation detection system based on plastic scintillator and PMT

Coltman and Marshall proposed a method for measuring the light emitted from the reaction between a scintillator and radiation using PMTs [13]. The advantage of detection using a scintillator and PMT is that it is possible to measure various radiations by changing the scintillator and to measure high count rate with shorter resolution time as compared to other detectors. This can be observed in Figure 18.

The plastic scintillator comprises a polymer material and the scintillator of a first solute and second solutes. When radiation enters the polymeric material of the plastic scintillator, the unstable polymer releases energy to become stable. The emitted energy is transmitted to the first solute of the scintillator, which then emits energy in the form of a flash in the ultraviolet region. As the wavelength of the ultraviolet region does not correspond to the flash response characteristic of the PMT, the wavelength of the ultraviolet region is shifted to a wavelength suitable for the PMT using the second solute.

Scintillators are classified into organic and inorganic scintillators. Organic scintillators include liquid, organic crystal, and plastic scintillators, while inorganic scintillators include gas, glass, and inorganic crystal scintillators. and the scintillators to be used in this study must have the following characteristics [14].

-The conversion efficiency (fluorescence efficiency) from radiation energy to fluorescent energy should be high.

- The generated fluorescence should have good transparency.

-The decay time of fluorescence should be short.

-The fluorescence spectrum distribution should match the wavelength sensitivity distribution of the photocathode surface of PMT.

In this study, we use an organic scintillator. A plastic scintillator is obtained by dissolving an organic scintillator in a solvent, and then polymerizing it into a solid solution. Polystyrene, PSF, PBAC, and styrene are used as the solvent, and p-terphenyle+POPOP and p-terphenyle+tetraphenyl butadiene are used as the solute. Plastic scintillators can be used for β-ray measurements and are easy to manufacture in many forms. Polystyrene is used as the scintillator material and the production of scintillators using polystyrene is difficult than that using other materials; however, it has twice the detection performance

as compared to other polymer materials [15]. In the form of a scintillator, a circular scintillator having a diameter of 50 mm is produced for fitting with the PMT geometry.
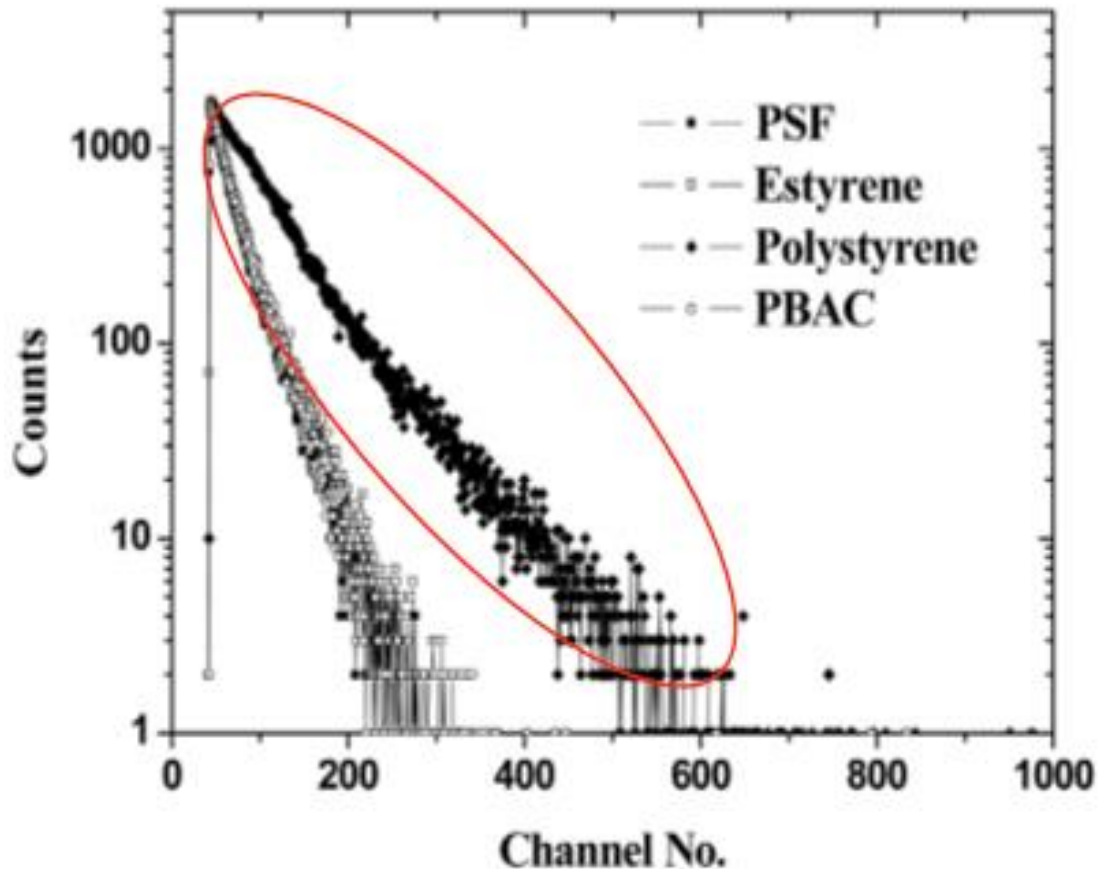
Figure 18 Detection performance according to polymer material

A scintillator and PMT are used to construct the detector and data processor. As for the scintillator, a plastic scintillator (EPIC CRYSTAL) is used, as shown in Figure 19, and as for PMT, the PMT R877 and R878 model of Hamamatsu is used, as shown in Figure 20 and Figure 21 [16]. Plastic scintillators are physically and chemically stable in the reaction with water and undergo little damage when contacted directly with water. Plastic scintillators exhibit relatively low backscattering due to their low effective atomic number. In addition, they can reduce the background level because of their low sensitivity to gamma rays.
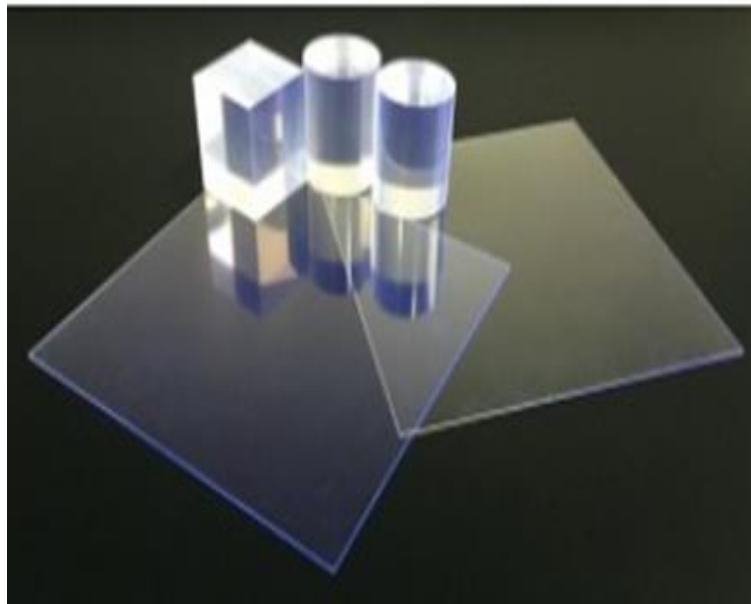
Figure 19 Plastic scintillator for beta nuclide monitoring in water sample
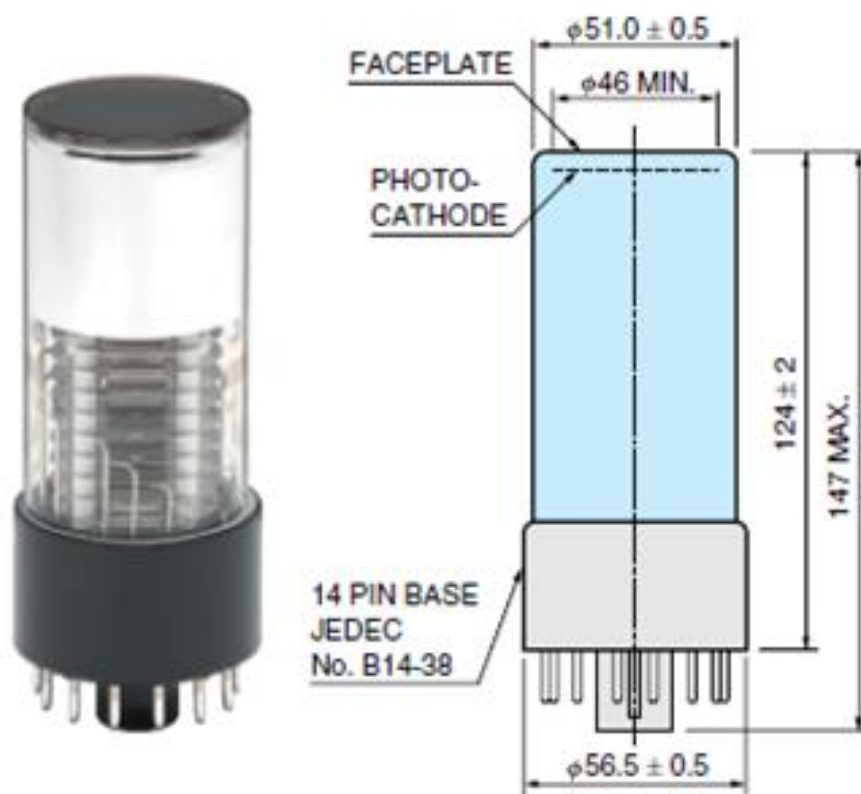
Figure 20 Dimensional outline of PMT R878
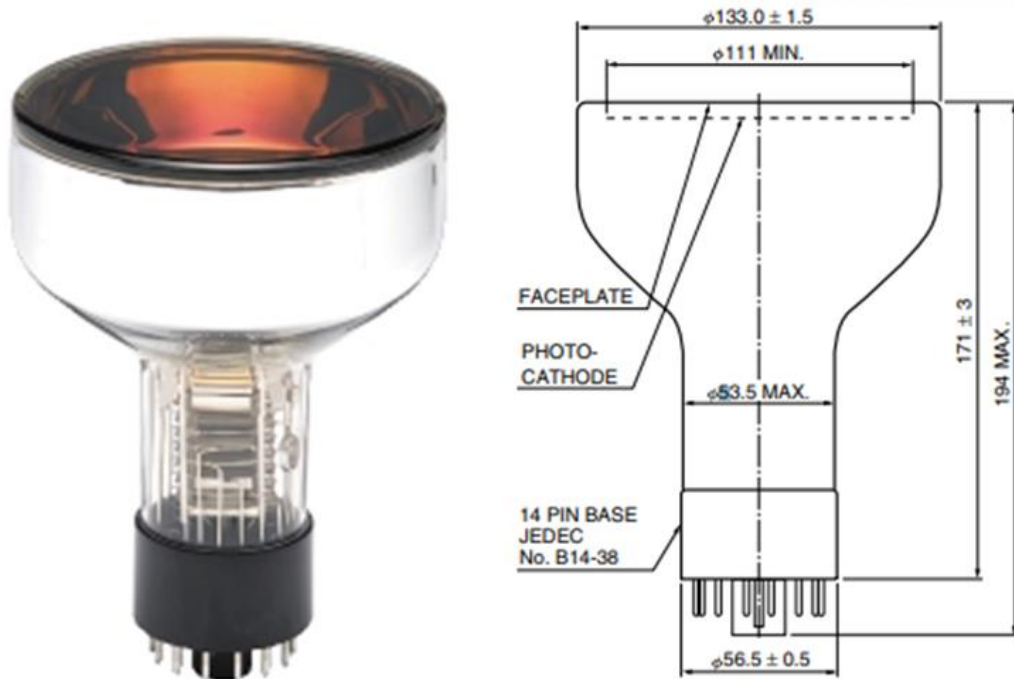
Figure 21 Dimensional outline of PMT R877

Light is emitted through an interaction between radiation and the scintillator, and transmitted to the photocathode, which releases electrons. A dynode, which is a multi-level metal plate designed to emit more electrons than the incident electrons, is used to accelerate the electrons. The dynode comprises 6 to 10 stages and applies voltage with sequential increment. The electrons emitted at each front end are accelerated and incident at the rear end so that multiplication occurs.

A resistor is connected to each dynode to apply a high voltage (HV) at 0. At this time, the PMT is shielded with an alloy, such as Fe or Ni. This is to prevent deviation of the electron migration path by the magnetic field, and a light shield is required to minimize the interference of light.

Current flows as the electrons with charge move, and this current is only on the order of nanoamperes. The preamplifier comprises a capacitor, which converts charge (current) into voltage. At this time, as the voltage generated by the current is on the order of microvolts, a main amplifier is used to generate a voltage between 0 and 10 V.
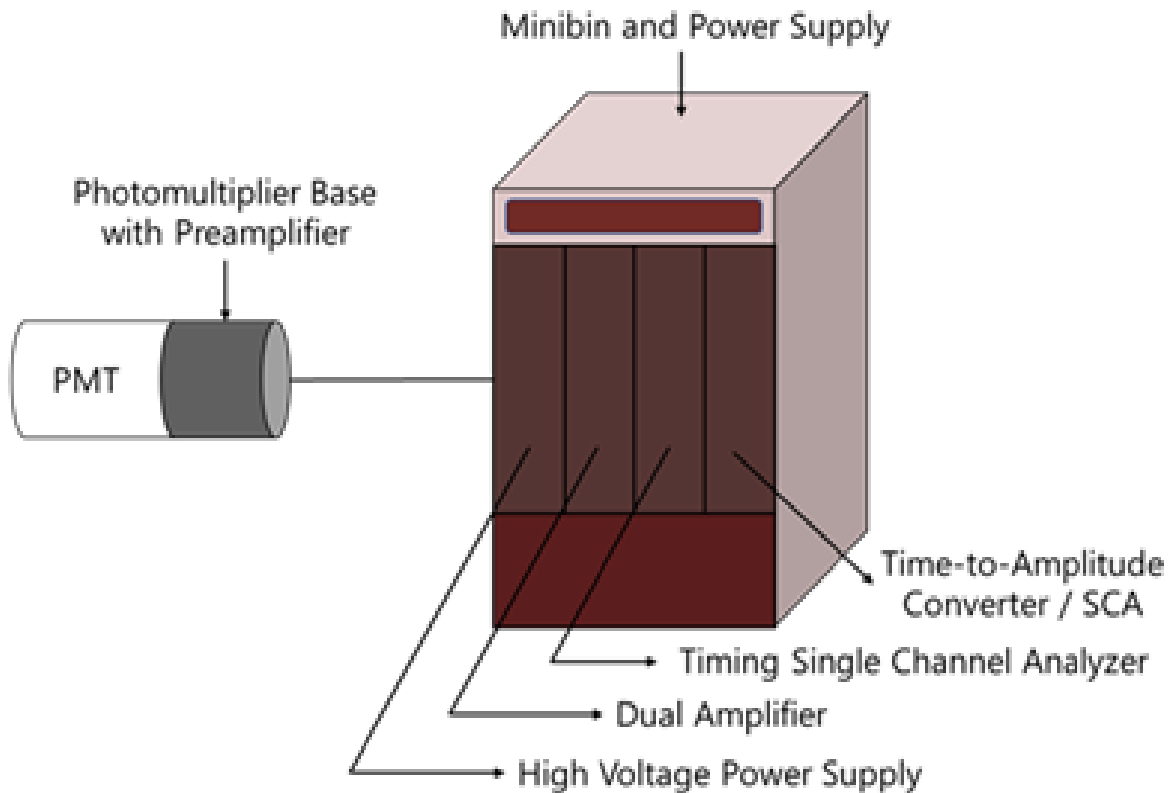
Figure 22 Electronic setting for scintillator and PMT based monitoring system

The NIM module-based spectroscopy system is used for constructing a beta nuclide characterization and detection module. The system is constructed using a 276 Photomultiplier Base with Preamplifier, 855 Dual Amplifier, 551 Timing Single-Channel Analyzer, 567 Time-to-Amplitude Converter/SCA, and 556 High-Voltage Power Supply. The overall electronic setting for the scintillator and PMT-based monitoring system is shown in Figure 22 [17-21].

The 276 Photomultiplier Base with Preamplifier, shown in Figure 23, is used with a 10-section PMT fitted into a standard 14-pin socket and incorporates a low-noise preamp. In addition, both the preamplifier and anode can be output, and it has an internal transistor protection circuit function.

Figure 24 shows the 855 Dual Amplifier and 551 Timing Single Channel Analyzer. The 855 Dual Amplifier comprises two 575 A amplifiers in 1-wide NIM for multi-detector-based energy spectroscopy with automatic reference reconstruction and threshold control, which determine amplification through coarse and fine gains.

The 551 Timing Single Channel Analyzer is a single-channel analyzer, which serves as a timing signal induction with a delay adjustable range of 0.1–11 μs. Figure 25 shows the 567 Time-to-Amplitude

Converter/SCA and 567 High-Voltage Power Supply. The 567 Time-to-Amplitude Converter/SCA allows time spectroscopy in the range of 10 ns to 2 ms for output delay and width selection. The 567 High-Voltage Power Supply provides appropriate power to the preamplifier and PMT.

Figure 23 276 Photomultiplier Base with Preamplifier

Determination of amplification

(Coarse and fine gain)

Determination of delay time

(250 ns)
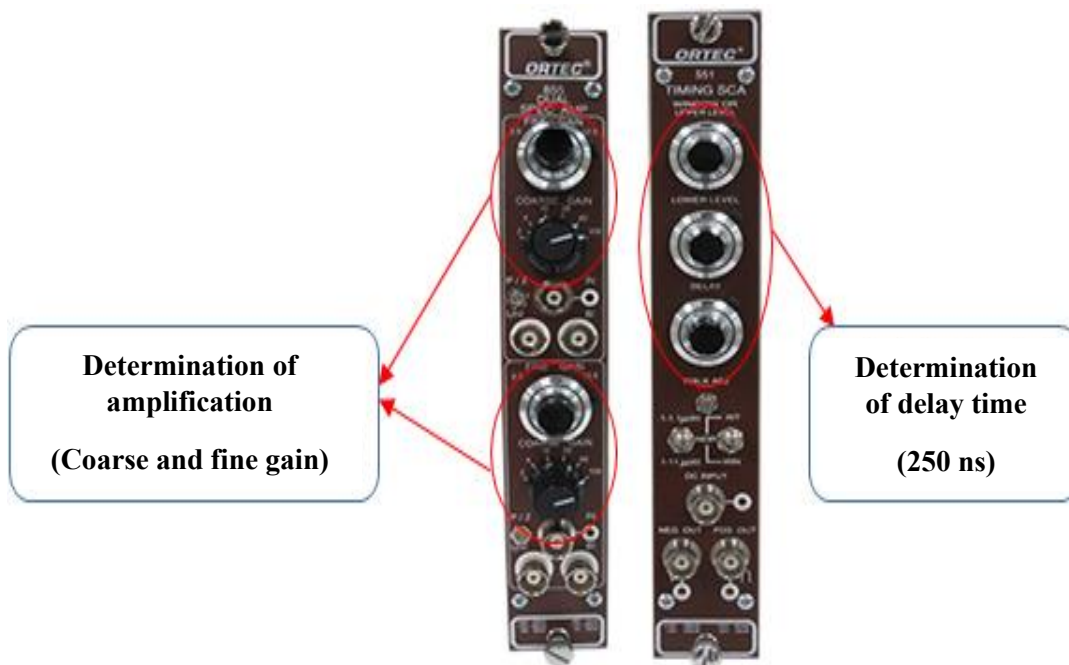
Figure 24 855 Dual Amplifier and 551 Timing Single Channel Analyzer

Selection of entire
spectrum range

(500 ns)

Apply adequate voltage at preamplifier and PMT

(1.25 kV)
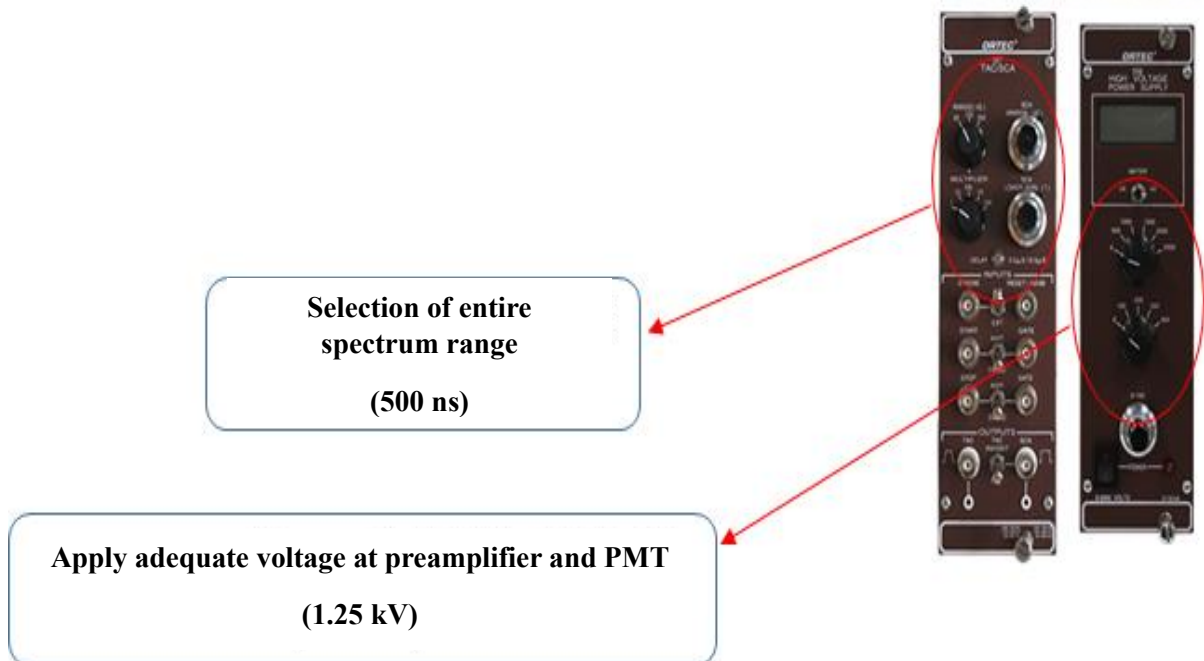
Figure 25 Time-to-Amplitude Converter/SCA and 567 High Voltage Power Supply

3.1.4 Simulation for interaction of plastic scintillators

3.1.4.1 Detection efficiency change simulation according to air layer

Simulations are performed to determine the effect of the air layer between the plastic scintillator and beta nuclide. The space between the scintillator and the water sample is defined as the air layer, which means that the beta rays can react with the air before the scintillator. Therefore, as the thickness of the air layer increases, the distance between the scintillator and the sample increases; thus, the beta particle is more likely to react with the air. This is also expected to affect the MDA, and hence, the air layer thickness is set as an efficiency characteristic variable. A geometrical model is established in which an air layer is formed between the scintillator and the radionuclide. The geometrical model used is shown in Figure 26, where the blue section indicates the scintillator, the green section indicates the water containing the radioactive source, the yellow section indicates the acrylic structure, and the red section indicates the air layer. The source terms are simulated using ^{3}H and ^{14}C. As low-energy beta nuclides are affected by the air layer, the representative low-energy beta nuclides ^{3}H and ^{14}C are selected for the simulation.

36
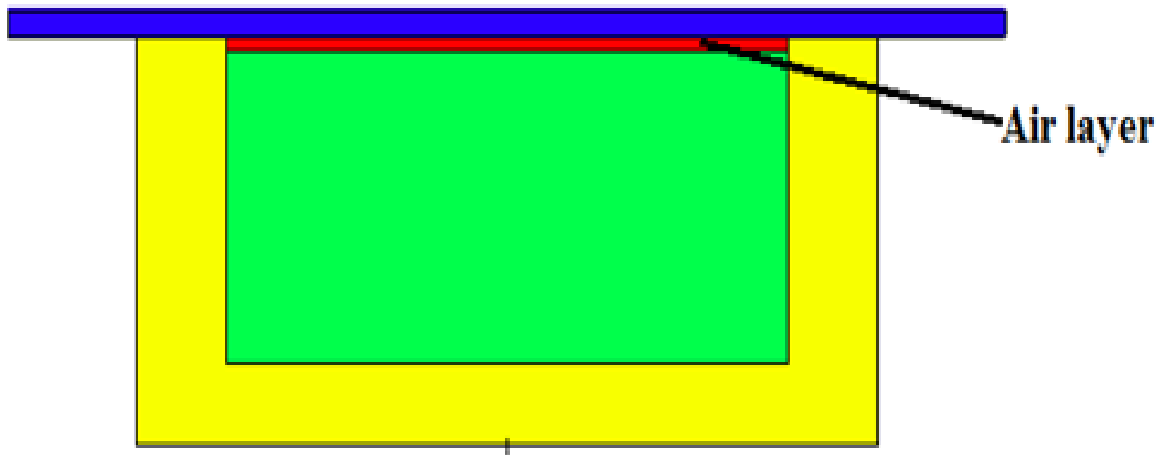
Figure 26 Simulation model of detection efficiency calculation for air layer

3.1.4.2 Detection efficiency simulation for thickness of plastic scintillator

  To determine the scintillator thickness, the efficiency of the plastic scintillator is calculated via MCNP6. Modeling is performed on two types of plastic scintillators with thicknesses of 1 and 5 mm. The modeled system is shown in Figure 27, and the components used in this simulation are shown in Table 11.
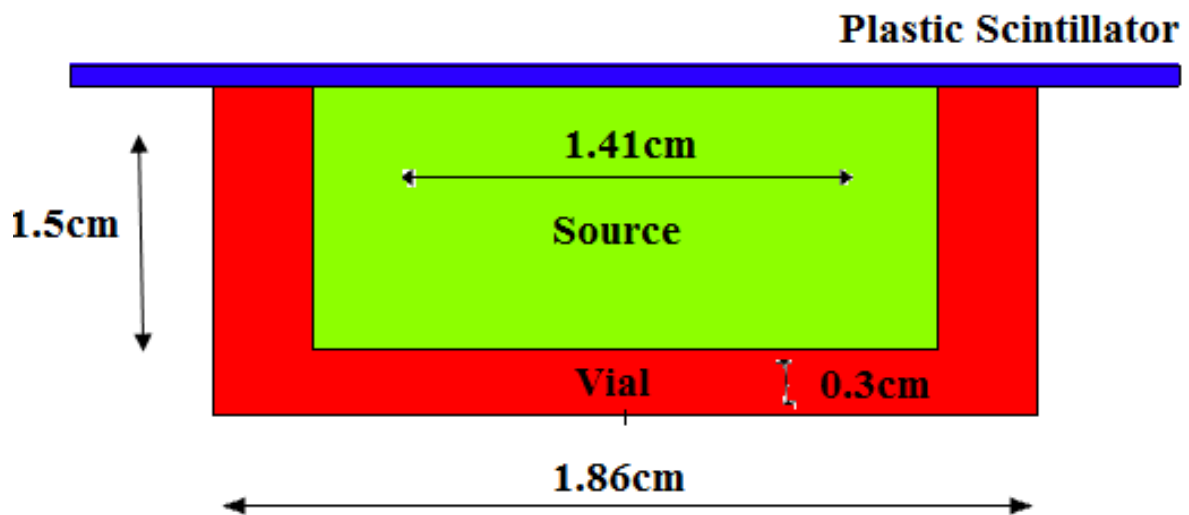
Figure 27 Simulation model of detection efficiency calculation for thickness of plastic scintillator

Table 11 Information of material component used for simulation

Component	Composition	Density (g/cm^3)
Plastic scintillator	Polystyrene	1.05
Vial	Polyethylene	0.93
Radioactive source	Approximate by water	1

3.1.4.3 Detection efficiency simulation for diameter of scintillator and height of water sample

A simulation is performed by setting two variables for the structural optimization of the sample and scintillator. The first variable is the diameter of the scintillator, which affects the cross-sectional area where the source and scintillator react. The second variable is the height of the water sample, which affects the volume and concentration of the sample to be measured. Based on the two variables, the concept of figure of merit (FOM) is introduced to perform effective modeling of the detection part. FOM is defined as the product of measurement efficiency and the volume of the sample, and is introduced to evaluate the effect of scintillator diameter and water depth on the measuring time, to achieve reasonable counting statistics. FOM is defined in the below equation, where ε and V indicate the simulation efficiency and water volume, respectively.

$$FOM = \varepsilon \times V$$

Equation 1. Equation for FOM of the simulation efficiency and sample volume

If the same number of counts is reached, a higher value of FOM would result in a shorter measurement period. To confirm the influence of the water sample height, a simulation is performed with varying the height (6, 12, 30, and 50 mm) while maintaining the same scintillator diameter (Figure 28). To confirm the influence on the scintillator diameter, modeling is performed by fixing the height of the water sample and varying the diameter (2, 3, and 5 cm). Figure 29 shows a geometrical simulation model for different diameters of the plastic scintillator at a constant height of the water sample. The used values of scintillator diameters and water sample heights are selected to confirm the tendency of each variable.
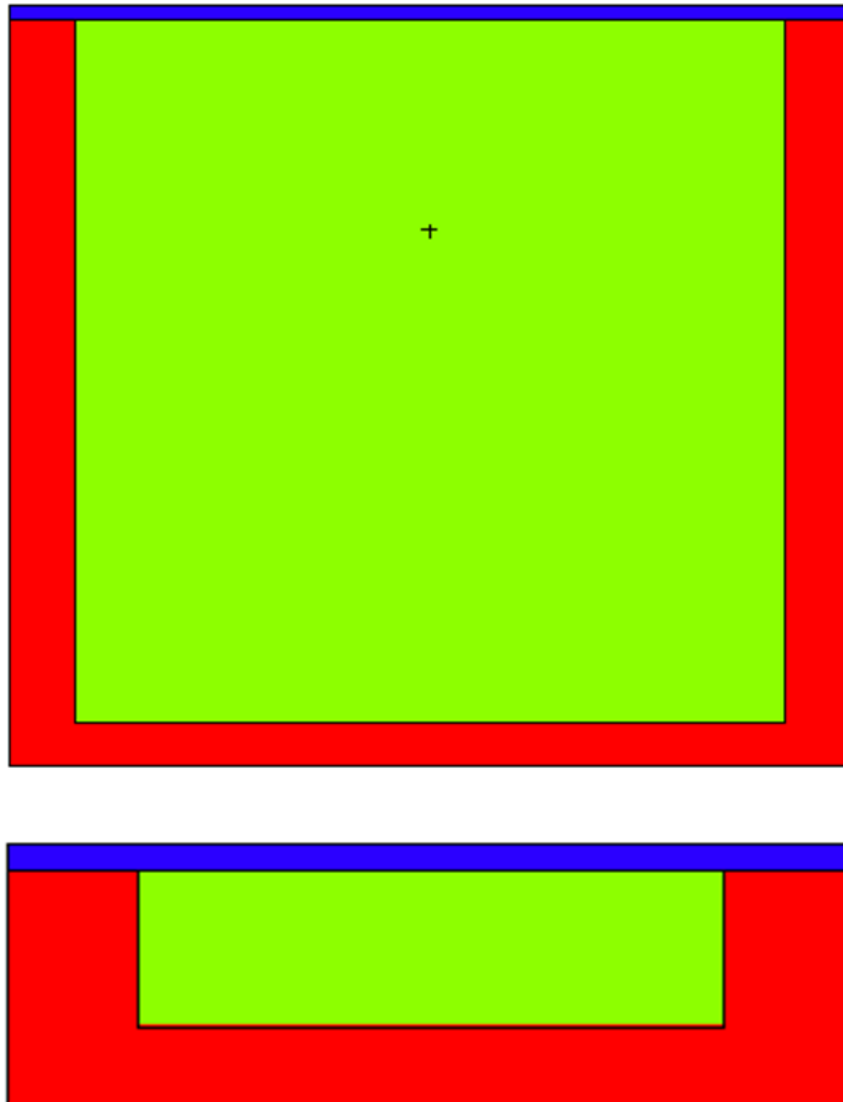
Figure 28 Geometrical simulation model for same diameter of plastic scintillator and different height of water sample
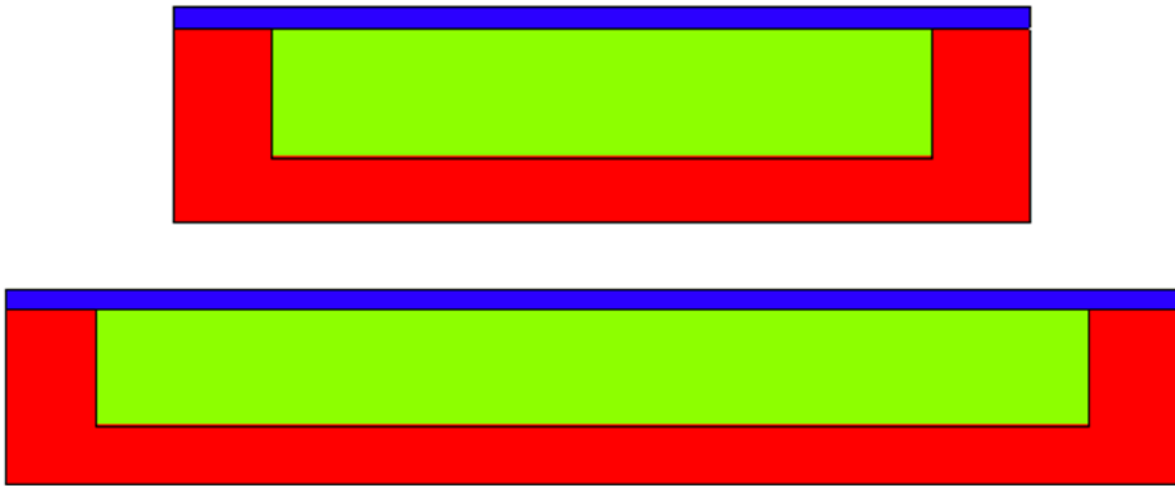
Figure 29 Geometrical simulation model for different diameter of plastic scintillator and same height of water sample

3.2 Pretreatment of water sample

The groundwater and seawater around nuclear facilities contain various substances besides radionuclides. The large-sized suspended particles not only affect the attenuation of beta rays but also reduce the efficiency in terms of optics. Organics and microorganisms may remain in the detection part and cause physical defects such as corrosion. In addition, if pure water is prepared by removing various ions in water, only the influence of tritium present in the water form can be analyzed. Based on these reasons, a pretreatment system is constructed to produce groundwater and seawater as pure water.

3.2.1 Target components in groundwater

The major constituents of groundwater include Ca^{2+}, Mg^{2+}, Na^+, HCO_3^-, Cl^-, and SO_4^{2-}, which play an important role in the evaluation and classification of groundwater quality. Ca^{2+}, Mg^{2+}, Na^+, K^+, and HCO_3^- are controlled by the solubility, component ratio, and behavior characteristics of the aquifer-constituting minerals. The dissolution characteristics are mainly determined by the solubility differences of calcite, plagioclase, K-feldspar, silver hornblende, and biotite [16]. According to the project of "IAEA Interlaboratory Exercise for Water Chemistry" conducted by the Korea Atomic Energy

Research Institute, the items for analyzing groundwater components include pH, conductivity, HCO_3, SO_4, Cl, F, B, NH3, Na, K, Ca, Mg, and Li [17].

In addition, according to the research results of groundwater circulation in the Yangsan and Gampo fault zone formed in the southeast of the Korean peninsula, the analysis results of the major components of groundwater in the measurement area are presented in Table 12. The order of the amount of cation content is Ca> Na> Mg> K and that of the anion content is HCO_3> SO_4> Cl> NO_3. The origin of ionic components in groundwater can be divided into natural supply by the water–rock reaction and supply of pollutants related to human activities. In the absence of specific pollutants, such as organic matter, HCO_3^- is a component that is supplied to groundwater by natural reactions. The F component in the granite groundwater can be classified as a representative component in which the small amount of F− represents the water–rock reaction as the major source of elution by substituting (OH^-) of mica. On the other hand, NO_3 components are classified as representative components of environmental pollutants. As such, various ions are found to be present in the groundwater due to geological effects [18].

Table 12 Groundwater components by geological structure

Rock type	pH	ORP (mV)	EC (μS/cm)	DO (mg/L)	Ca^{2+}	Mg^{2+}	Na^+	K^+	Sr^{2+}	Fe	Si	HCO_3^-	SO_4^{2-}	Cl^-	NO_3^-	F^-
Andesite/Biotite granite	6.30	8.90	207	1.79	23.0	3.60	15.9	2.36	0.14	N.D	7.25	59.0	20.0	19.6	3.70	N.D
Andesite/Biotite granite	6.59	90.2	363	2.91	42.8	3.12	43.8	1.53	0.40	N.D	7.70	154	35.0	16.1	1.20	1.05
Andensite/Granite	5.65	133	194	5.59	19.7	4.40	17.7	0.99	0.15	N.D	12.8	67.0	15.0	15.3	6.50	N.D
Andesite/Biotite granite	5.88	117	216	5.84	17.1	6.33	17.4	1.01	0.14	N.D	21.0	99.2	9.00	16.8	2.10	N.D
Andesite/Biotite granite	8.16	-9.30	252	1.74	18.7	0.94	28.6	0.28	1.08	0.27	6.12	70.2	47.9	12.6	N.D	0.89
Eonyang granite/ Deagu formation/ Andensite	7.34	-24.5	253	0.95	22.2	8.62	31.6	0.35	0.32	N.D	18.8	140	19.0	11.0	N.D	1.25
Eonyang granite/ Deagu formation	6.80	-28.0	582	3.16	58.4	15.2	41.1	23.3	1.41	N.D	7.56	296	24.0	37.3	N.D	0.21
Tertiary diorite/ Granite	6.08	21.2	703	1.71	66.6	23.2	28.4	4.84	0.35	2.42	14.3	41.2	163	67.6	N.D	0.01
Tertiary diorite/ Granite	7.14	-24.6	268	6.06	16.6	4.29	21.8	3.44	0.08	1.98	8.49	76.3	38.3	18.6	N.D	0.08
Deagu formation/ hornfels	6.15	66.5	135	2.30	11.6	3.00	6.65	1.15	0.08	0.01	4.10	33.7	13.3	9.20	7.12	0.04

3.2.2 Target components in seawater

To operate a nuclear power plant, considerable cooling water is inevitably required. The used cooling water is inevitably discharged to the surrounding waters as a product of the power plant operation. In general, the increase in temperature in the surrounding waters due to the operation of the power plant cooler in the temperate seas is reported to be 8–12, which directly or indirectly affects the marine environment in the surrounding waters. The number of species of zooplankton and phytoplankton in the waters around the nuclear power plant site varies depending on the season. Following are the main components of seawater:

- Seaweeds: large seaweeds (red algae, green algae, brown algae), salt plants, marine flowering plants

- Marine plankton: Phytoplankton, zooplankton, protozoa, microalgae

- Marine microorganisms: soothing bacteria, archaea, fungi

- Suspended matter: a solid substance that exists in the form of fine particles in water. In natural water, it is a small particle with a diameter of 2 mm or less, which is mainly formed by clay minerals.

- Salinity: Na^+, Mg^{2+}, Ca^{2+}, K^+, SO_4^{2-}, Br^-

Table 13 shows the types of zooplankton that emerge from the sea near the Wolseong nuclear power plant. A total of 63 species of zooplankton emerge from the surveyed area, including 32 species that can be identified to the species level [19].

Table 13 List of zooplankton occurred in the study area

Noctiluca scintillans	Corycaeus longistylis
	Corycaeus spp.
Ctenophora	Oithona spp.
Siphonophora	Oncaea spp.
Hydromedusa	Euterpina acutifrons
	Clytemnestra scutellata
Evadne nordmanni	
Evadne tergestina	Hyperiidea
Penilia avirostris	Gammaridea
Podon spp.	
	Euphausiacea egg
Ostracoda	
	Mysidacea
Acartia omorii	
Acartia negligens	Sagitta enflata
Acartia pacifica	Sagitta spp.
Acartia erythrea	
Acrocalanus gibber	Oikopleura spp.
Candacia longimana	Doliolidae spp.
Canthocalanus pauper	Salpidae spp.
Calanus sinicus	
Centropages furcatus	Fish egg
Centropages tenuiremis	
Clausocalanus sp.	Polychaeta larvae
Ctenocalanus vanus	Polychaeta trochophores
Eucalanus crassus	Bivalvia larvae
Eucalanus subcrassus	Gastropoda larvae
Eucalanus subtenuis	
Labidocera rotunda	Cirriped nauplii and cypris
Paraeuchaeta plana	
Paraeuchaeta aculeatus	Anomura larvae
Paraeuchaeta sp.	Brachyura larvae
Pseudodiaptomus marinus	Macrura larvae
Undinula vulgaris	Euphausiacea larvae
Temora discaudata	
Hemicyclops japonicus	Echinodermata larvae
Microsetella norvegica	
Mecynocera clausi	Tadpole larvae
Corycaeus affinis	Fish larvae

A total of 54 species of algae (7 species of blue-green algae, 12 species of green algae, 9 species of brown algae, and 26 species of red algae) are observed in the Kori Nuclear Power Plant Drainage, of which red algae account for 48%. Among the algae, the green algae (Ulvaceae) and red algae (Corallinaceae) are the most diverse, comprising seven species. The red algae of Halimeniaceae comprises six species and the blue-green algae of Oscillatoriaceae comprises five species [20] (Table 14).

Table 14 Marine algal species found at the discharge canal of Gori NPP

(W: Winter, Sp: Spring, Su: Summer. A: Autumn)

Species	2003				2004				2005				2006			
	W	Sp	Su	A	W	Sp	Su	A	W	Sp	Su	A	W	Sp	Su	A
Cyanophyta																
Lyngbya confervoides	+				+		+		+		+		+	+	+	
L. lutea		+		+		+				+						
Microcoleus chthonoplastes							+				+				+	
Oscillatoria brevis	+	+	+	+	+	+		+	+	+		+	+	+		+
O. nigro-viridis																
Calothrix confervicola									+							
Brachytrichia quoyi												+				
Chlorophyta																
Ulothrix flacca												+				
Enteromorpha clathrata					+				+	+				+		
E. compressa	+	+		+	+	+	+	+	+	+	+	+	+	+	+	+
E. intestinalis	+	+	+	+	+	+	+	+	+	+	+	+	+	+	+	+
E. linza	+								+	+	+		+	+		+
E. prolifera	+		+	+	+	+	+	+	+	+	+	+	+	+	+	+
Ulva conglobata																
U. pertusa	+	+	+		+	+	+		+		+	+	+	+		
Urospora penicilliformis																
Cladophora opaca																
C. pusilla																+

45

C. sericea				+			+	+	+						+	
Phaeophyta																
Ectocarpus arctus																
Colpomenia sinuosa	+				+	+								+		
Sphacelaria rigidula	+										+			+		+
Dictyota dichotoma					+											
Pachydictyon coriaceum																
Padina arborescens	+	+	+		+	+	+		+	+	+		+	+	+	
Sargassum fulvellum	+		+													
S. horneri	+	+	+				+				+			+	+	
S. patens		+					+									
Rhodophyta																
Porphyra tenera																
Gelidium amansii	+	+	+		+	+	+	+	+	+	+				+	
G. divaricatum																
Pterocladiella capillacea													+			
Amphiroa beauvoisii	+	+	+	+	+	+	+	+	+	+	+				+	
A. ephedraea																
Corallina pilulifera		+	+			+	+	+	+		+	+		+	+	+
Lithophyllum okamurae																
Lithothamnion cystocarpioideum																
Pneophyllum zostericolum		+														
Titanoderma tumidulum									+							
Grateloupia acuminata																
G. divaricata																
G. livida			+													
G. lanceolata																

G. ramosissima	+	+			+	+	+	+	+	+	+					
Prionitis cornea					+											
Caulacanthus ustulatus	+	+	+	+	+	+	+	+	+	+	+	+	+	+	+	+
Chondrus ocellatus	+															
Hypnea charoides																
H. saidana																
Ahnfeltiopsis flabelliformis	+	+	+				+	+	+	+	+					
Lomentaria catenata							+									
Ceramium paniculatum																
C. tenerrimum																
Symphyocladia latiuscula																

3.2.3 Filtration for pretreatment

A pretreatment system is constructed to remove various ions, organics, and microorganisms contained in seawater and groundwater and to produce pure water that satisfies the standard specification for reagent water [21]. Based on the membrane filter, a seawater desalination process and a system for removing various particles and ions are designed.

Reverse osmosis (RO) is the process of producing pure water by applying high pressure to the RO membrane (Toray Chemical, RE4040-SHN, 40 "). The RO process is equipped with a booster pump (SPECK, D-91154 Roth) to apply high pressure to the RO membrane. In seawater RO (SWRO), fouling occurs due to the floating matter, colloid, organic/inorganic compounds, and biological growth. Therefore, a micro filtration (MF) filter (Hanyeon Industry, BDS Cartridge filter, 20 ", 1 μm) and an activated carbon (AC) filter (Hanyeon Industry, BDC Cartridge filter 20") are used as pretreatment to prevent the degradation of the RO membrane. The MF filter removes most suspended particles such as silica, clay, yeast, and bacteria having a size of 0.05 to 0.1 μm to 1 μm [22-24].

AC filters are used to remove the dissolved organics and particulate matter. The filters are also used as a pretreatment for the RO membrane, as well as for ion-exchange resins to remove residual chlorine and organics that have a significant effect on the performance of ion-exchange resins.

As RO membranes pass water but rarely pass ions or molecules dissolved in the water, this process removes most of the sea's ions (Cl^-, Na^+, SO_4^{2-}, Mg^{2+}, Ca^{2+}, and K^+). In addition, as non-ion materials are removed when passing through the RO membrane, the performance of the facility is determined by the condition of the RO membrane.

The ultrapure mixed-phase ion-exchange resin (THERMAX, TULSION MB-115, 25L) is a treatment method for removing residual ions in water and obtaining high-purity pure water with a low amount of salinity. The water passed through the ion-exchange resin is finally passed through a 0.2 μm final filter (Hanyeon Industrial Co., Ltd., MP Cartridge filter, 10") to remove microorganisms and particles. The conductivity can be determined using the conductivity meter installed in the pretreatment system. The solenoid valve prevents the injection of water when the equipment is switched off [25].

Based on the considerations, the pure water manufacturing equipment is designed; the overall flowchart is shown in Figure 30 and the constructed system is shown in Figure 31.
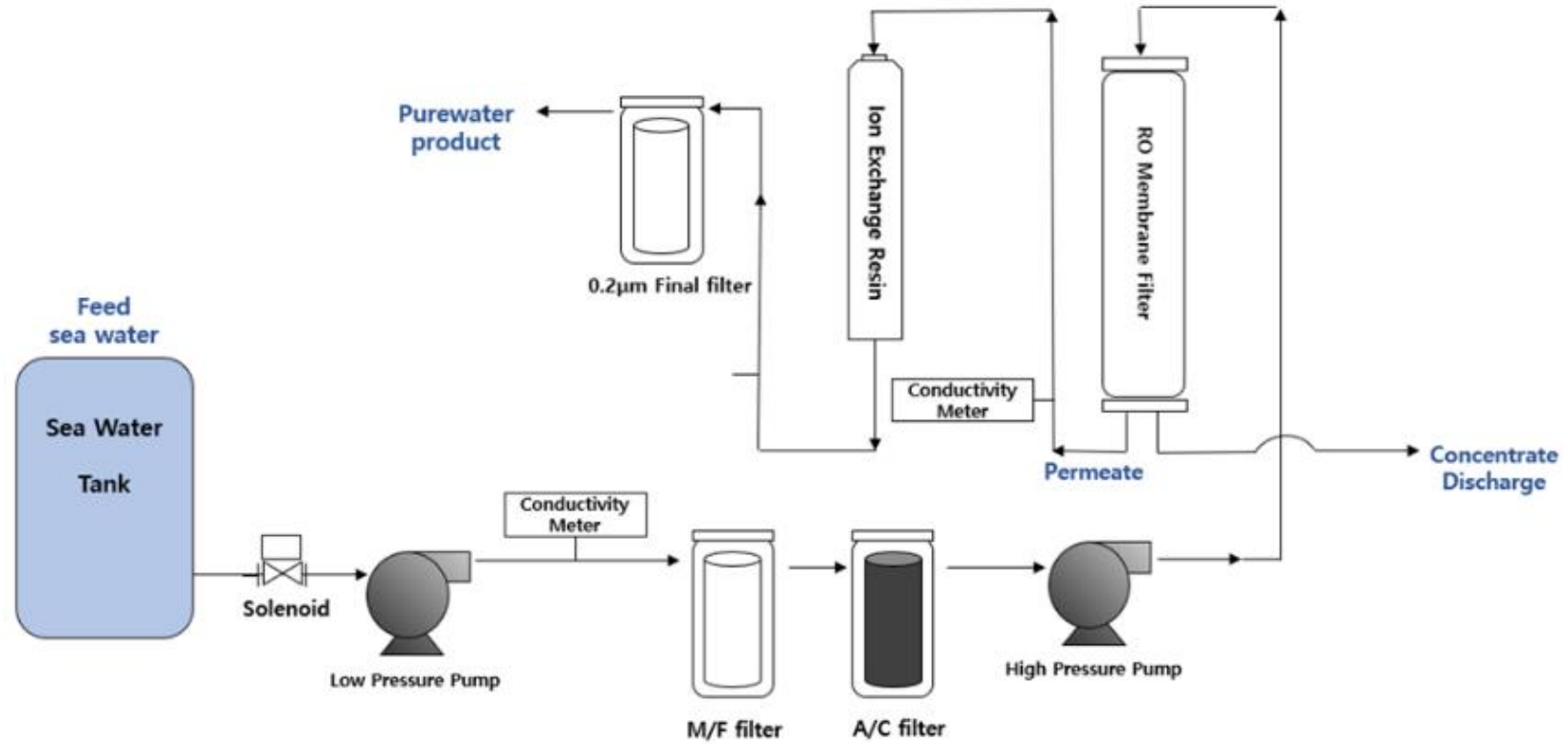
Figure 30 The overall flow chart for pure water manufacturing equipment

R/O Filter

M/F Filter

A/C Filter

Final Filter

Ion Exchange Filter
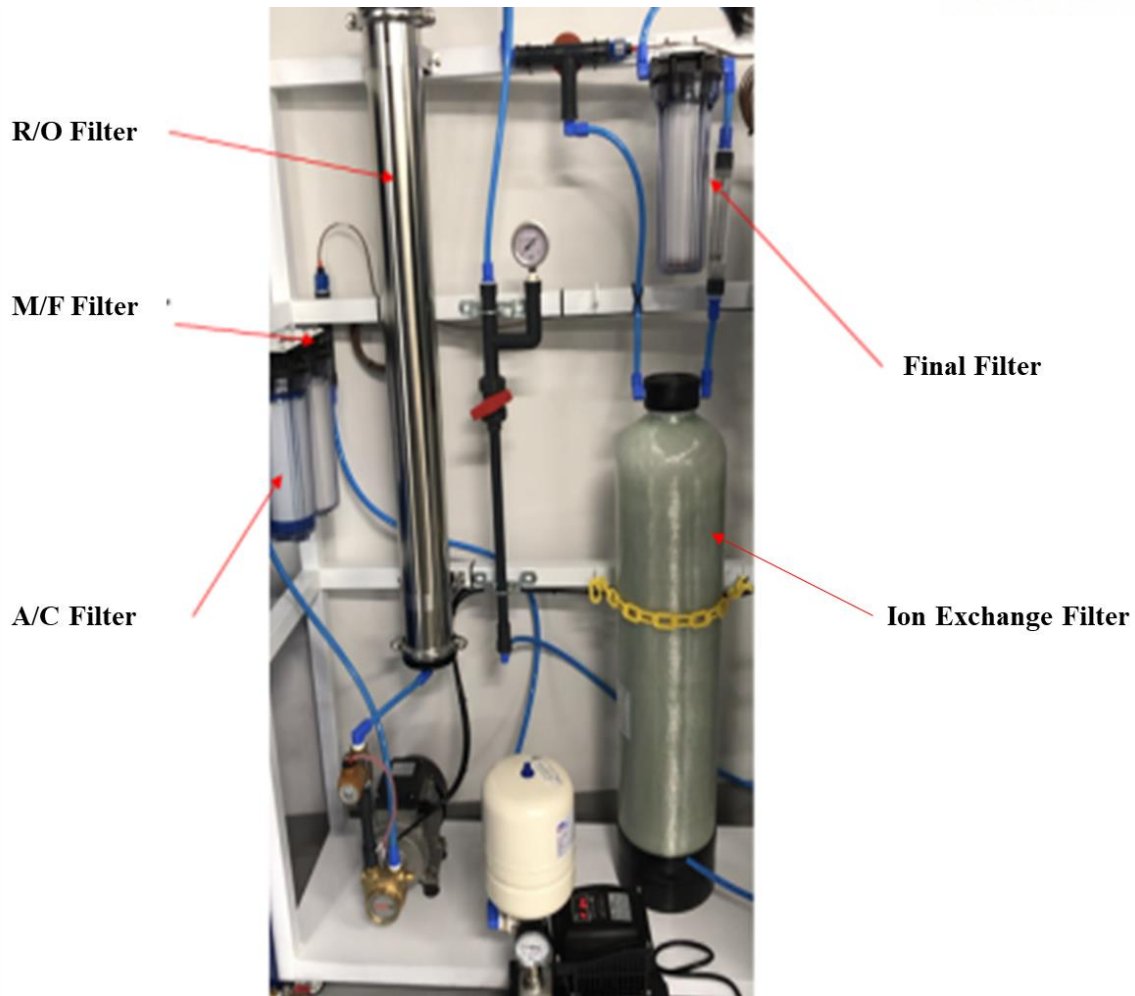
Figure 31 Constructed pretreatment system for pure water manufacturing equipment

3.3 Coincidence circuit

3.3.1 Basic algorithm for coincidence circuit

The coincidence circuit aims to check the time coincidence between pulses in two or more systems. There is a circuit that generates a logic pulse of constant width, and a signal from the outside is used as it is as a logic pulse. A simultaneous counting circuit is expected to produce output only when two pulses coincide in time, but in reality, even if there is a little time lag to applying a finite-width pulse to the ADN circuit, the output will appear. Thus, the time resolution is determined by the sum of the pulse widths applied to each input.

The coincidence circuit system uses a "simultaneous counting technique" to improve efficiency and eliminate background. The coincidence circuit indicates that only pulses that enter two input terminals within a certain period are recognized as the count values. This method sets the range of pulse magnitudes to screen out the beta ray of a particular nuclide and excludes anything else by the recoupling counting technique, and then obtains the final count.

Two PMTs are used to construct the coincidence counting technique. First, two PMTs are placed on both sides of the chamber. When radiation reacts with scintillation and emits light in multiple directions, it is simultaneously detected by both PMTs. Each output of the PMTs enters the preamplifier input, while the output goes to the main amplifier of ORTEC 855 DUAL SPEC. The output of the main amplifier must be connected to the UNI terminal to obtain a single pulse. This output is connected to the input of the ORTEC 551 TIMING single channel analyzer (SCA). After setting the upper and lower limits in the timing SCA, the delay time is set. The output must be connected to the NEG OUT terminal, which has a pointed pulse, and not to the POS OUT terminal, which has a gentle pulse, because the time information is important.

The output from the timing SCA is connected to the start and stop terminals of the time-to-amplitude converter (TAC)/SCA. At this time, the timing SCA output with a lower delay time should be connected to the start terminal, while that with a larger delay time should be connected to the stop terminal. The output of TAC is connected to the input of the multi-channel analyzer (MCA), whose output is connected to the multichannel analyzer emulation software (MAESTRO).

If the coarse gain related to amplification is changed to 10, 20, or 40 in the 855 Dual Amplifier, the higher the amplification, the more noise generated from the PMT is affected by the amount of light. Therefore, it is an effective way to reduce the background count rate by removing as much of the noise signal generated from PMT as possible, through the coincidence circuit. Figure 32 shows the configuration of the detection signal processing electronics flow diagram and the actual experimental settings of the coincidence circuit-based NIM module. Table 15 presents information regarding the model and specification of each component of the coincidence circuit. Figure 33 shows the constructed coincidence system.
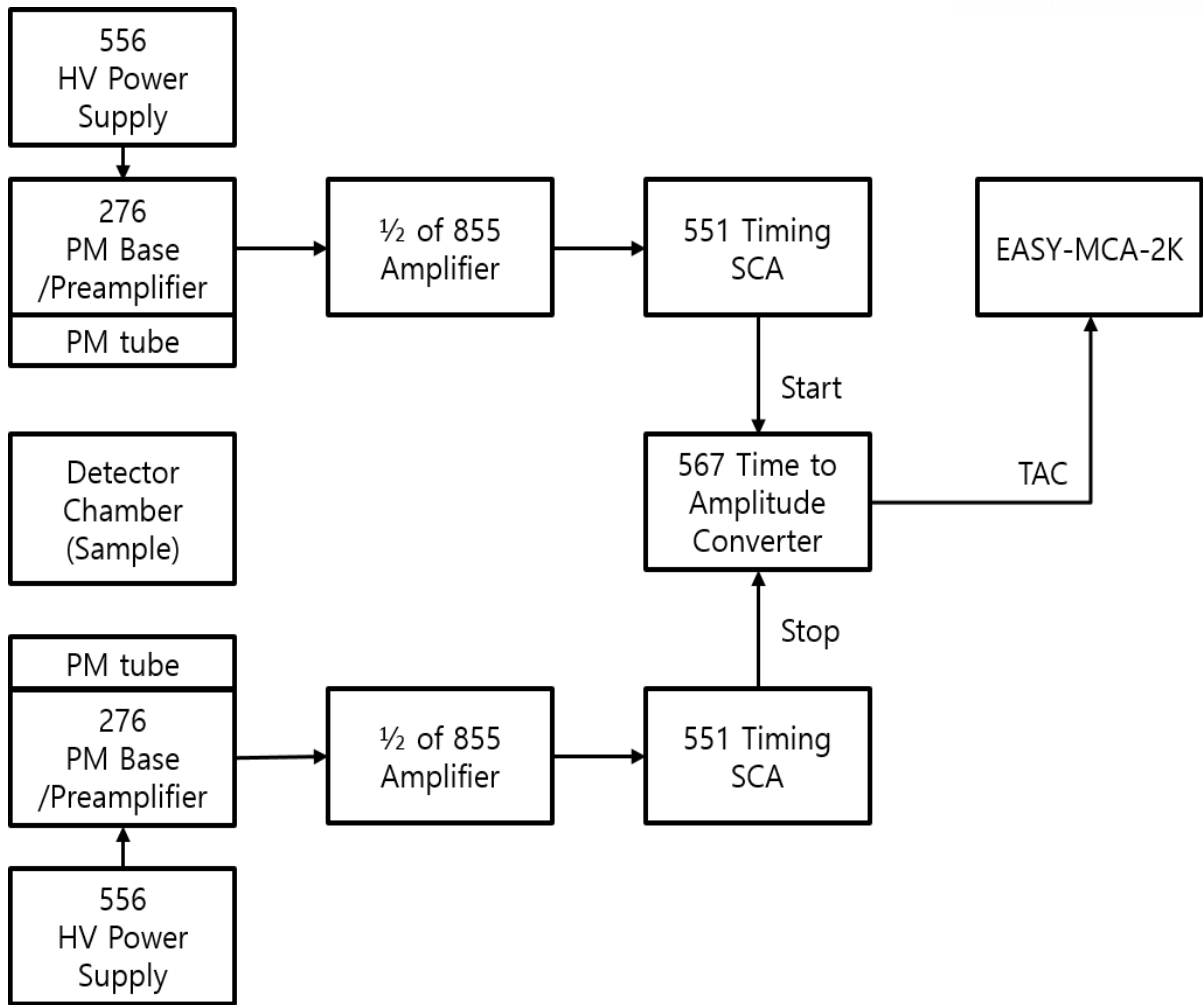
Figure 32 The configuration of the detection signal processing electronics flow diagram

Table 15 Information of model and specification of each component of coincidence circuit

Component	Manufacturer	Model name	Specification
H.V supply	ORTEC	556 HIGH VOLTAGE POWER SUPPLY	· Suitable for operating with PMT · 0 to ±3 kV · 0 to 10 mA · Lower noise · Stable supplying high voltage
PMT	HAMAMATSU	R877, R878	· High energy resolution and stability · Stable gain · 8 dynode stages · Anode to Cathode Voltage: 1500 V
Preamplifier	ORTEC	276 Photomultiplier Base with Preamplifier	· For use with 10-stage PMTs that fit standard 14-pin sockets · Built-in low-noise preamplifier · Both preamplifier output and anode output
Amplifier	ORTEC	855 DUAL SPEC AMP	· For scintillation detectors · Low-input noise
Timing SCA	ORTEC	551 Timing Single Channel Analyzer	· Single-channel analyzer and timing signal derivation · Trailing-edge constant-fraction timing provides walk <±3 ns for 100:1 dynamic range
TAC	ORTEC	567 TAC	· Start to stop conversion time is less than 5 ns · Multiplying factor: 1, 10, 100, 1K, 100K
MCA	ORTEC	EASY-MCA	· 2k or 8k resolution · Easy to connect with MAESTRO
Software	ORTEC	MAESTRO	· Spectroscopy system · Enhanced peak fitting calculation

Figure 33 The actual experimental settings of the coincidence circuit based NIM module

Figure 34 shows a schematic of the coincidence circuit. The 556 High-Voltage Power Supply can vary from 0 to 3 kV in kV units and from 0 to 10 mA in mA units. Appropriate power corresponding to the preamplifier and PMT should be supplied. This experiment is performed by setting a power of 1.25 kV because this is a suitable value for the used PMTs [26].

In the case of the 855 Dual Amplifier, the amplification is determined through the coarse and fine gains. The experiment is conducted by changing the coarse gain to 10, 20, 40, and 100. In the case of the 551 Timing SCA, the delay time, which plays the most important role in the simultaneous summation circuit, is input. The total area of the TAC spectrum is 500 ns, and the delay time between two PMT signals is set to 250 ns, so that the signals are collected near 512 channels corresponding to 250 ns for the simultaneous incoming signal. Finally, the spectrum is identified and analyzed through EASY-MCA 2K [27].
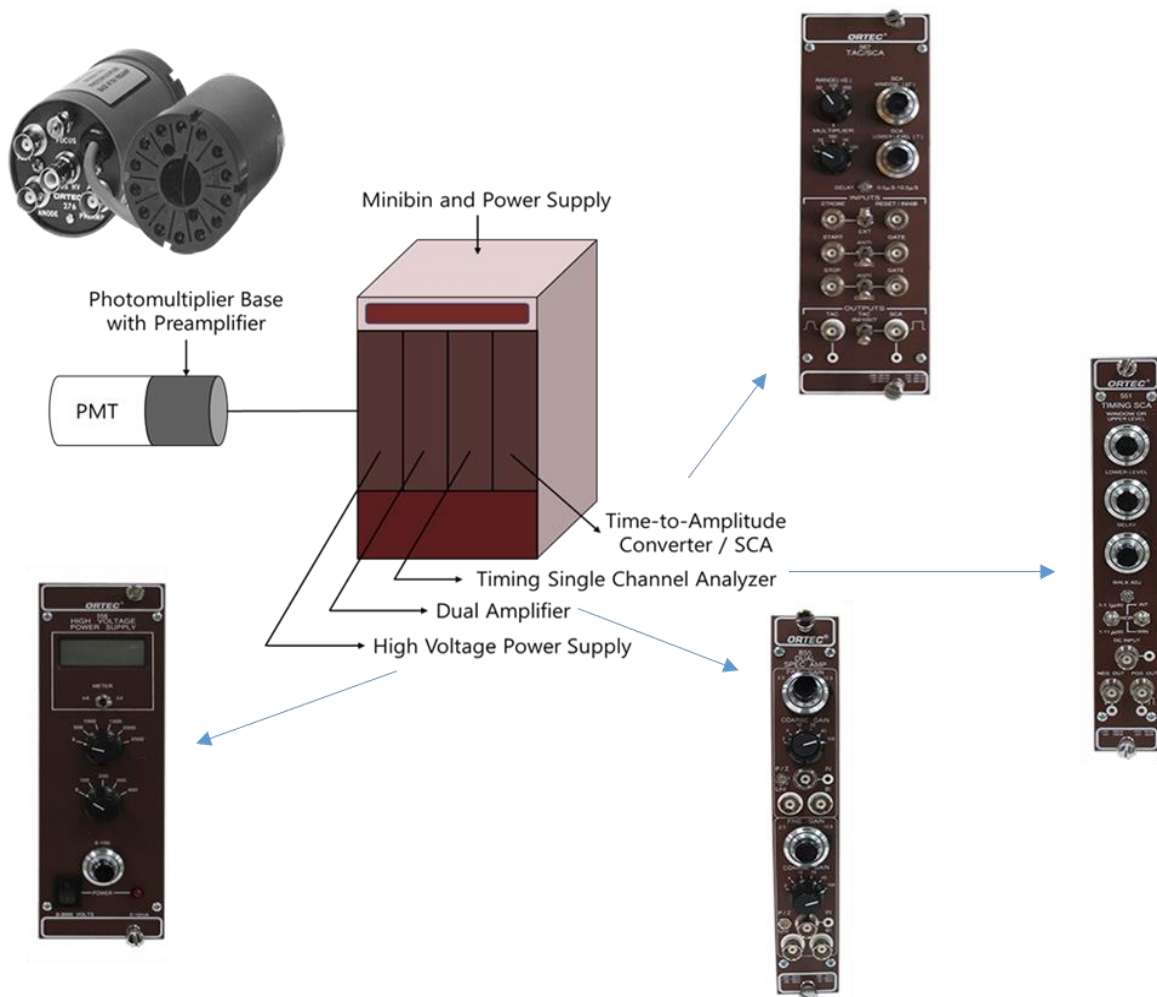
Figure 34 Schematic of the electronics setting for coincidence circuit

3.4 Background suppression

Even if there is no radionuclide, background radioactivity exists. Background radioactivity is a measure of the amount of ionizing radiation present in an environment at a particular point that is not emitted from the radioactive source.

Natural radiation can have various sources, including both natural and artificial. These include man-made medical X-rays, fallouts from nuclear tests and nuclear accidents, as well as cosmic radiation from naturally occurring radioactive materials (such as radon and radium) and environmental radiation.

In addition, PMT-based measurement systems can be affected by the measurement of the external light signal. To define the only measurements by radioactive sources, the elimination of background radiation and noise is very important. Therefore, the physical methods and software used for reducing such background radiation and noise are described here.

3.4.1 Physical methods for eliminating background

3.4.1.1 Dark box for external light

It is important to eliminate as much of the noise signal from PMT as possible, through the coincidence circuit. In addition, it is very important to minimize the effect of the amount of light during the actual experiment. For this purpose, an $800 \times 500 \times 250$ mm^3 dark box with two PMTs is used, as shown in Figure 34. On one side of the dark box, only the signal and power ports connected to the PMT are cut out, as shown in Figure 35 and Figure 36, to completely block the external light [28]. Two inflow paths (φ12 mm) are provided at the front and back to allow liquids containing sources to flow to the front and rear sides. On each side, two RS-232 adapters (DSUB 9 standard), two SHV adapters (φ 13 mm), and two BNC adapters (φ 12.7 mm) are mounted. RS-232 is the preamp's power supply cable connection, SHV is the HV cable connection, and BNC is the adapter for the voltage pulse signal cable connection [35-37]. Figure 37 shows the external view for the data connection cable with dark box.
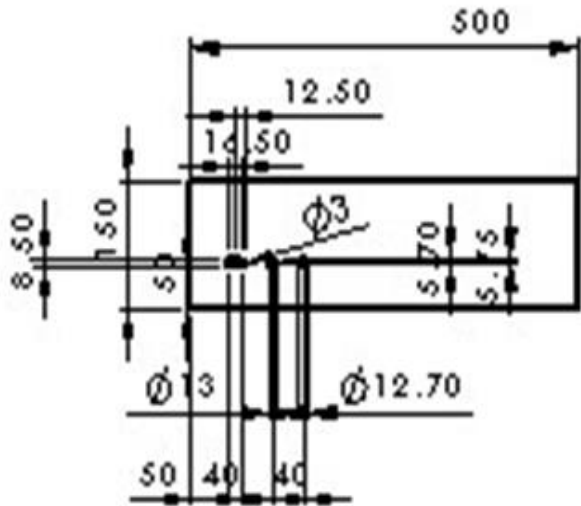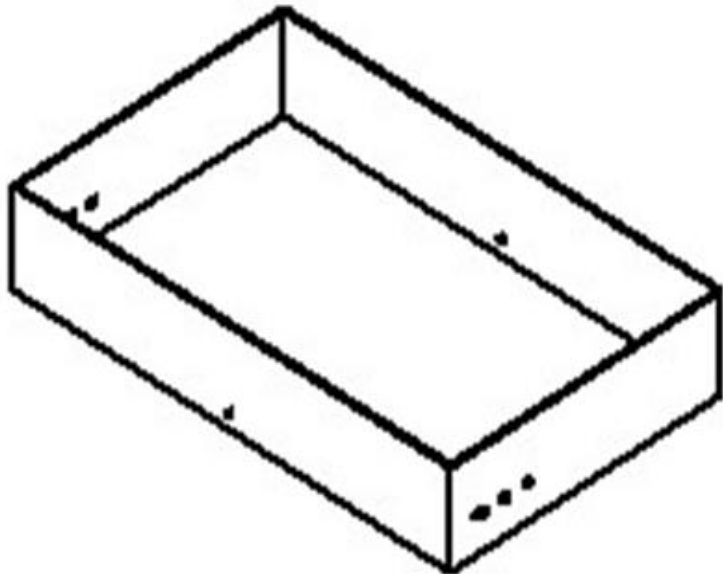
Figure 35 3D view(upper) and x-axis view(bottom) of dark box
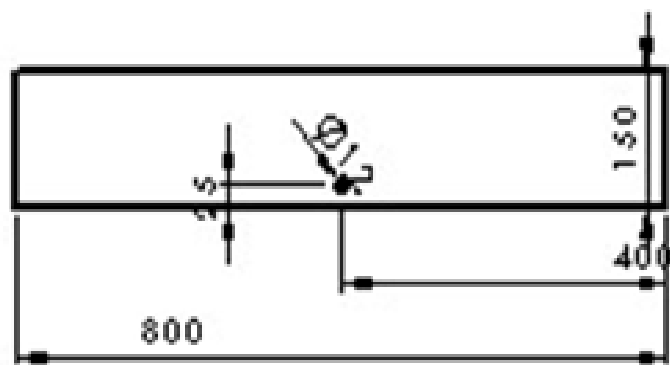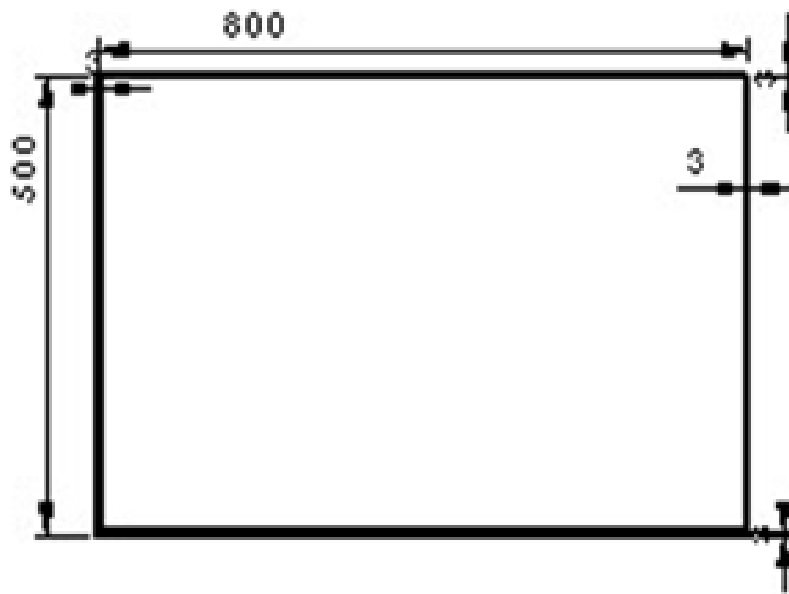
Figure 36 z-axis view(upper) and y-axis view(bottom) of dark box

Figure 37 External view and connection cable at side part of dark box

A blackout cloth is put on the detection unit and the dark box is closed, and then, the blackout cloth is put on the dark box again to minimize the influence of external light. The flow path, scintillator, and acrylic support structure are fixed through an acrylic bonding material. The experiment is conducted using a liquid containing a source after confirming that the water does not leak.

3.4.1.2 Lead box for shielding background radiation

A lead box for shielding is applied to minimize the effects of background and external radiation. Detailed drawings of the shield box are shown in Figure 38 and Figure 39, respectively. The dimensions shown in the figure are the outermost dimensions, including the thickness; the hinge is located at two points and one door lock exists. There is no internal partition, and the material is made of steel (2.0t) and lead (5.0t). The actual shielded box is shown in Figure 40.
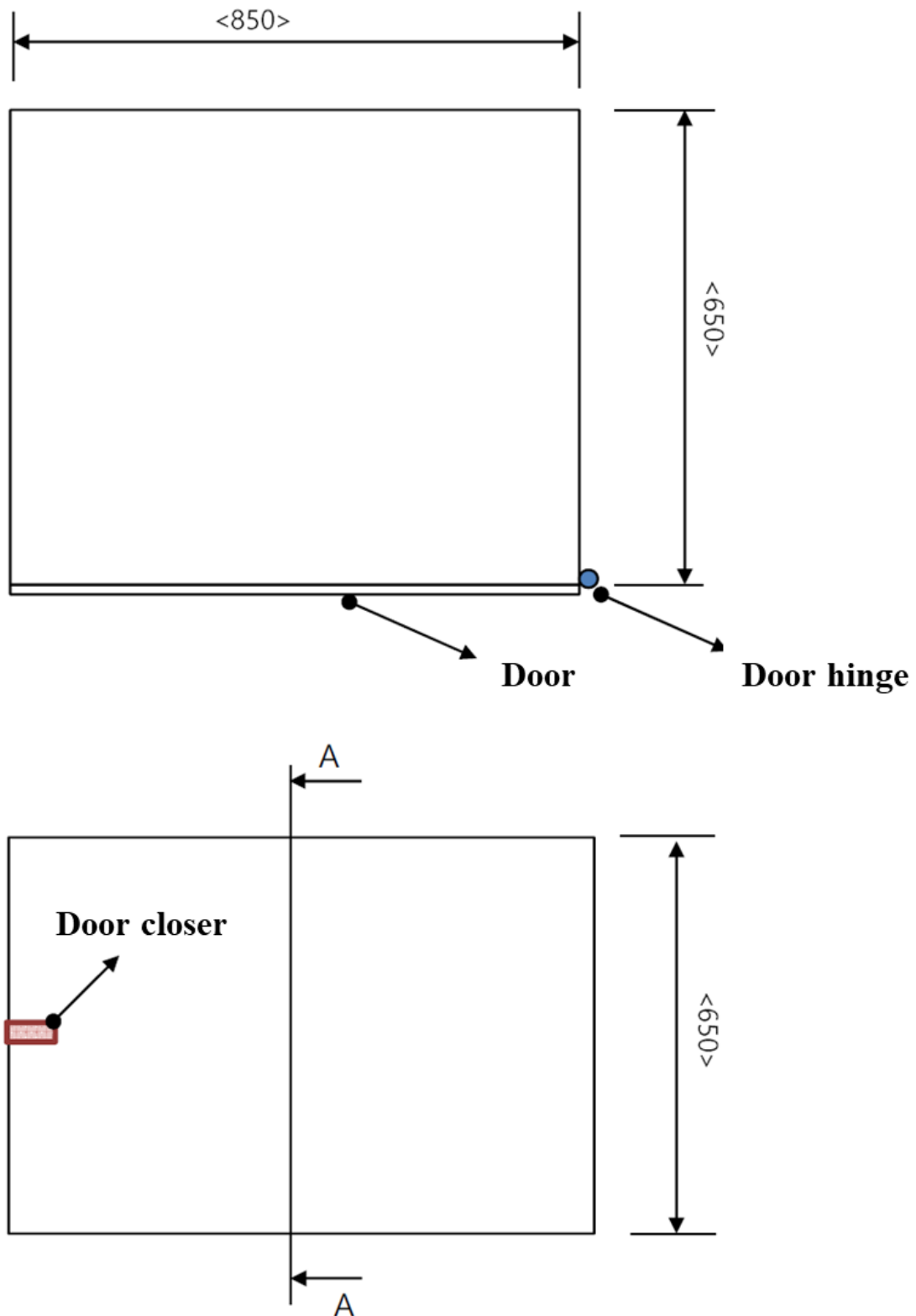
Figure 38 Front and top side of blueprint for lead shielding box
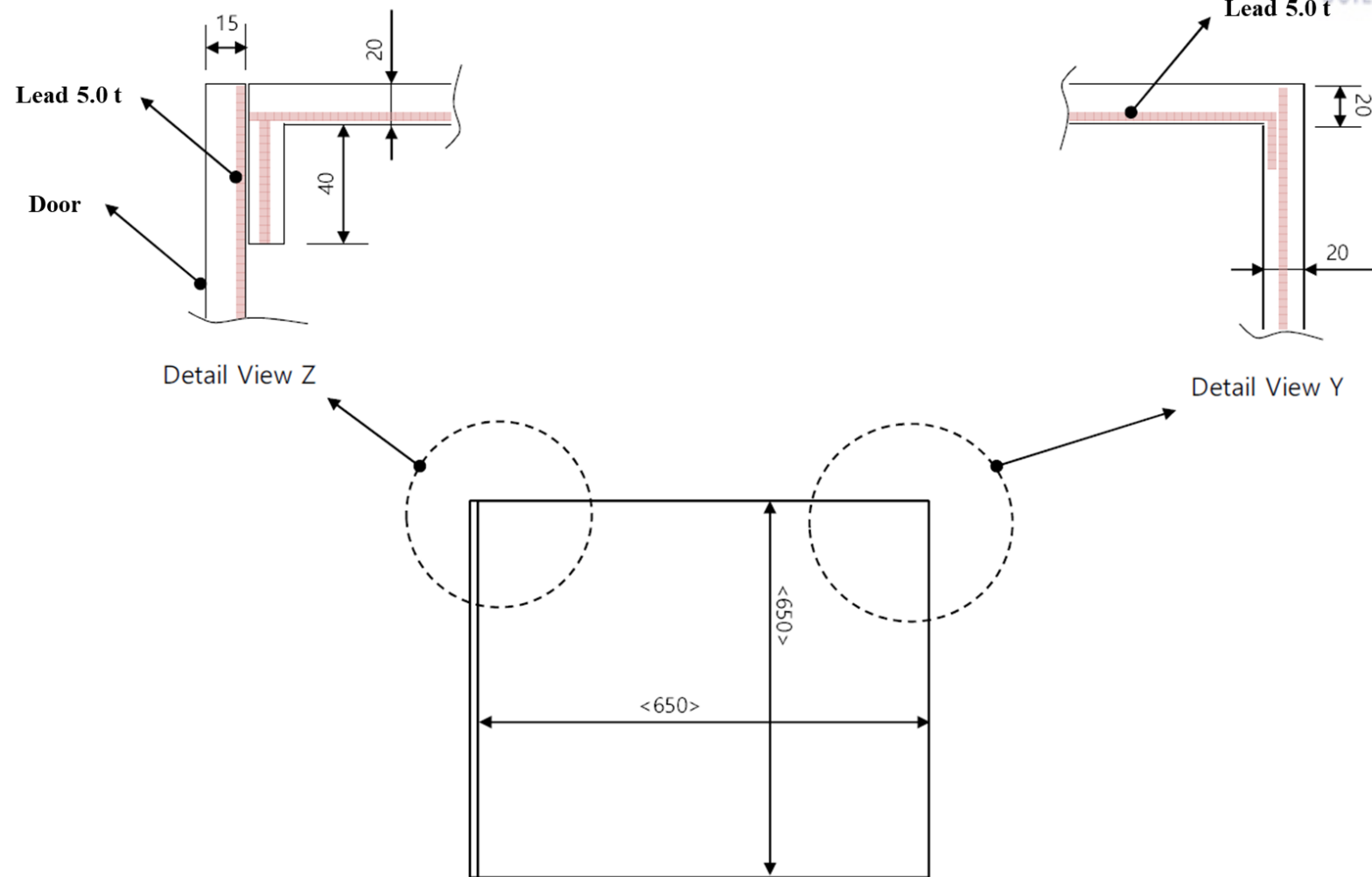
Figure 39 Side view of detail blueprint for lead shielding box

Figure 40 External view of lead box for shielding background radiation

3.4.2 Software for eliminating background

The measured data using the radiation detector may include not only radiation values (meaningful data) by the radiation source but also unnecessary signals (meaningless data) generated by electrical noise or statistical fluctuation. Unnecessary data distort the actual radiation monitoring, so their removal is essential. If one or two data values are suddenly relatively large without continuity, they might not be generated by the radiation source. However, data generated by the radiation source may have a continuity with the adjacent value. Therefore, it is important to distinguish between the value obtained from noise or fluctuation and that obtained from the radiation source.
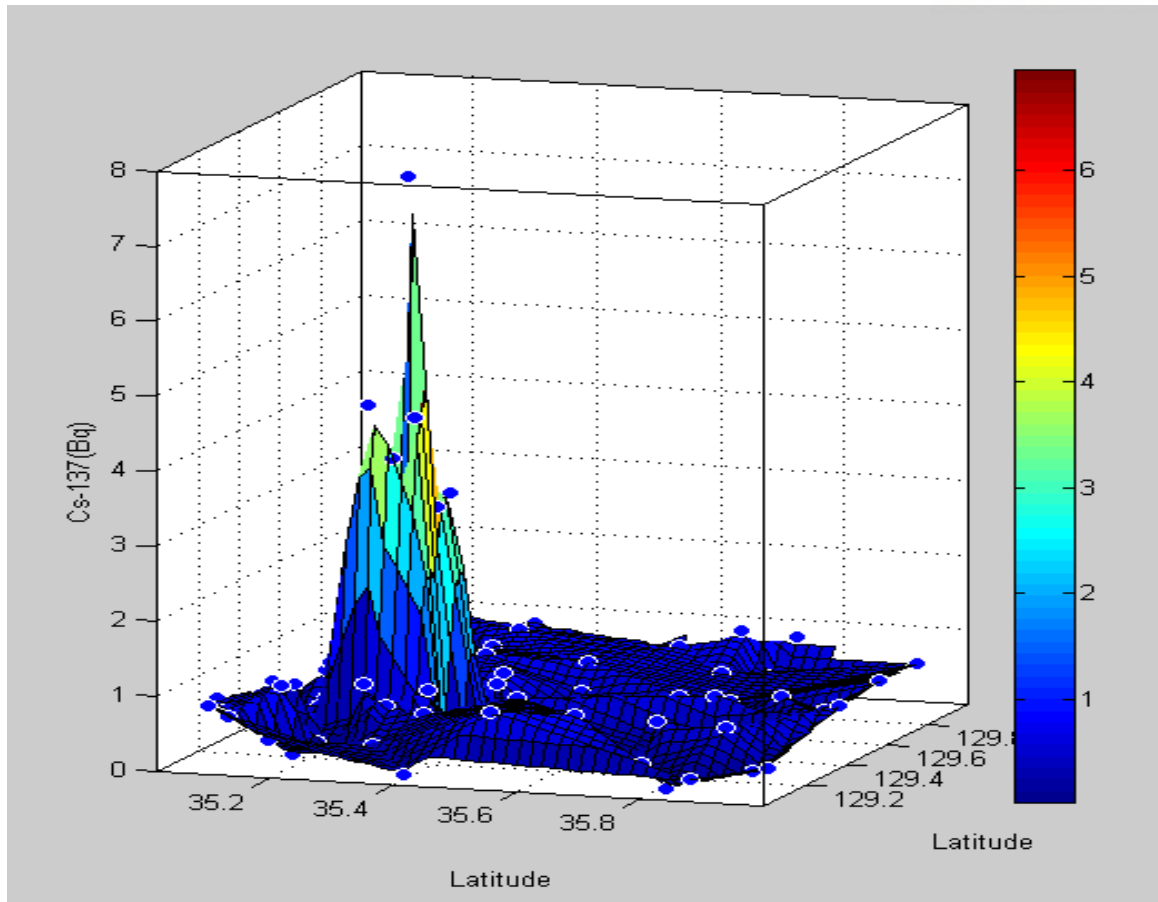
Figure 41 Example for detected data due to radiation source

Figure 41 shows an example of data from the radiation source. There are several points or areas where data values are relatively high. In this case, one or two pieces of data do not appear to be insignificantly large and tend to increase or decrease around the specific data values.
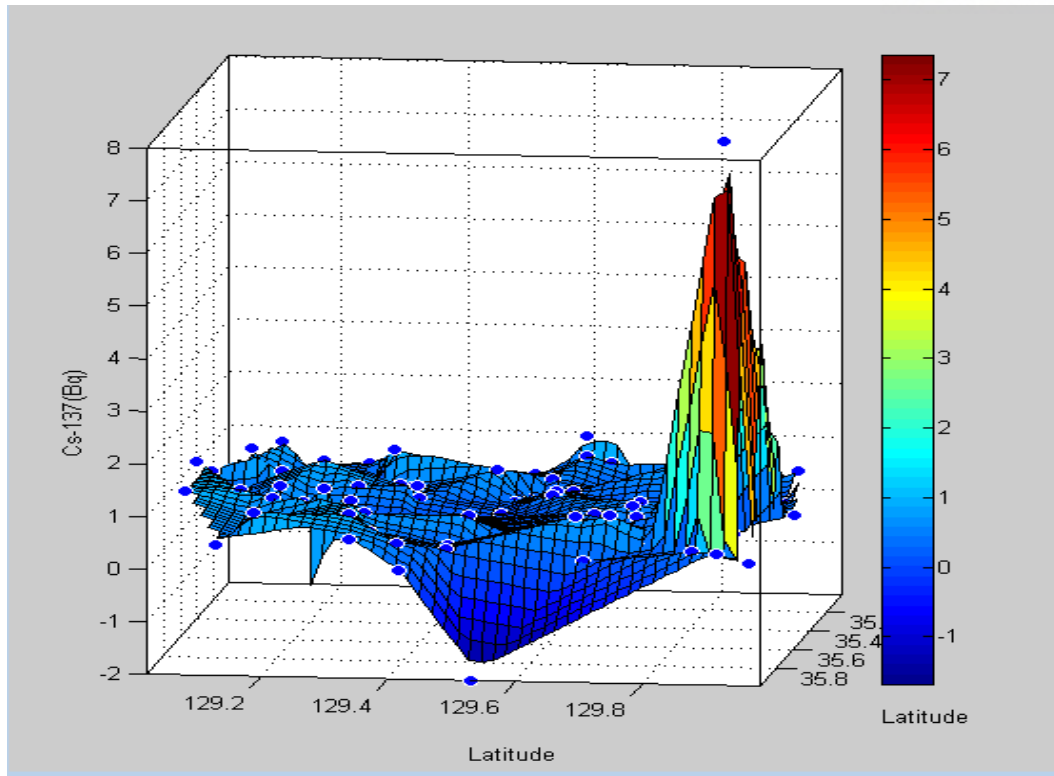
Figure 42 Example for meaningless data due to noise or statistical fluctuation

Figure 42 shows that the value at one point is extremely high without continuity compared to those at the surrounding points. There are also negative data that cannot be taken as radiation values, which can be judged as noise or fluctuations in the instrument rather than the actual detected data values. Therefore, there is a need for an algorithm that extracts only meaningful data values by considering two cases: data that are not related to other data and negative value data. Negative values can be easily removed using conditional statements in the program. On the other hand, the distinction between the case of meaningless data, such as suddenly high values due to noise, and meaningful data due to the presence of a radiation source is defined in consideration of continuity with its before and after data. The method of comparing the data just before and after the specific value is defined as the "3-point comparison method," and is described as follows:

- Calculate the average value, including the value at a specific point and just before and after that value
- If the value at a specific point falls within the range of mean $\pm 1.96 \times$ standard deviation (), it is regarded as having continuity and specific data are considered as the radiation value. (A value of 1.96 is used because the radiation detection statistically follows the Poisson distribution, and if the

number of samples is 30 or more, the normal distribution can be applied, which corresponds to the
95% confidence interval accepted by social myths.)

-Otherwise, it is judged to be meaningless by noise or statistical fluctuation

3.5 Experimental characteristics of beta nuclide in water

3.5.1 Experiment for interaction between beta ray and scintillator

Basic experiments were performed to characterize the reaction of beta nuclides and plastic scintillators,
using ^{3}H, ^{14}C, ^{32}P, and ^{90}Sr radionuclides. The maximum energy of the beta nuclide is listed in Table 16.
To ensure the ease of use of the open source during the experiment, the radioactive source is carried in
a vial. The mass of the radioactive material is confirmed for management. For the experiment, a specific
amount of the source is diluted with distilled water to prepare a sample, and the measurement of a single
nuclide and a sample mixed with two radionuclides is performed.

Table 16 Maximum energy of used radionuclide

Radioactive nuclide	Maximum energy
^{3}H	18.6 keV
^{14}C	156.5 keV
^{32}P	1710 keV
^{90}Sr	546.2 keV

The procedure for manufacturing the beta radionuclide source is as follows.

1. Extract 500 μl of the source
2. Check the mass of the extracted source
3. Mix the source (500 μl) and distilled water (5,500 μl)
4. Check the mass of the mixture
5. Encapsulate the sample case with wrapping
6. Calculate the specific activity

Table 17 lists the information on the prepared single beta nuclide sample, including information regarding initial radioactivity, mass, and date of manufacture for ^{3}H, ^{14}C, ^{32}P, and ^{90}Sr. Table 18 lists information about the mixed beta nuclide source produced. Information including initial radioactivity, mass, and date of manufacture for mixed beta-nuclide sources of ^{90}Sr+^{32}P, ^{90}Sr+^{14}C, ^{90}Sr+^{3}H, ^{3}H+^{32}P, ^{3}H+^{14}C, and ^{14}C+^{32}P is also shown.

Table 17 Information of beta ray emitting nuclide source

	^{3}H	^{14}C	^{32}P	^{90}Sr
Initial radioactivity (Bq)	3.52E+08	3.90E+03	3.89E+03	3.90E+03
Mass of total source(g)	4.97E+00	5.01E+00	5.00E+00	5.00E+00
Date of production	170701	170701	170701	170701
Radioactivity concentration (Bq/g)	**7.08E+07**	**7.79E+02**	**7.77E+02**	**7.81E+02**
Mass of source case before sampling (g)	3.39E+01	9.44E+00	8.68E+00	7.38E+00
Mass of source case after sampling (g)	3.34E+01	8.92E+00	8.18E+00	6.88E+00
Extracted sample mass (g)	4.92E-01	5.17E-01	5.01E-01	5.01E-01
Radioactivity extraction (Bq)	**3.48E+07**	**4.03E+02**	**3.89E+02**	**3.91E+02**
Sample case mass (g)	4.94E+00	4.94E+00	4.91E+00	4.94E+00
Sample case+Water+Sample mass(g)	1.08E+01	1.10E+01	1.11E+01	1.09E+01
Water+Sample mass (g)	5.85E+00	6.03E+00	6.16E+00	5.99E+00
Radioactivity concentration (Bq/g)	**5.95E+06**	**6.69E+01**	**6.32E+01**	**6.53E+01**

Table 18 Information of mixed beta ray emitting nuclide source

	^{90}Sr+^{32}P		^{90}Sr +^{14}C		^{90}Sr +^{3}H		^{3}H +^{32}P		^{3}H+^{14}C		^{14}C +^{32}P	
	^{90}Sr	^{32}P	^{90}Sr	C^{14}C	^{90}Sr	^{3}H	^{3}H	^{32}P	^{3}H	^{14}C	^{14}C	^{32}P
	3.90E+03	3.89E+03	3.90E+03	3.90E+03	3.90E+03	3.52E+08	3.52E+08	3.89E+03	3.52E+08	3.90E+03	3.90E+03	3.89E+03
	5.00E+00	5.00E+00	5.00E+00	5.01E+00	5.00E+00	4.97E+00	4.97E+00	5.00E+00	4.97E+00	5.01E+00	5.01E+00	5.00E+00
Date of production	170701	170701	170701	170701	170701	170701	170701	170701	170701	170701	170701	170701
Radioactivity concentration (Bq/g)	**7.81E+02**	**7.77E+02**	**7.81E+02**	**7.79E+02**	**7.81E+02**	**7.08E+07**	**7.08E+07**	**7.77E+02**	**7.08E+07**	**7.79E+02**	**7.79E+02**	**7.77E+02**
Mass of source case before sampling (g)	6.88E+00	8.18E+00	9.13E+00	8.91E+00	8.63E+00	3.34E+01	3.29E+01	7.89E+00	3.24E+01	8.41E+00	7.90E+00	7.67E+00
Mass of source case after sampling (g)	6.38E+00	7.67E+00	8.63E+00	8.41E+00	8.13E+00	3.29E+01	3.24E+01	7.39E+00	3.19E+01	7.90E+00	7.40E+00	7.17E+00
Extracted sample mass (g)	5.04E-01	5.02E-01	5.01E-01	5.02E-01	5.01E-01	5.01E-01	5.06E-01	5.04E-01	5.00E-01	5.09E-01	5.02E-01	5.01E-01
Radioactivity extraction (Bq)	**3.93E+02**	**3.90E+02**	**3.91E+02**	**3.91E+02**	**3.91E+02**	**3.55E+07**	**3.58E+07**	**3.92E+02**	**3.54E+07**	**3.97E+02**	**3.91E+02**	**3.89E+02**
Total radioactivity (Bq)	**7.84E+02**		**7.82E+02**		**3.55E+07**		**3.58E+07**		**3.54E+07**		**7.80E+02**	
Sample case mass (g)	4.91E+00		4.93E+00		4.89E+00		4.85E+00		4.89E+00		4.92E+00	
Sample case+Water+Sample mass(g)	1.09E+01		1.09E+01		1.09E+01		1.09E+01		1.09E+01		1.09E+01	
Water+Sample mass (g)	6.00E+00		5.99E+00		6.00E+00		6.00E+00		6.00E+00		5.99E+00	
Radioactivity concentration (Bq/g)	**1.31E+02**		**1.31E+02**		**5.91E+06**		**5.98E+06**		**5.90E+06**		**1.30E+02**	

3.5.2 Experiments with flow rate change

  Table shows the source information used in the experiment. The date of manufacture for all sources is March 15, 2018, and the initial radioactivity is 3,863 Bq for ^{90}Sr, 3,907 Bq for ^{14}C, and 393,700,000 Bq for ^{3}H. The total mass of water and the source in a beaker is measured by an electronic balance. The mass of each sample is 76.50 g for ^{90}Sr, 71.00 g for ^{14}C, and 76.50 g for ^{3}H. The radioactivity concentration of the sample is confirmed by injecting 0.25 g, 0.50 g, 0.75 g, and 1.00 g of the radioactive source. The radioactivity concentrations ^{90}Sr are 2.51 Bq/g, 5.02 Bq/g, 7.53 Bq/g, and 10.04 Bq/g; those of ^{14}C are 2.75 Bq/g, 5.51 Bq/g, 8.26 Bq/g, and 11.01 Bq/g; and those of ^{3}H are 253,206.78 Bq/g, 506,413.56 Bq/g, 759,620.35 Bq/g, and 1,012,827.13 Bq/g. The radioactivity concentration of each sample is derived considering the corresponding half-life [32]. The details regarding the used sources are described in Table 19–21.

Table 19 Source information of ^{3}H for flow rate experiment

	^{3}H			
Initial radioactivity (Bq)	393,700,000			
Mass (g)	5.00			
Date of production	2018.03.15			
Radioactivity concentration (Bq/g)	387,319,597.11			
Extracted sample mass (g)	0.25	0.50	0.75	1.00
Radioactivity extraction (Bq)	**19,370,318.81**	**38,740,637.61**	**58,110,956.42**	**77,481,275.23**
Water + sample mass (g)	76.50	76.50	76.50	76.50
Radioactivity concentration (Bq/g)	**253,206.78**	**506,413.56**	**759,620.35**	**1,012,827.13**

Table 20 Source information of ^{14}C for flow rate experiment

	^{14}C			
Initial radioactivity (Bq)	3,907			
Mass (g)	5.00			
Date of production	2018.03.15			
Radioactivity concentration (Bq/g)	**3,906.86**			
Extracted sample mass (g)	0.25	0.50	0.75	1.00
Radioactivity extraction (Bq)	**195.51**	**391.02**	**586.53**	**782.03**
Water + sample mass (g)	71.00	71.00	71.00	71.00
Radioactivity concentration (Bq/g)	**2.75**	**5.51**	**8.26**	**11.01**

Table 21 Source information of ^{90}Sr for flow rate experiment

	^{90}Sr			
Initial radioactivity (Bq)	3,863			
Mass (g)	5.00			
Date of production	2018.03.15			
Radioactivity concentration (Bq/g)	**3,835.95**			
Extracted sample mass (g)	0.25	0.50	0.75	1.00
Radioactivity extraction (Bq)	**191.95**	**383.91**	**575.86**	**767.81**
Water + sample mass (g)	76.50	76.50	76.50	76.50
Radioactivity concentration (Bq/g)	**2.51**	**5.02**	**7.53**	**10.04**

The procedure for manufacturing the beta nuclide source is as follows.

① Extract 0.25 g, 0.50 g, 0.75 g, and 1.00 g of each radioactive material through precision balance.

② Check the mass of the extracted radioactive source, the initial mass of the sample case, and the mass after sampling.

③ Fill the sample case with radioactive source (0.25 g, 0.50 g, 0.75 g, and 1.00 g) and water (76.25 g, 76.00 g, 75.75 g, 75.50 g for ^{90}Sr and 3H, 70.75 g, 70.50 g, 70.25 g, 70.00 g for ^{14}C) by using a micropipette.

④ Measure the mass of the sample case containing distilled water and the source.

⑤ Calculate the radioactivity concentration of the produced sample.

⑥ Inject distilled water containing the radioactive source into the acrylic support structure using a micropipette.

When the flow rate experiment is performed, the flow rate is changed by the peristaltic pump with the silicone tubes from the front and rear of the dark box. The used peristaltic pump is shown in Figure 43. In the case of the peristaltic pump, it is set to measure the correct flow rate through calibration, and the flow rate is set to 600 mL/min, 800 mL/min, and 1,000 mL/min. The pump is operated to check the value that can flow without retaining liquid in the flow path and scintillator acrylic support structure, as shown in Figure 44. For flow rates of less than 600 m/min, the water sample cannot pass through the flow path and scintillator acrylic support structure. Therefore, the experiments are conducted with varying flow rates of 600 mL/min, 800 mL/min, and 1,000 mL/min.

OmniSpense ELITE®

Figure 43 Peristaltic pump for experiments with flow rate change

Figure 44 Experimental setting for flow rate determination

The experiment is performed by deriving the minimum detectable activity (MDA) value according to the flow rate change, source concentration changes, and coarse gain change of the 855 Dual Amplifier. MDA is calculated at 95% confidence interval through Equation (2), and the MDA is confirmed by inputting the background count and detection efficiency obtained through the experiment [33].

$$\frac{2.71 + 4.65 \times \sqrt{N_b}}{T \times \frac{\varepsilon}{100} \times V_c}$$

Equation 3. Equation for minimum detectable activity

MDA: Minimum detectable activity (Bq/g)

N_b: Background count

T: Measurement time

ε: Detection efficiency

V_c: Volume of sample

Detection efficiency is defined as

$$\varepsilon = \frac{C_g - N_b}{A} \times 100\%$$

Equation 4. Equation for calculating detection efficiency

ε: Detection efficiency (%)

C_g: Total count rate (cps)

N_b: background count rate (cps)

A: Activity (Bq)

The flow rates are varied to 0 mL/min, 600 mL/min, 800 mL/min, and 1,000 mL/min. The radioactivity concentrations are changed by injecting 0.25 g, 0.50 g, 0.75 g, and 1.00 g for each source. The coarse gain of the 855 Dual Amplifier is changed to 10, 20, and 40, and the MDA values are derived by performing experiments on 48 cases.

3.5.3 Detection characteristics according to amplification change

In plastic scintillators and PMT-based measurement systems, the main amplifier has a significant effect on the measurement results. As the main amplifier amplifies the signal generated from the PMT, it is very important to determine the count rate in a measurement system that judges the data of a signal of a certain size as significant data. Increasing the amplification degree increases the output value, and

a small amplification degree directly affects the measurement efficiency because the output value is small.

Figure 45 shows the measured spectrum with varying degrees of amplification using ^{90}Sr. The peak region in the middle of the spectrum is the result of the scintillator and the other values are due to the background.
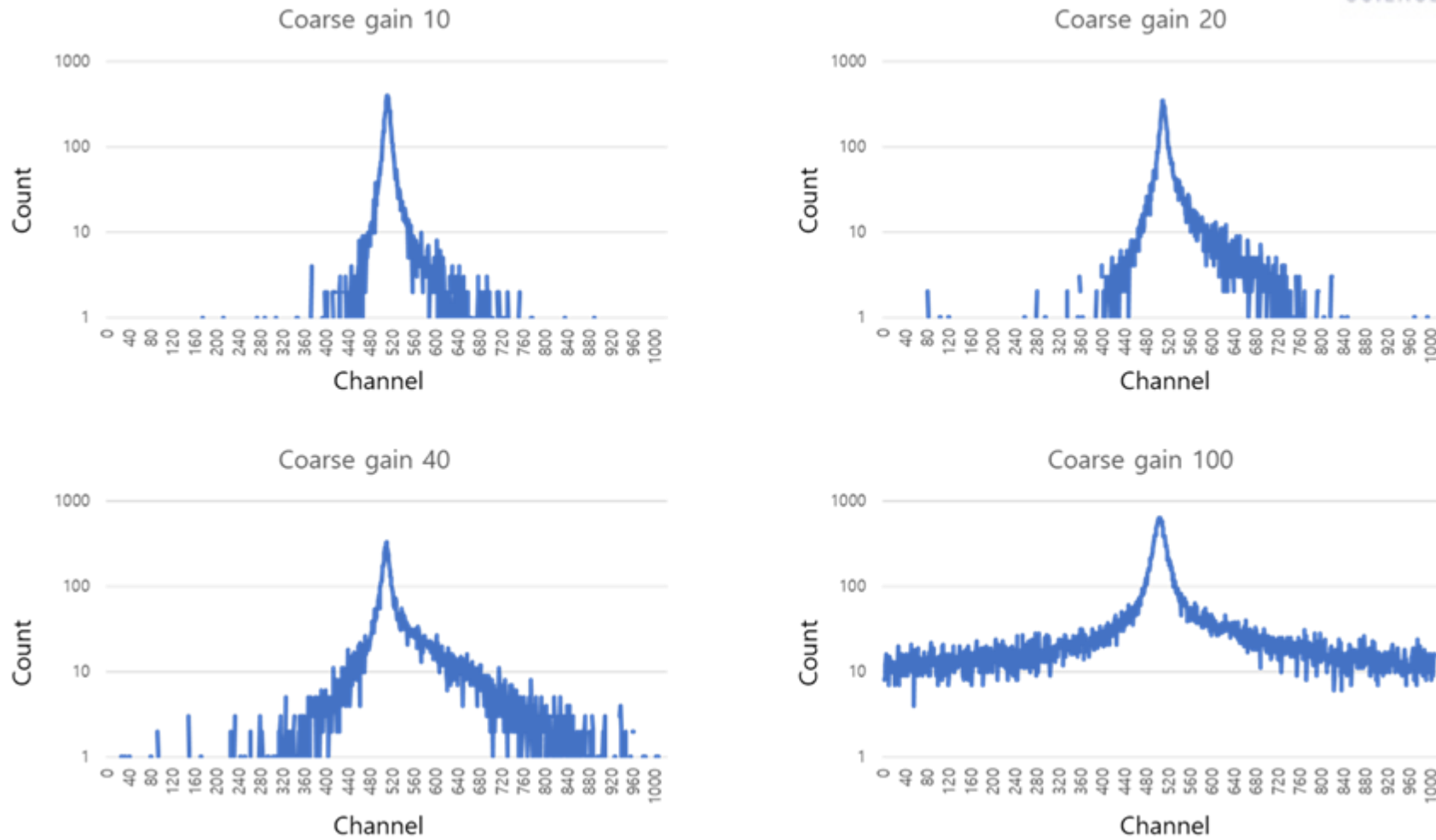
Figure 45 Measured spectrum by amplification changes with coarse gain 10, 20 40 and 100

As the amplification degree increases, the background value and the value measured by the source tend to increase together. It is expected that the optimization of the detection system is necessary to reflect these characteristics.

3.6 Separation detection method for beta nuclides

To detect various beta radionuclides in water, an analytical method is proposed. A method for detecting beta nuclides with different energies depending on the energy in the medium of water is suggested.

3.6.1 Concept for beta detection with nuclide separation

The seawater and groundwater around nuclear facilities may contain various radionuclides, including tritium. Tritium is usually in the form of water, so it can easily enter the body through ingestion or inhalation. Tritium can cause serious internal exposure if it enters the body. Therefore, tritium monitoring is essential.

Beta nuclides have a spectral energy distribution based on their maximum energy. To investigate the effect of a single nuclide in this mixed beta nuclide, a method of separating tritium from the mixed source is suggested.

As tritium is contained in groundwater or seawater in the form of water, only the impact on tritium can be identified if only pure water is separated from the field samples. In addition, tritium and other beta nuclides differ in detection efficiency for plastic scintillators. Therefore, only tritium is separated from other nuclides and radioactivity is analyzed by applying appropriate measurement conditions.

The pretreatment method is applied to RO and ion-exchange resin to separate tritium by applying a high-pressure treatment system. In addition, a pretreatment system based on physical filtering with MF and AC filters for other nuclides without tritium is applied for separating the analysis method.

The detection system conditions according to the target nuclide are selected for the separated samples. When the amplification degree of the main amplifier is changed, not only the signal due to radioactivity but also the value of background radioactivity is amplified and reflected in the result. Therefore, the appropriate amplification degree for each nuclide is derived and the measurement method for each nuclide is applied.

3.6.2 Radionuclide separation analysis with amplification change

Increasing the amplification of the main amplifier amplifies the signal generated by the PMT and increases the measured signal. As tritium emits low energy, it is possible to perform stable counting by applying a high amplification degree.

Pure water can be produced through the application of a pretreatment system, so water including only tritium can be measured separately. The measurement efficiency can be increased by applying a high amplification degree to water samples containing only the separated tritium.

However, in case of relatively high-energy beta nuclides, such as strontium, high amplification amplifies and measures signals from not only radiation but also background radiation. Relatively high-energy beta nuclides can achieve sufficiently stable counts with the application of appropriate amplification degrees.

Therefore, a method of applying high amplification to water samples containing tritium only by pretreatment and applying appropriate amplification to relatively high beta nuclides is suggested.

4. Results and discussion

4.1 Results of detection efficiency simulation

4.1.1 Detection efficiency simulation of air layer

The air layer thickness is one of the experimental condition variables of the detection part design. The change in the detection efficiency according to the change in this variable is simulated using MCNP. The results of the simulations performed on ^{3}H and ^{14}C radionuclides are listed in Table 22 and Table 23, respectively. In the case of tritium, the detection efficiency decreases as the thickness of the air layer between the plastic scintillator and beta nuclide increases. In the case of ^{14}C having higher beta energy than tritium, the influence of detection efficiency by the air layer cannot be confirmed. The experiments are conducted with no air layer between the scintillator and the beta radionuclide in the detection characteristics and quantification experiments, to not affect the measurement of ultra-low energy tritium.

Table 22 Simulation results for detection efficiency change according to thickness of air layer in case of ^{3}H

Thickness of air layer (cm)	Detection efficiency (%)	Error (%)
0	0.0018	0.047
0.025	0.0016	0.062
0.05	0.0014	0.067
0.1	0.0008	0.088
0.2	0.0003	0.141

Table 23 Simulation results for detection efficiency change according to thickness of air layer in case

of ^{14}C

Thickness of air layer (cm)	Detection efficiency (%)	Error (%)
0	0.117	0.0070
0.025	0.116	0.0076
0.05	0.118	0.0075
0.1	0.116	0.0076
0.2	0.118	0.0075

4.1.2 Detection efficiency simulation of scintillator thickness

MCNP simulations are performed on plastic scintillators with thickness of 1 and 5 mm to confirm the effect of detection efficiency on the thickness of the plastic. The simulation results confirm that the efficiencies of the 1- and 5-mm plastic scintillators show the same result. The calculated results are listed in Table 24. The efficiency is not affected by the thickness of the plastic scintillator. It can be seen that the detection efficiency for ^{3}H in water is relatively low due to the short range of beta. The high efficiency of $^{90}Sr/^{90}Y$ is confirmed mainly by the high-energy beta emitted from ^{90}Y ($E_{max} = 2.23$ MeV).

Table 24 Detection efficiency simulation for plastic scintillators thickness of 1 mm and 5 mm

	Detection efficiency of 1 mm scintillator (%)	Error (%)	Detection efficiency of 5 mm scintillator (%)	Error (%)
^{3}H	0.002	0.047	0.002	0.047
^{14}C	0.107	0.007	0.107	0.007
^{32}P	5.650	0.001	5.650	0.001
$^{90}Sr/^{90}Y$	4.620	0.002	4.620	0.002

The reason for the same efficiency regardless of the thickness of the plastic scintillator can be explained by Figure 46. In both cases a) and b), the amount of energy deposited is different, but the nonzero energy deposition of beta particles in the scintillator is considered as a count in the F8 tally of MCNP6.
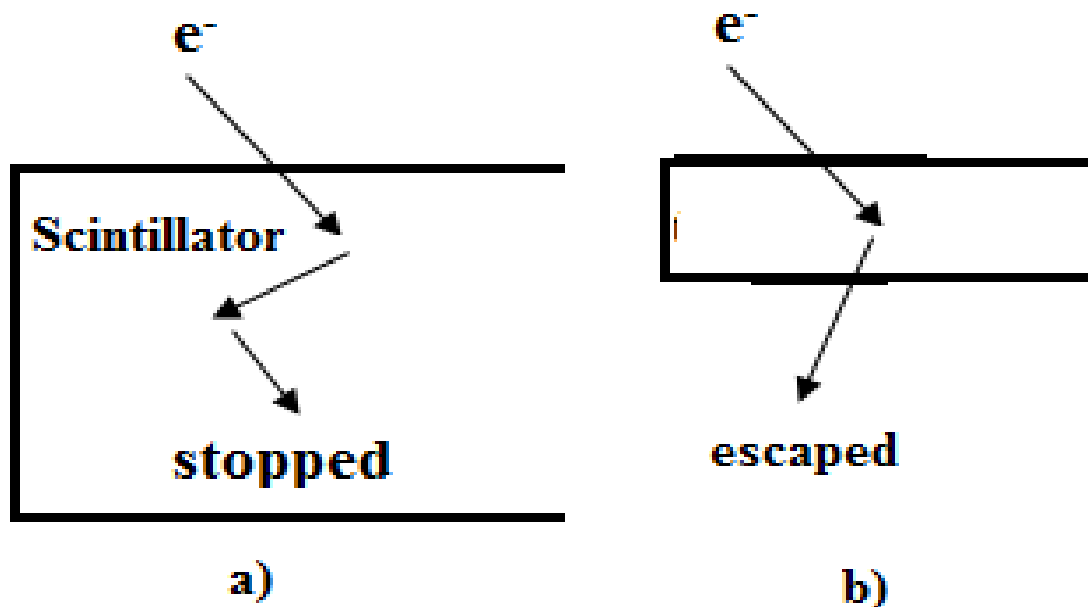
Figure 46 Energy deposition mechanism for interaction between beta particle and plastic scintillator

The energy deposition spectra of ^{3}H (Figure 47) and ^{14}C (Figure 48) are very similar regardless of the thickness of the plastic scintillator. On the other hand, in the case of ^{32}P (Figure 49) and ^{90}Sr/^{90}Y (Figure 50), the energies deposited in plastic scintillators of 1 and 5 mm thicknesses are different. Low-energy tritium and ^{14}C show the same energy deposition results regardless of the plastic scintillation thickness. That is, it is confirmed that even a 1 mm thickness of the plastic scintillator is sufficient for beta detection. However, the relatively high-energy ^{32}P and ^{90}Sr show different energy deposition trends for each thickness. As a result of defining the efficiency by the reaction using the F8 tally of MCNP6, it is confirmed that the same results are obtained for 1 and 5 mm. The same efficiency despite the different thickness is explained by the range property of beta nuclides in Figure. In both cases, the amount of deposition energy is different; however, any non-zero energy deposition of beta particles within the scintillator would be regarded as one count in F8 tally.
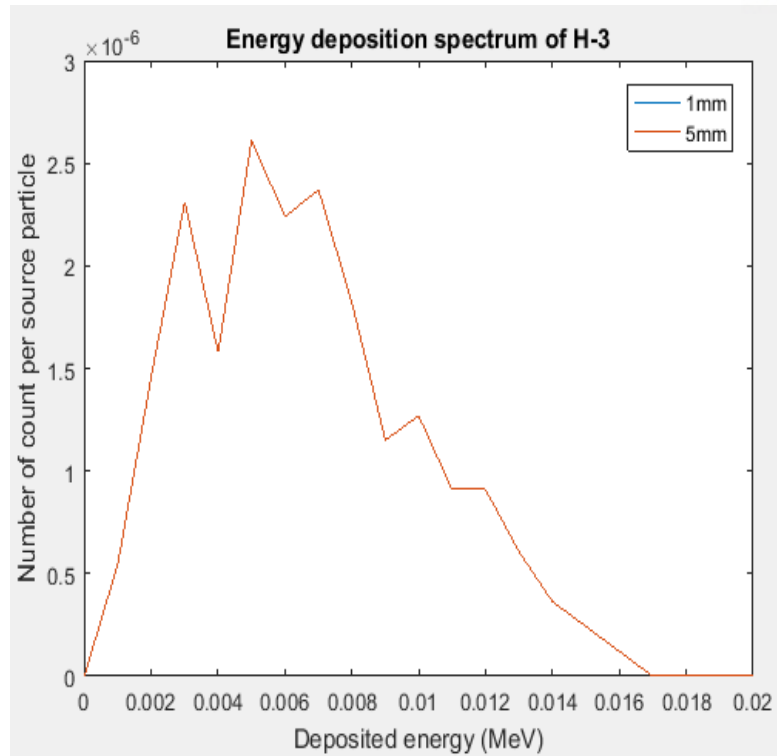
Figure 47 Energy deposition spectrum of ^{3}H
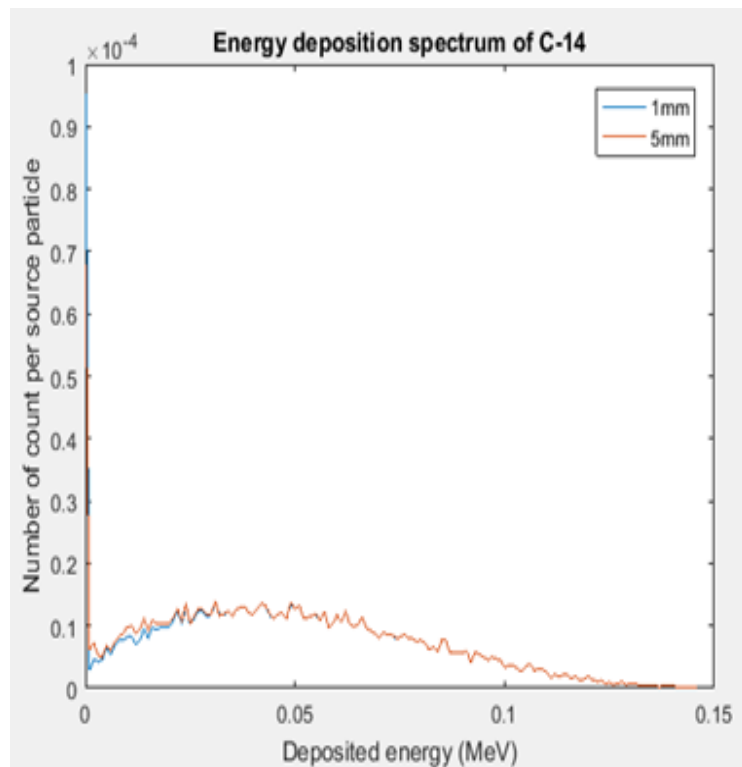
Figure 48 Energy deposition spectrum of ^{14}C
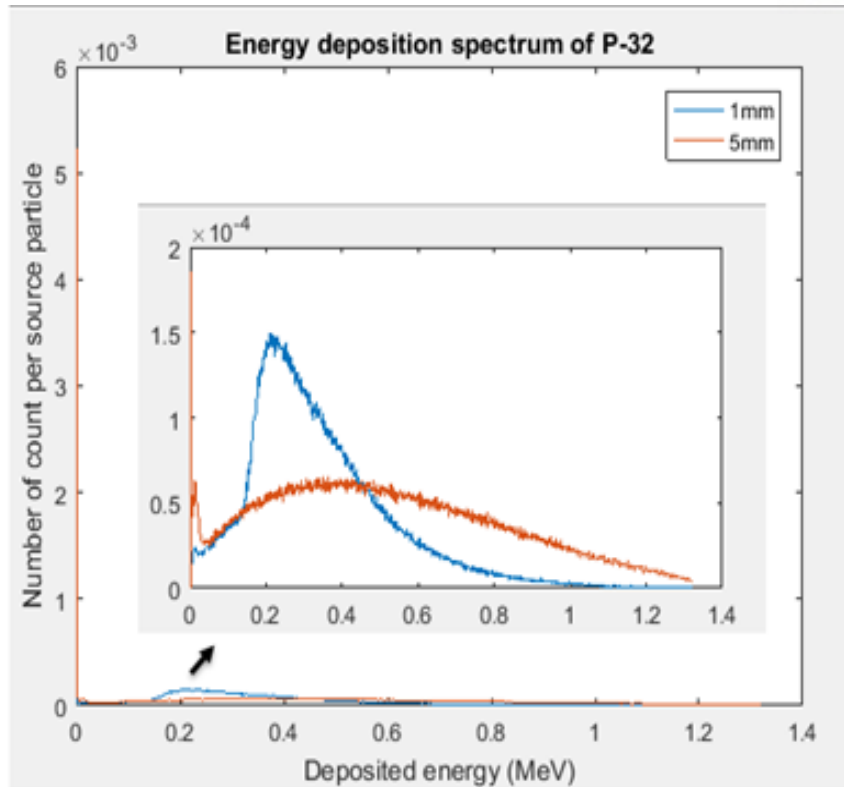
Figure 49 Energy deposition spectrum of ^{32}P
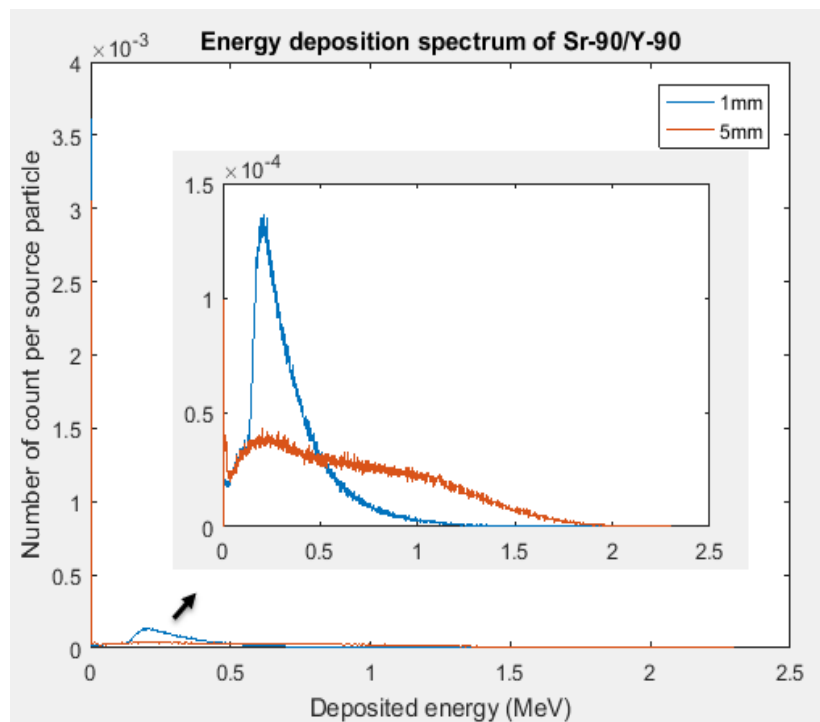
Figure 50 Energy deposition spectrum of ^{90}Sr/^{90}Y

4.1.3 Detection efficiency simulation of height of water sample and diameter of plastic scintillator

Simulations are performed on ^{3}H, ^{14}C, ^{32}P, and ^{90}Sr/^{90}Y radioactive sources. In the detection of short-range beta rays, the cross-sectional area of the reaction between the source and the scintillator is considered as the main variable in terms of the geometrical factor. Variables affecting the detection efficiency are defined by the height of the water sample and the diameter of the scintillator. The variation of the detection efficiency is simulated by MCNP. An increase in the height of the water sample indicates an increase in the sample mass, which is expected to affect the MDA. The height of the water sample is identified as the efficiency characteristic variable and the simulation using this variable. As the height of the water sample increases, the detection efficiency value tends to decrease (Figure 51). The change in the detection efficiency does not appear to be large, depending on the scintillator diameter, but it is confirmed that the detection efficiency increases with the scintillator diameter.
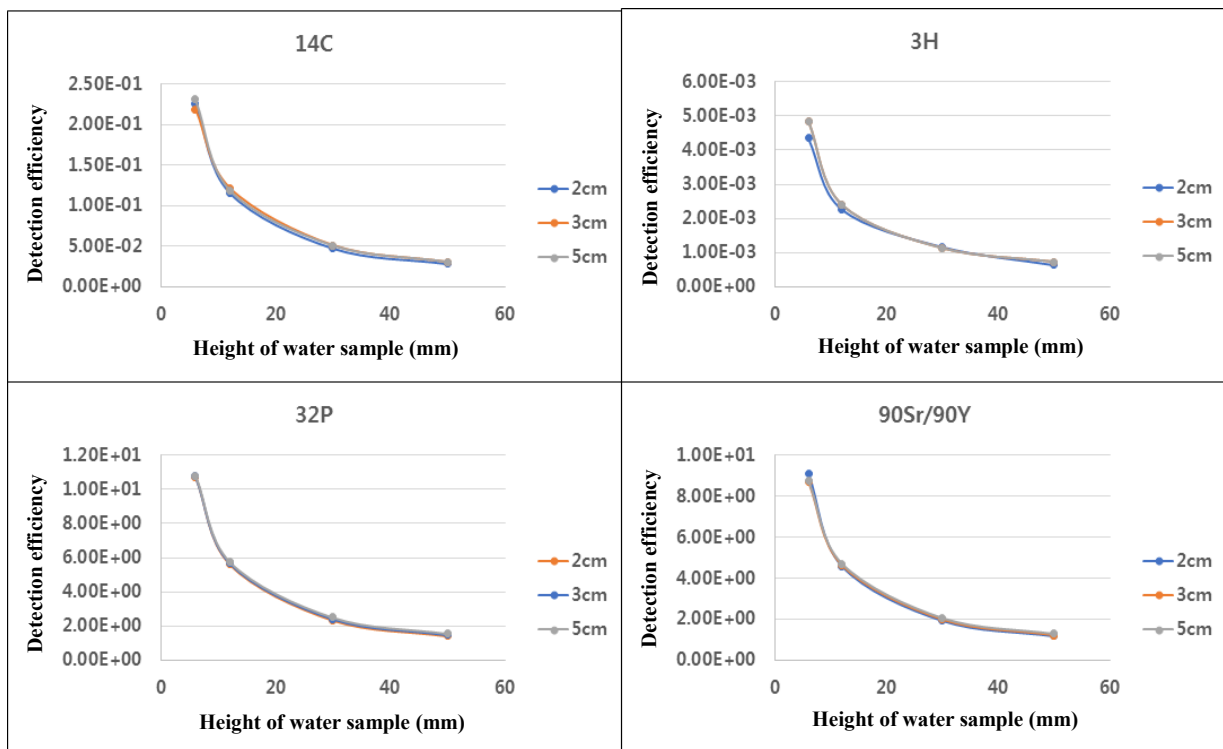
Figure 51 Simulation results of detection efficiency about height of water sample and diameter of plastic scintillator on ^{3}H, ^{14}C, ^{32}P and ^{90}Sr/^{90}Y

The concept of FOM is applied to evaluate the height of the water sample and diameter of the scintillator. The value of FOM is related to the radioactivity concentration and efficiency of the source, and thus, the measurement time required to reach a certain level. The value of FOM is proportional to the measuring time. If the same number of counts is reached, a higher value of FOM would result in a shorter measurement period. The FOM values for four major beta-emitting radionuclides are shown in Figure 52, where the blue, red, and green lines indicate the scintillator's diameter of 2, 3, and 5 mm respectively.
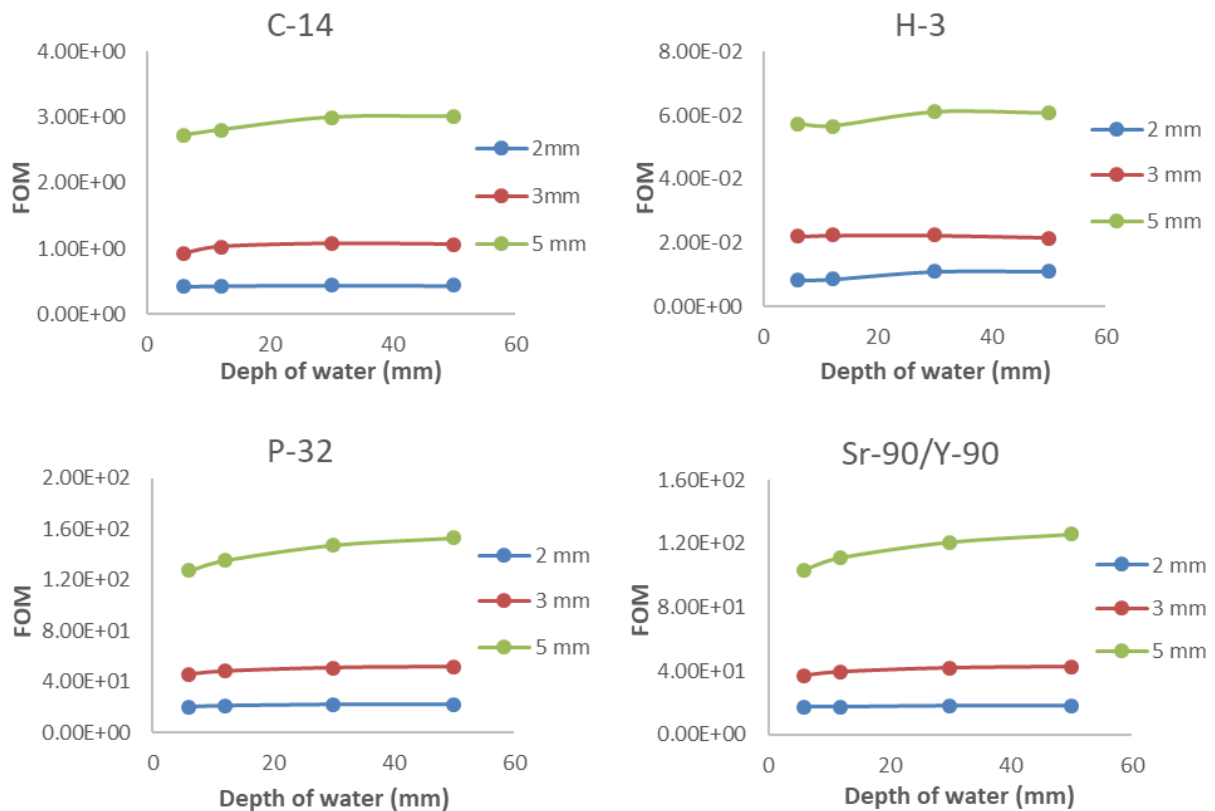
Figure 52 FOM result for diameter of scintillator and depth of water

The FOM for a 5-mm-diameter scintillator is much higher than those for 2- and 3-mm-diameter scintillators. In other words, a scintillator having 5 mm diameter needs the shortest counting time to reach a reasonable statistic count. Change in water depth has an insignificant effect on FOM values. The FOMs for ^{32}P and ^{90}Sr/^{90}Y are much higher than those for ^{3}H and ^{14}C (2,000 and 40 times in general, respectively).

Based on the FOM and the assumption that all radionuclides have similar activity concentration, the measurement of ^{3}H and ^{14}C would require 2,000 and 40 times longer to acquire reasonable counting statistics compared to that of ^{32}P or ^{90}Sr/^{90}Y.

The simulation results are reflected in fabricating scintillator acrylic support structures for a basic experiment. The scintillator diameter is set to 50 mm, which is the same as the PMT diameter. This is the maximum value for a plastic scintillator diameter. The height of the water sample is set to 2 cm, which is the smallest value, while securing a space in connecting the tube on both sides of the scintillator support structure.

To increase the cross-sectional area between the scintillator and water sample, many scintillators should be inserted within a limited volume. Based on the PMT size, the acrylic structure of the detector is set as not exceeding the PMT diameter.

MCNP simulations are used to confirm the detection efficiency by increasing the number of scintillators in the acrylic structure. The number of scintillators range from three to thirteen. If the number of scintillators is one or two, the multilayer scintillator type is not applicable. In addition, when the number of scintillators is more than 13, laser processing of the acrylic structure is impossible. Therefore, the number of scintillators ranges from 3 to 13, and as the number of scintillators is increased from 3 to 13, the detection efficiency increases. The relation between the number of scintillators and detection efficiency of tritium is plotted in Figure 53.
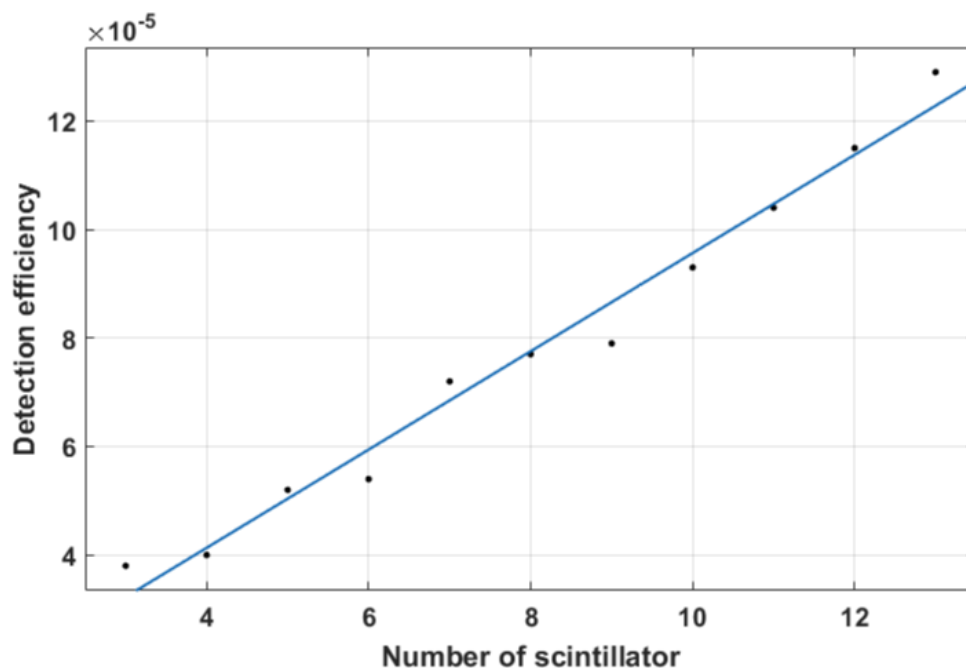
Figure 53 Simulation result of detection efficiency with the number of scintillators

4.2 Filtration performance results

To evaluate the performance of the water purification system for tritium separation, seawater samples are collected and purified using a pretreatment equipment. The water sample applying the pretreatment equipment is requested to be analyzed by the Korea Quality Testing Institute (KQT), a nationally recognized institution. The water condition is analyzed, and the analysis items and results are listed in Table 25.

In addition, the concentrations of ions and salts in water are analyzed. Cl^- and NO_3 are analyzed by ion chromatography, and the remaining items are analyzed by inductively coupled plasma mass spectrometry. The analysis results are listed in Table 26.

For all analysis items, values below the detection limit are detected and most of the material is filtered out to confirm that only pure water is produced.

Table 25 Analysis item and result of treated water sample for water condition

Analysis item	Detection limit	Result
Electrical conductivity	-	0.080 $\mu S/cm^{-1}$
pH at 25℃	-	6.80
Electrical resistivity	-	12.5 $M\Omega \cdot cm$
Heating at 110℃	1 mg/L	Not detected
Total Organic Carbon (TOC)	0.1 mg/L	Not detected
Bacteria	1 CFU/mL	Not detected
Endotoxin	0.005 EU/mL	Not detected

Table 26 Analysis result of the concentrations of ions and salts in treated water sample

Analysis item	Detection limit	Result
SiO_2	0.005 mg/L	Not detected
Na	0.001 mg/L	Not detected
Cr	0.001 mg/L	Not detected
Fe	0.001 mg/L	Not detected
Ni	0.001 mg/L	Not detected
Pb	0.001 mg/L	Not detected
Cl^-	0.005 mg/L	Not detected
NO_3^-	0.005 mg/L	Not detected

4.3 Experiment for detection characteristic of beta ray with plastic scintillator

4.3.1 Interaction characteristic experiment

To compare the simulated value with the actual measured value, samples are prepared using a standard source and the count is measured. The measurement time set to 600 s and the background count is 3,485. PMT is used in the model R878 and measured under the conditions of 50 mm in diameter for plastic scintillators. The net count is defined as the total count minus the background count value and the efficiency is calculated as (net count/600/extracted radioactivity) × 100%. The comparison between the real detection and simulation is described in Table 27.

Table 27 Comparison between real detection and simulation

	Real detection		Simulation	
	Net count. (Gross count)	Detection Efficiency (%)	Detection efficiency (%)	Error (%)
Background	3,485	Not available	-	-
^{3}H	Not available (3,429)	Not available	0.002	0.047
^{14}C	241 (3,726)	0.10 $\pm$ 3.93E-02	0.107	0.007
^{32}P	9,224 (12,709)	5.54 $\pm$ 2.98E-02	5.650	0.001
^{90}Sr/^{90}Y	21,570 (25,055)	4.60 $\pm$ 2.90E-02	4.620	0.002

Comparing the detection efficiency of the simulation with the actual measurements, most of the radionuclides show similar results. However, in the case of tritium, there is no difference between the background and measured values. To detect very-low-energy beta nuclides, such as tritium, the application of a method for increasing the efficiency of the detection unit will be required. All other nuclides are expected to be detected in the environment in which tritium measurements are defined.
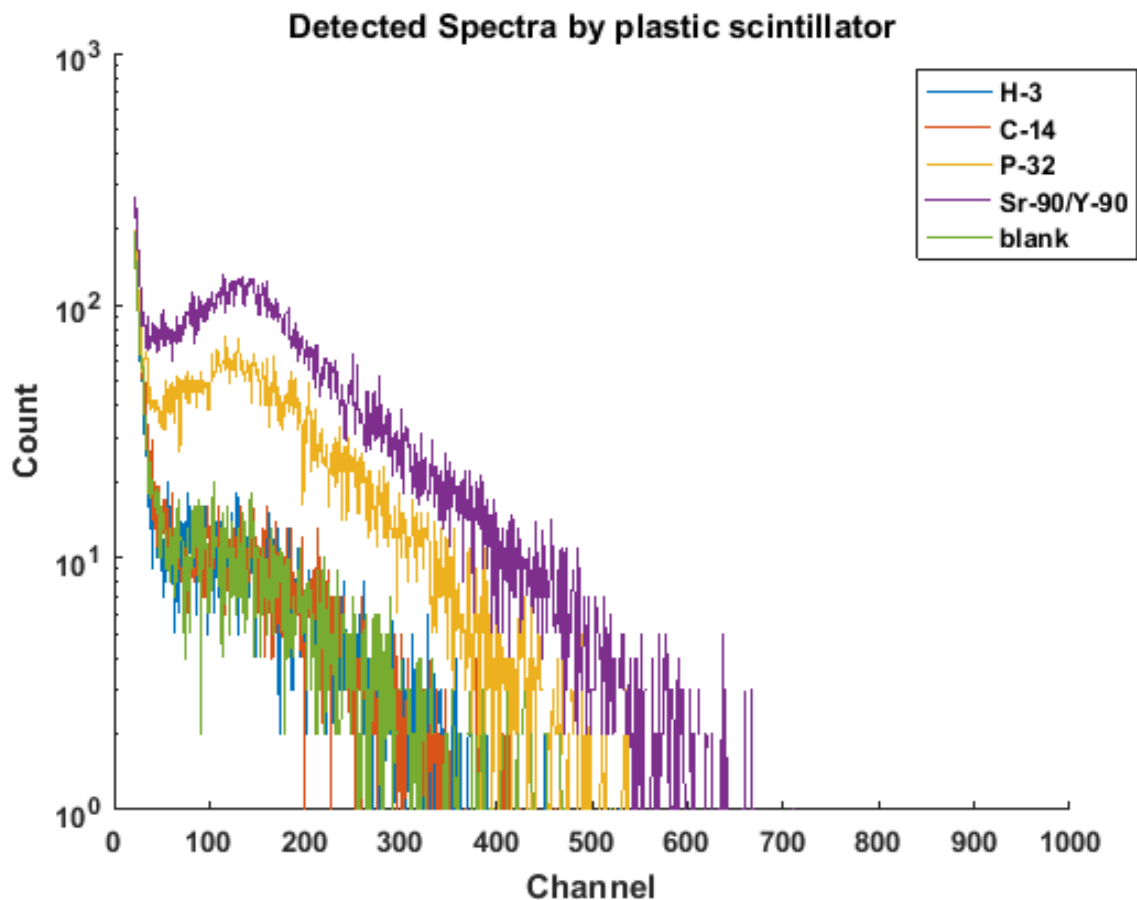
Figure 54 Detected spectrum for single beta radionuclide

To confirm the detection characteristics of beta radionuclides, the spectrum for each radionuclide is confirmed. Figure 54 shows the measured spectrum for a single radionuclide. Tritium and ^{14}C, which have relatively low beta energy, are found to be very similar to the background spectrum. In the case of relatively high-energy nuclides, such as ^{32}P and ^{90}Sr/^{90}Y, the results show a clear difference from the background.

To confirm the change in the spectrum, the background spectrum is removed from the measured spectrum of each radionuclide. The spectrums obtained for each radionuclide are shown in Figure 55.
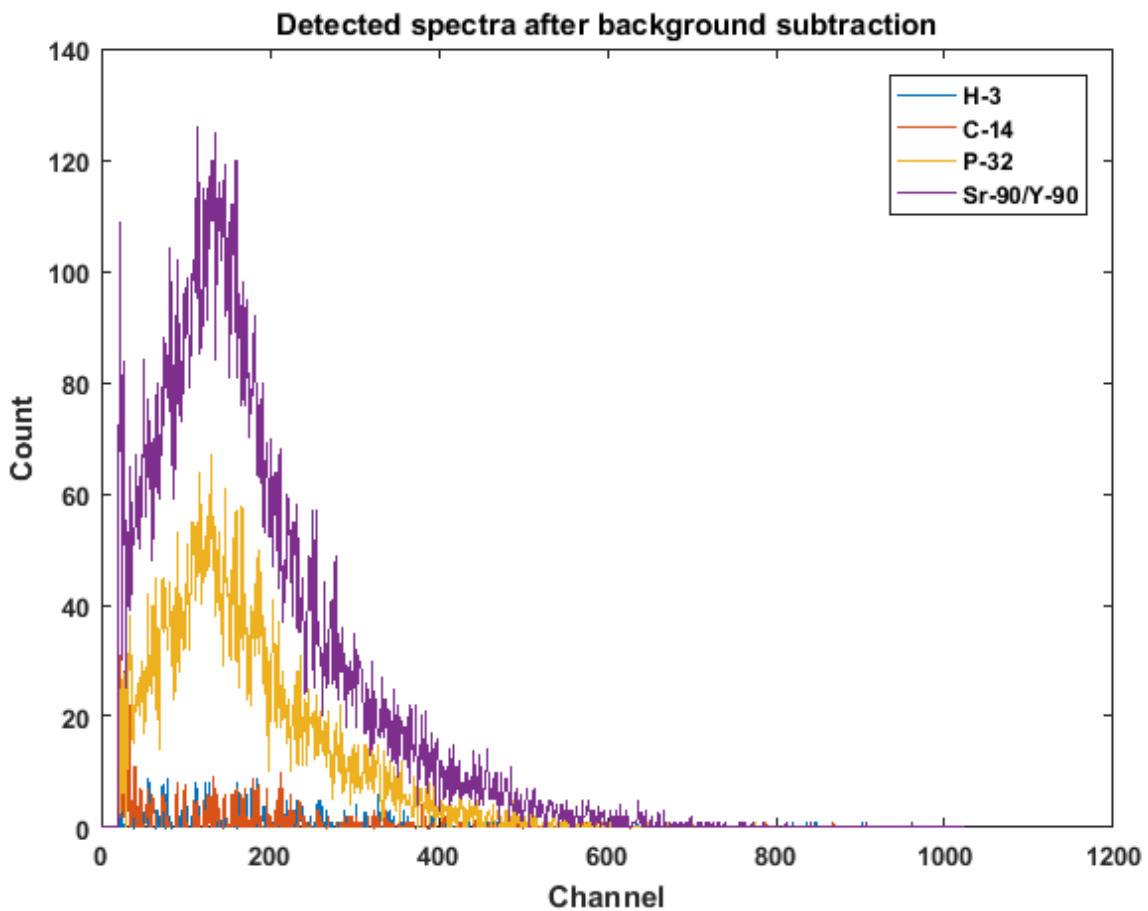
Figure 55 Detected spectrum background subtracted for single beta radionuclide

In the case of ^{32}P and ^{90}Sr/^{90}Y, even if the background is removed, the spectrum showing a constant distribution is found. On the other hand, tritium and ^{14}C show a small value when the spectrum is removed.

Besides the spectrum for a single radionuclide, the spectra are measured by mixing two radionuclides on four prepared nuclides. The measured spectra are shown in Figure 56. The mixed radionuclides are also well-measured for the relatively high energies of ^{32}P and ^{90}Sr/^{90}Y. ^{3}H and ^{14}C are found to have no effect on the measurement, even when mixed.
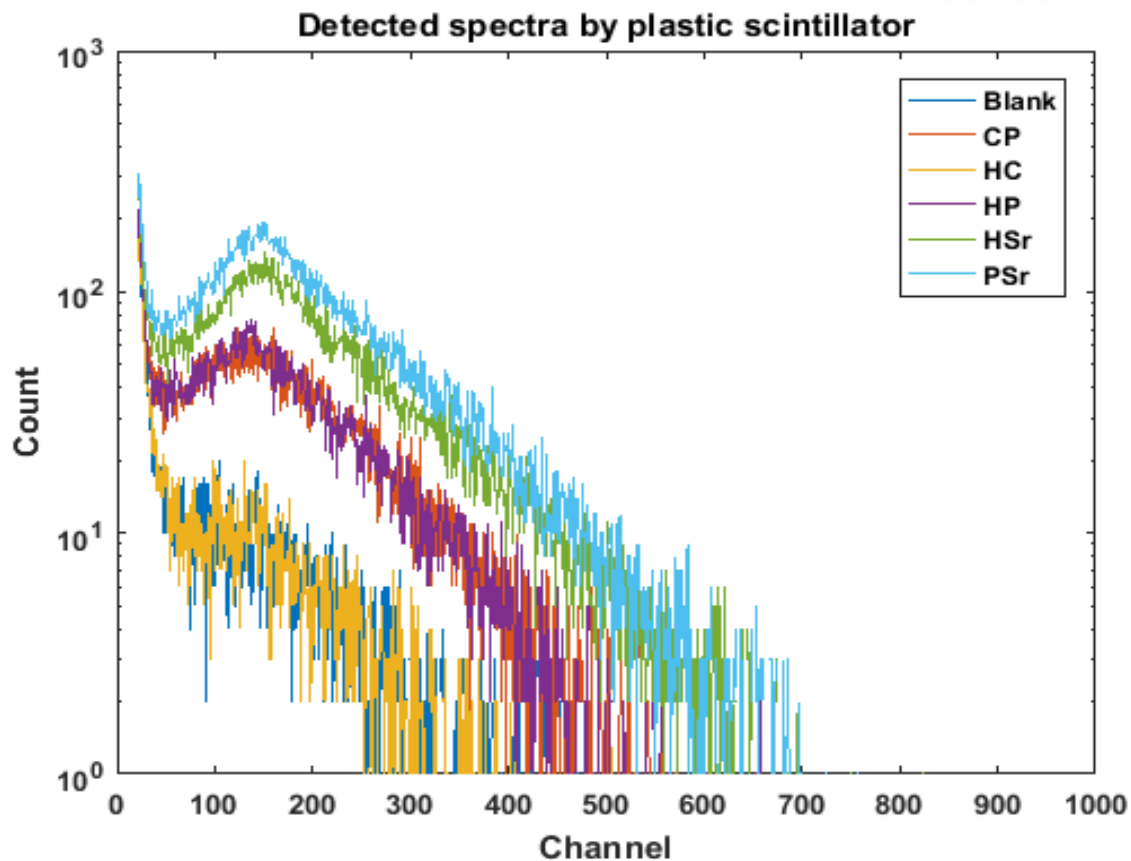
Figure 56 Detected spectrum for double beta radionuclide

4.3.2 Detection characteristics according to flow rate change

An external pump must be used to inject the water sample into the detection part. As the flow rate is generated when the source is injected, an experiment for determining the effect of flow rate is performed. The flow rate is changed to 0 mL/min, 600 mL/min, 800 mL/min, and 1,000 mL/min to derive the MDA. First, before performing the experiment by injecting the source, a change in the background count rate according to the flow rate change through the distilled water is performed. Figure 57 and Figure 58 show the background spectrum as the flow rate changes. As shown in Table 28, even if the flow rate is changed, there is no significant difference in the background count rate.
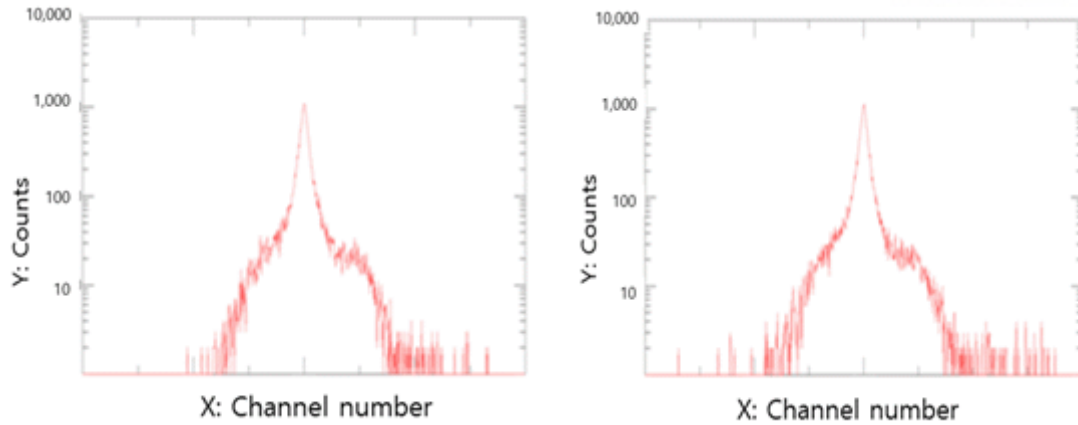
Figure 57 Background spectrums for 0 mL/min (left) and 600 mL/min (right) of flow rate
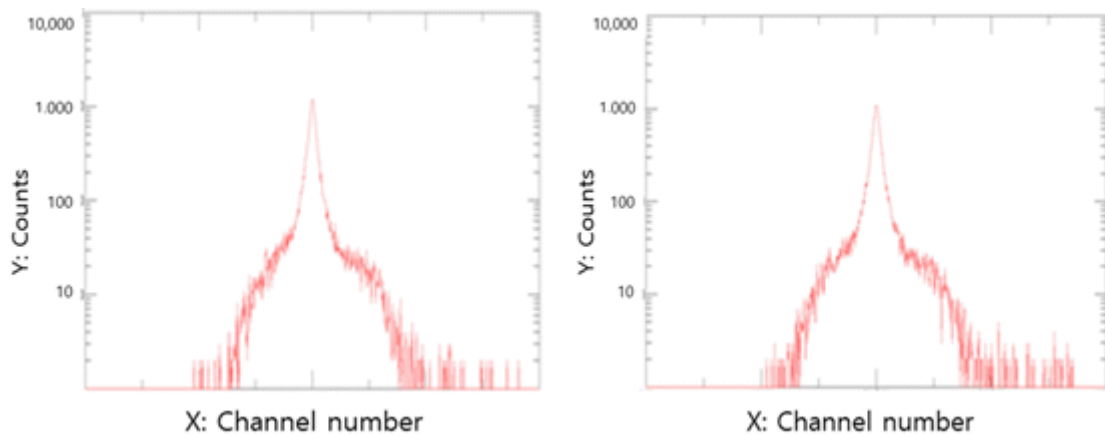
Figure 58 Background spectrums for 800 mL/min (left) and 1,000 mL/min (right) of flow rate

Table 28 Background count rate change according to flow rate change

Background count rate at flow rate of 0 mL/min	Background count rate at flow rate of 600 mL/min	Background count rate at flow rate of 800 mL/min	Background count rate at flow rate of 1,000 mL/min
31.12 ± 0.23 cps	31.12 ± 0.17 cps	31.39 ± 0.12 cps	31.24 ± 0.19 cps

To determine the influence of the detection according to the flow rate change when the source is injected, the background count rate and total count rate after injecting the radioactive source are measured. For ^{90}Sr, a source with a radioactivity concentration of 10.04 Bq/g is used. Table 29 shows

the background count rate before injecting the source and the total count rate after injecting the source. Although there is a significant difference before and after source injection, it is confirmed that there is no change according to the flow rate.

Table 29 Background and total count rates according to flow rate change using ^{90}Sr source

Flow rate	0 mL/min	600 mL/min	800 mL/min	1,000 mL/min
Background count rate (cps)	7.60 ± 0.23	7.60 ± 0.23	7.60 ± 0.23	7.60 ± 0.23
Total count rate (cps)	33.05 ± 0.12	32.4 ± 0.15	32.88 ± 0.25	32.54 ± 0.19

Table 30 shows the calculated MDA according to the measurement time, where an MDA of ~1/10th the value of the actually injected radioactivity concentration is indicated. Even if there is a change in the flow rate, the radioactivity concentration value to be measured can be confirmed in ~40 s in all cases. Figure 59 shows the MDA derived according to the flow rate and detection time change. There is no significant difference between each detected data. In the case of ^{90}Sr, it is confirmed that the radiation measurement is not affected by the change in flow rate.

Table 30 ^{90}Sr MDA calculation according to flow rate change

Flow rate	0 mL/min	600 mL/min	800 mL/min	1,000 mL/min
Time (sec)	Derived MDA (Bq/g)	Derived MDA (Bq/g)	Derived MDA (Bq/g)	Derived MDA (Bq/g)
1	6.12 ± 0.187	6.28 ± 0.193	6.17 ± 0.189	6.25 ± 0.193
10	1.94 ± 0.060	1.99 ± 0.061	1.95 ± 0.060	1.98 ± 0.061
20	1.37 ± 0.042	1.41 ± 0.044	1.38 ± 0.043	1.40 ± 0.044
30	1.12 ± 0.035	1.15 ± 0.036	1.13 ± 0.035	1.14 ± 0.036
40	**0.97 ± 0.030**	**0.99 ± 0.031**	**0.97 ± 0.030**	**0.99 ± 0.031**
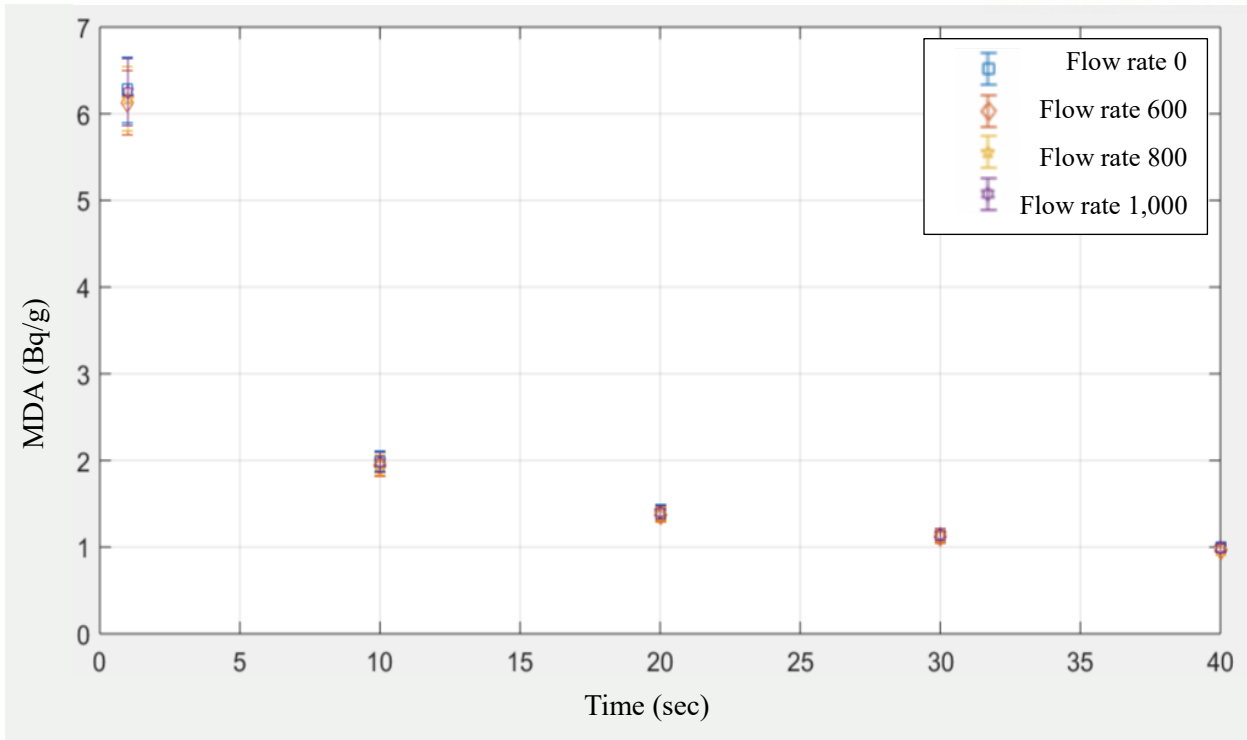
Figure 59 Derived MDA according to flow rate and detection time change in case of ^{90}Sr

The radioactivity of 11.01 Bq/g concentration for ^{14}C source is used. However, as shown in Table 31, the total counting rate is 0.02 cps higher, or rather lower, than the background counting rate, which means that accurate experimental results cannot be obtained. In future experiments, it may be necessary to increase the amount of source and the measurement time, or use higher radiation concentration values.

Table 31 Background and total count rates according to flow rate change using ^{14}C source

Flow rate	0 mL/min	600 mL/min	800 mL/min	1,000 mL/min
Background count rate (cps)	7.71 ± 0.18	7.72 ± 0.20	7.69 ± 0.13	7.73 ± 0.11
Total count rate (cps)	7.66 ± 0.15	7.62 ± 0.16	7.71 ± 0.17	7.68 ± 0.11

In case of tritium, a source with a radioactivity concentration of 1,012,827.13 Bq/g is used. Table 32 shows the background count rate before injecting the source and the total count rate after injecting the source. Although there is a significant difference before and after source injection, there is no change according to the flow rate.

Table 32 Background and total count rates according to flow rate change using ^{3}H source

Flow rate	0 mL/min	600 mL/min	800 mL/min	1,000 mL/min
Background count rate (cps)	7.13 ± 0.14	7.13 ± 0.14	7.13 ± 0.14	7.13 ± 0.14
Total count rate (cps)	15.18 ± 0.20	15.03 ± 0.22	15.72 ± 0.15	15.15 ± 0.20

The time required to derive an MDA of 1/10th the initial source is derived. Table 33 shows the calculated MDA as the measurement time and the flow rate change. It is estimated that ~400 s are required to satisfy the target MDA, and that the value of the measurement according to the change in the flow rate does not have a significant difference. Figure 60 shows the derived MDA according to the flow rate and detection time change. There is no significant difference between each detected data. In the case of ^{3}H, it is confirmed that the radiation measurement is not affected by the change in flow rate.

Table 33 ^{3}H MDA calculation according to flow rate change

Flow rate	0 mL/min	600 mL/min	800 mL/min	1,000 mL/min
Time (sec)	Derived MDA (Bq/g)	Derived MDA (Bq/g)	Derived MDA (Bq/g)	Derived MDA (Bq/g)
3	1,110,916 ± 22,409	1,119,657 ± 28,152	1,029,719 ± 25,891	1,102,904 ± 27,731
10	617,856 ± 14,173	613,261 ± 15.420	564,000 ± 14,181	604,085 ± 15,189
100	195,383 ± 4,482	193,930 ± 4,876	178,352 ± 4,485	191,028 ± 4,803
200	138,156 ± 3,170	137,129 ± 3,982	126,114 ± 3,171	135,077 ± 3,397
300	112,804 ± 2,588	111,965 ± 3,448	102,971 ± 2,590	110,290 ± 2,774
400	**97,691 ± 2,241**	**96,965 ± 3,084**	**89,176 ± 2,243**	**95,514 ± 2,402**
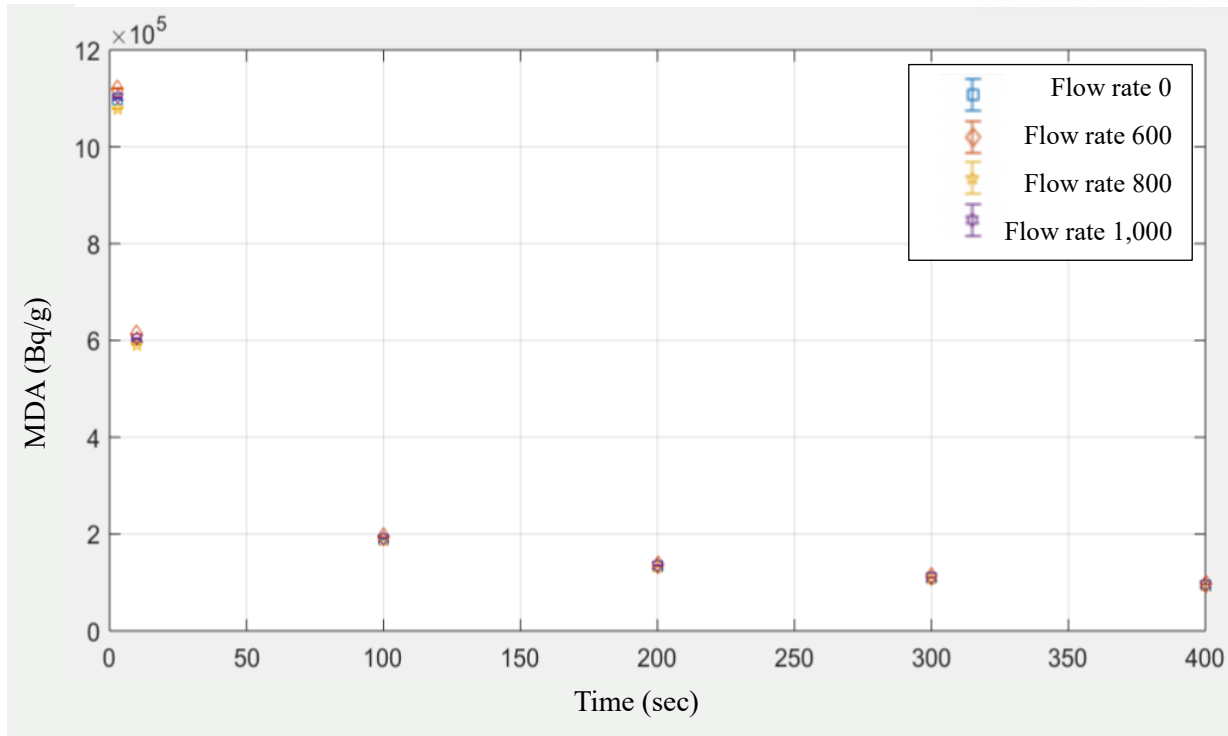
Figure 60 Derived MDA according to flow rate and detection time change in case of ^{3}H

4.3.3 Detection characteristics with radioactivity concentration

As it is confirmed that there is no significant difference in the MDA value according to the flow rate, radiation analysis is conducted when the flow rate is 0 mL/min and the coarse gain of the 855 Dual Amplifier is 10. Table 34 shows the actual measured background and total count rates corresponding to the radioactivity concentrations of 2.51 Bq/g, 5.02 Bq/g, 7.53 Bq/g, and 10.04 Bq/g for ^{90}Sr. Based on the measurement results, the MDA values according to the radioactivity concentrations are derived using the background count and detection efficiency. The calculated MDA corresponding to the measurement time is derived. Table 35 shows the MDA results. The time required to derive the MDA of the injected radioactivity concentration level is determined, and that required to derive the MDA level corresponding to 1/10th of the injected radioactivity concentration is confirmed. Figure 61 is a graph showing the measurement results.

Table 34 Background and total count rates corresponding to the radioactivity concentrations for ^{90}Sr

Radioactivity concentration	2.51 Bq/g	5.02 Bq/g	7.53 Bq/g	10.04 Bq/g
Background count rate (cps)	7.25 ± 0.16	7.41 ± 0.12	7.48 ± 0.11	7.60 ± 0.23
Total count rate (cps)	12.95 ± 0.18	19.42 ± 0.21	26.32 ± 0.18	33.05 ± 0.12

Table 35 Derived MDA according to detection time for ^{90}Sr with different radioactivity concentrations

2.51 Bq/g		5.02 Bq/g		7.53 Bq/g		10.04 Bq/g	
Time (sec)	Derived MDA (Bq/g)	Time (sec)	Derived MDA (Bq/g)	Time (sec)	Derived MDA (Bq/g)	Time (sec)	Derived MDA (Bq/g)
8	**2.37 ± 0.062**	**2**	**4.59 ± 0.090**	**1**	**6.21 ± 0.101**	**1**	**6.12 ± 0.187**
100	0.67 ± 0.018	10	2.05 ± 0.040	10	1.96 ± 0.032	5	2.74 ± 0.084
200	0.47 ± 0.013	30	1.18 ± 0.024	20	1.39 ± 0.023	10	1.94 ± 0.060
300	0.39 ± 0.011	50	0.92 ± 0.018	30	1.13 ± 0.019	15	1.58 ± 0.049
400	0.34 ± 0.009	70	0.78 ± 0.016	40	0.98 ± 0.016	20	1.37 ± 0.042
500	0.30 ± 0.008	90	0.68 ± 0.014	50	0.88 ± 0.015	25	1.22 ± 0.038
600	0.27 ± 0.008	110	0.62 ± 0.013	60	0.80 ± 0.013	30	1.12 ± 0.035
700	0.25 ± 0.007	130	0.57 ± 0.012	**70**	**0.74 ± 0.013**	**35**	**1.04 ± 0.032**
800	**0.24 ± 0.007**	**150**	**0.53 ± 0.011**	80	0.69 ± 0.012	40	0.97 ± 0.030
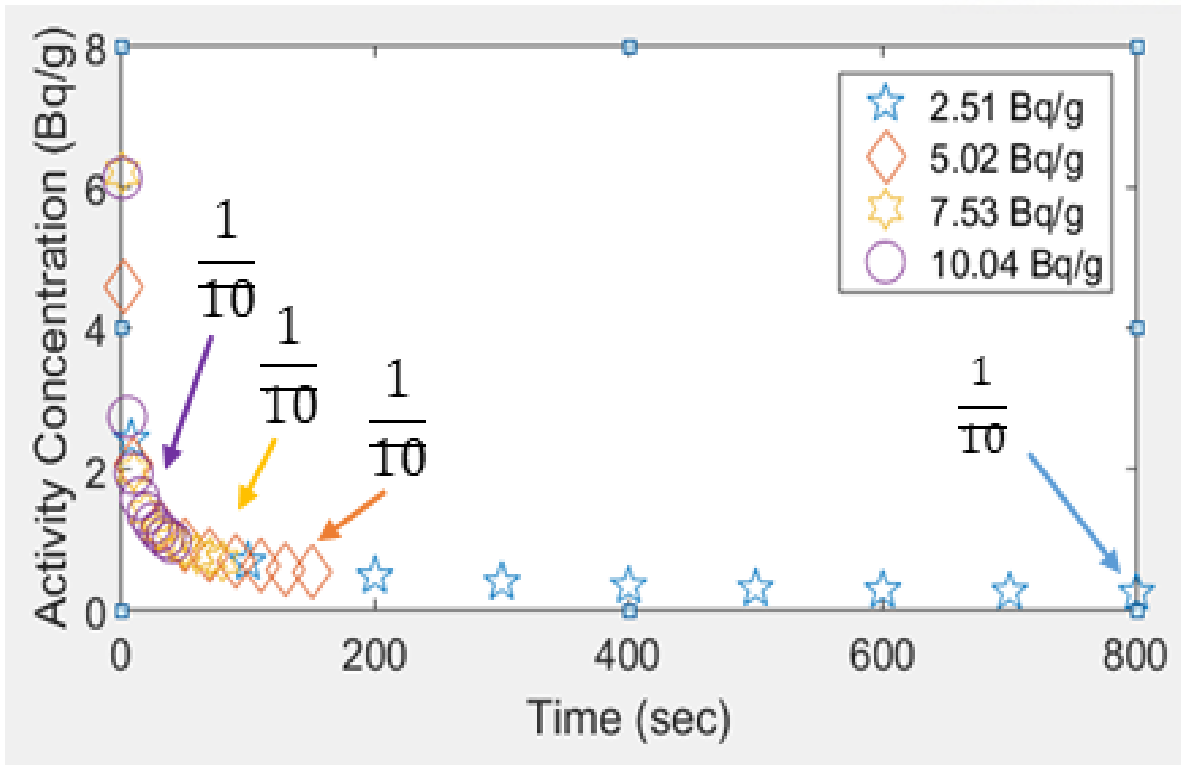
Figure 61 MDA change trend corresponding to measurement time per radioactivity concentration of ^{90}Sr

For ^{14}C, measurements are taken for source concentrations of 2.75 Bq/g, 5.51 Bq/g, 8.26 Bq/g, and 10.01 Bq/g. The result is described in Table 36. The total count rare measured after source injection is less than or equal to that of the background. Therefore, the case of ^{14}C cannot be defined.

Table 36 Background and total count rates corresponding to the radioactivity concentrations for ^{14}C

Radioactivity concentration	2.75 Bq/g	5.51 Bq/g	8.26 Bq/g	10.01 Bq/g
Background count rate (cps)	7.59 ± 0.12	7.55 ± 0.18	7.57 ± 0.11	7.73 ± 0.11
Total count rate (cps)	7.33 ± 0.10	7.49 ± 0.12	7.58 ± 0.13	7.70 ± 0.11

Table 37 shows the actual measured background and total count rates corresponding to the radioactivity concentrations of 253,206 Bq/g, 506,413 Bq/g, 759,620 Bq/g, and 1,012,827 Bq/g for ^{3}H. This radioactivity concentration value is much higher than those of the other radionuclides. In case of ^{3}H, a much higher concentration is used because tritium has extremely low beta energy, so it needs a

98

high concentration level to obtain a stable count rate. Based on the measurement results, the MDA values according to the radioactivity concentrations are derived using the background count and detection efficiency. The calculated MDA corresponding to the measurement time is derived. Table 38 shows the MDA results. The time required to derive the MDA of the injected radioactivity concentration level is determined. In addition, the time required to derive the MDA level corresponding to 1/10th of the injected radioactivity concentration is confirmed. Figure 62 is a graph showing the measured results.

Table 37 Background and total count rates corresponding to the radioactivity concentrations for ^{3}H

Radioactivity concentration	253,206 Bq/g	506,413 Bq/g	759,620 Bq/g	1,012,827 Bq/g
Background count rate (cps)	7.19 ± 0.12	7.40 ± 0.15	7.19 ± 0.14	7.13 ± 0.14
Total count rate (cps)	8.83 ± 0.10	11.09 ± 0.12	13.22 ± 0.14	15.18 ± 0.13

Table 38 Derived MDA according to detection time for ^{3}H with different radioactivity concentration

253,206 Bq/g		506,413 Bq/g		759,620 Bq/g		1,012,827 Bq/g	
Time (sec)	Derived MDA (Bq/g)	Time (sec)	Derived MDA (Bq/g)	Time (sec)	Derived MDA (Bq/g)	Time (sec)	Derived MDA (Bq/g)
90	252,730 ± 5,098	18	502,332 ± 11,543	7	739,398 ± 16,389	10	617,856 ± 14,173
1000	75,819 ± 1,530	1000	67,394 ± 1,549	100	195,626 ± 4,337	100	195,383 ± 4,482
3000	43,774 ± 883	1200	61,522 ± 1,414	250	123,724 ± 2,743	200	138,156 ± 3,170
5000	33,907 ± 684	1400	56,959 ± 1,309	400	97,813 ± 2,169	300	112,804 ± 2,588
9000	**25,273 ± 510**	**1800**	**50,233 ± 1,155**	**700**	**73,939 ± 1,639**	**400**	**97,691 ± 2,241**
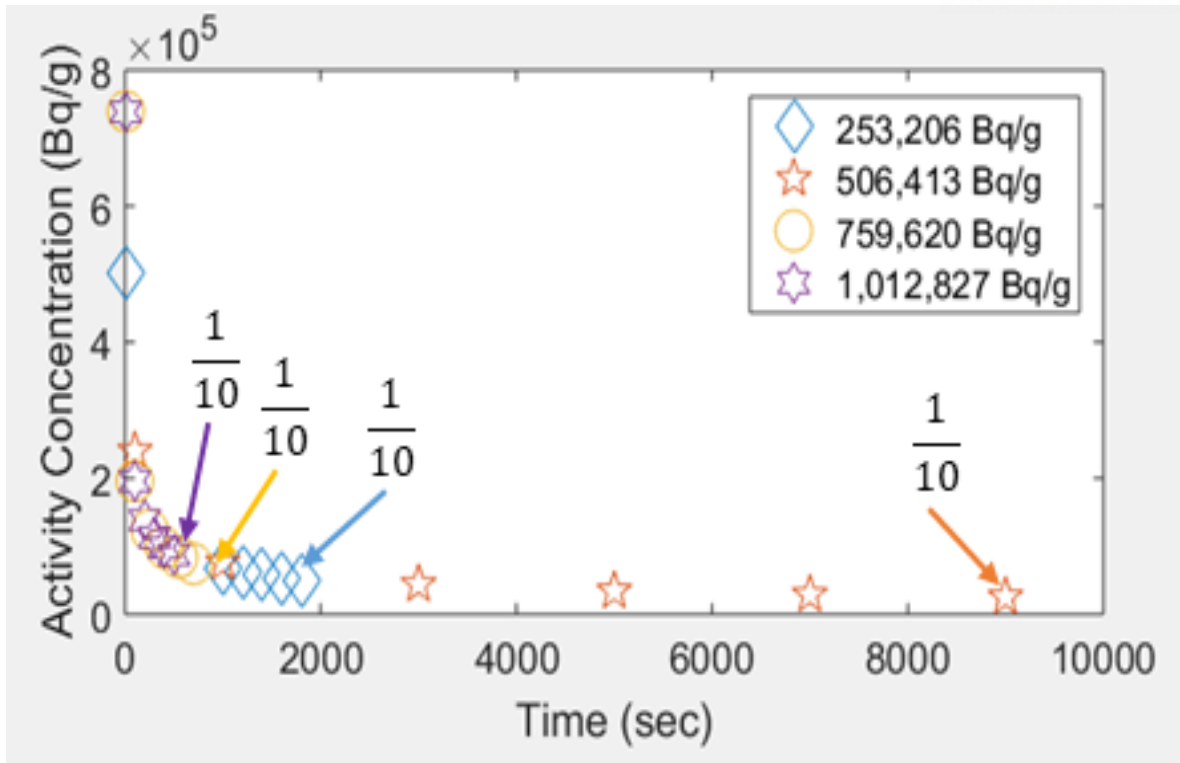
Figure 62 MDA change trend corresponding to measurement time per radioactivity concentration of ^{3}H

4.3.4 Detection characteristics due to amplification

Plastic scintillators and PMT-based radiation monitoring systems depend on the amplification of the main amplifiers. The radioactive source is injected, the amplification degree of the main amplifier is changed, and the measurement result is obtained.

For ^{90}Sr, the efficiency of the 855 Dual Amplifier at coarse gain 10 is $8.20 \pm 0.59\%$ for concentration 2.51 Bq/g, $8.64 \pm 0.62\%$ for concentration 5.02 Bq/g, $9.04 \pm 0.65\%$ for concentration 7.53 Bq/g, and $9.16 \pm 0.66\%$ for concentration 10.04 Bq/g. The average value of efficiency is ~$8.76 \pm 0.63\%$.

Efficiency at coarse gain 20 is $14.12 \pm 1.02\%$ at concentration 2.51 Bq/g, $16.33 \pm 1.18\%$ at concentration 5.02 Bq/g, $17.32 \pm 1.25\%$ at concentration 7.53 Bq/g, and $18.14 \pm 1.31\%$ at concentration 10.04 Bq/g. The average value is ~$16.48 \pm 1.19\%$.

The efficiency at coarse gain 40 is $30.71 \pm 2.22\%$ at concentration 2.51 Bq/g, $32.11 \pm 2.32\%$ at concentration 5.02 Bq/g, $34.60 \pm 2.50\%$ at concentration 7.53 Bq/g, and $32.76 \pm 2.37\%$ at concentration 10.04 Bq/g. The average is ~$32.54 \pm 2.35\%$. Figure 63 shows the total result of detection efficiency according to the coarse gain change.

As the 855 Dual Amplifier's coarse gain increases, ^{90}Sr shows higher efficiency and all values are within the error range. Considering the uncertainty of the micropipette and the difference between the temperature and sample temperature during micro-calibration, it is determined that all values are within the error range.
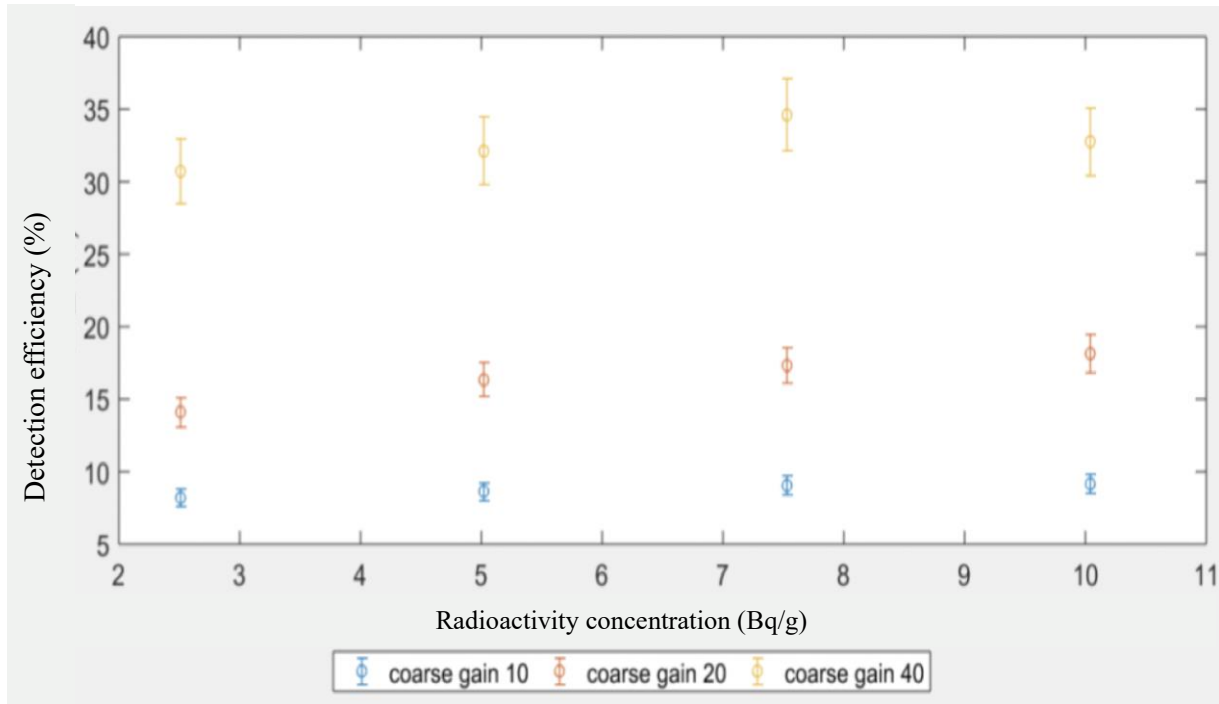
Figure 63 Detection efficiency according to coarse gain and radioactivity concertation change in case of [90]Sr

For ^{3}H, the efficiency at coarse gain 10 is 2.34E-05 ± 0.22E-05% at concentration 253,206 Bq/g, 2.63E-05 ± 0.25E-05% at concentration 506,413 Bq/g, 2.87E-05 ± 0.27E-05% at concentration 759,620 Bq/g, and 2.87E-05 ± 0.27E-05% at concentration 1,012,827 Bq/g. Total average is ~2.68E-05 ± 0.25E-05%.

The efficiency at coarse gain 20 is 2.84E-05 ± 0.27E-05% at concentration 253,206 Bq/g, 4.65E-05 ± 0.44E-05% at concentration 506,413 Bq/g, 7.23E-05 ± 0.69E-05% at concentration 759,620 Bq/g, and 9.22E-05 ± 0.87E-05% at concentration 1,012,827 Bq/g. The average is ~5.98E-05 ± 0.57E-05%.

Efficiency at coarse gain 40 is 5.03E-04 ± 0.48E-04% at concentration 253,206 Bq/g, 6.86E-04 ± 0.65E-04% at concentration 506,413 Bq/g, 6.61E-04 ± 0.63E-04% at concentration 759,620 Bq/g, and 6.59E-04 ± 0.62E-04% at concentrations 1,012,827 Bq/g. The average is ~6.27E-04 ± 0.59E-04%. Figure 64 shows all the data for ^{3}H with a change in radioactivity concentration and coarse gain.

Similar to ^{90}Sr, ^{3}H shows higher efficiency as the 855 Dual Amplifier's coarse gain increases. In the case of tritium, the measured value is significantly increased at a coarse gain of 40, and thus, a stable measurement is possible. In the case of tritium measurement, it is confirmed that the tendency is within the error range. The results can be observed in Figure 64.
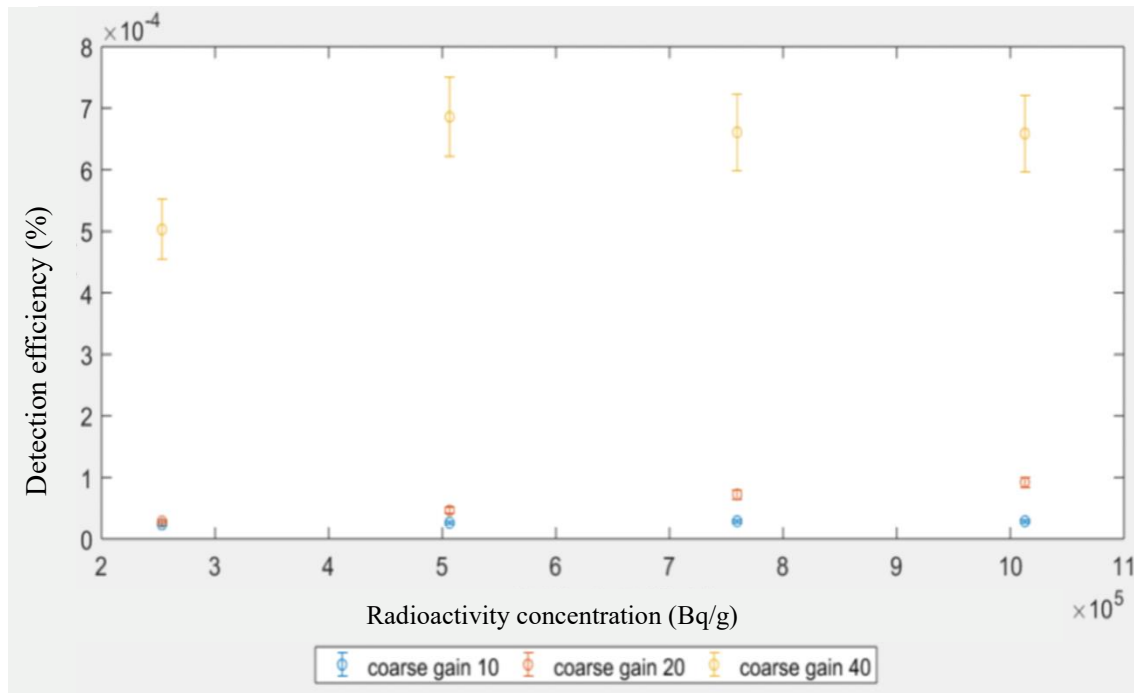
Figure 64 Detection efficiency according to coarse gain and radioactivity concertation change in case of ^{3}H

Characteristic experiments are performed using ^{90}Sr source and tritium source to confirm the effect of measurement on the change in amplification degree. The count rate change due to radioactivity concentration and coarse gain of the source are measured. Four radioactivity concentrations are used for Sr and tritium, and the used values of coarse gain are 10, 20, and 40. Based on the measurement results, the time required to derive the MDA of the intensity of the injected source and that of 1/10th the intensity of the injected source is derived.

For ^{90}Sr, experiments are performed for concentrations of 2.51 Bq/g, 5.02 Bq/g, 7.53 Bq/g, and 10.04 Bq/g. Table 39 shows the background and total count rates of ^{90}Sr 2.51 Bq/g at coarse gains 10, 20, and 40.

Table 39 Background and total count rates of ^{90}Sr 2.51 Bq/g at coarse gains 10, 20, and 40

Radioactive source	^{90}Sr		
Radioactivity concentration (Bq/g)	2.51		
Coarse gain	10	20	40
Background count rate (cps)	7.25 ± 0.16	8.55 ± 0.18	14.94 ± 0.15
Total count rate (cps)	12.95 ± 0.18	18.43 ± 0.14	36.43 ± 0.17

Table 40 shows the MDA according to the measurement time derived at each gain by using the measured background radioactivity and detection efficiency in case of 2.51 Bq/g of ^{90}Sr.

Table 40 Derived MDA according to measurement time per coarse gain for ^{90}Sr 2.51 Bq/g

Coarse gain 10		Coarse gain 20		Coarse gain 40	
Time (sec)	Radioactivity concentration (Bq/g)	Time (sec)	Radioactivity concentration (Bq/g)	Time (sec)	Radioactivity concentration (Bq/g)
8	**2.37 ± 0.062**	**3**	**2.29 ± 0.052**	**1**	**1.83 ± 0.021**
100	0.67 ± 0.018	10	1.26 ± 0.029	10	0.58 ± 0.007
200	0.47 ± 0.013	50	0.56 ± 0.013	20	0.41 ± 0.005
300	0.39 ± 0.011	100	0.40 ± 0.009	30	0.33 ± 0.004
400	0.34 ± 0.009	150	0.32 ± 0.008	40	0.29 ± 0.004
500	0.30 ± 0.008	200	0.28 ± 0.007	50	0.26 ± 0.003
600	0.27 ± 0.008	**250**	**0.25 ± 0.006**	**60**	**0.24 ± 0.003**
700	0.25 ± 0.007				
800	**0.24 ± 0.007**				

The time required to derive the MDA of the injected source intensity level and that of 1/10th the intensity of the injected source is 8 and 800 s for coarse gain 10, 3 and 250 s for coarse gain 20, and 1 and 60 s for coarse gain 40, respectively. Figure 65 shows the trend of the measurement result. The higher the radioactivity concentration and the higher the coarse gain, the lower is the MDA obtained.
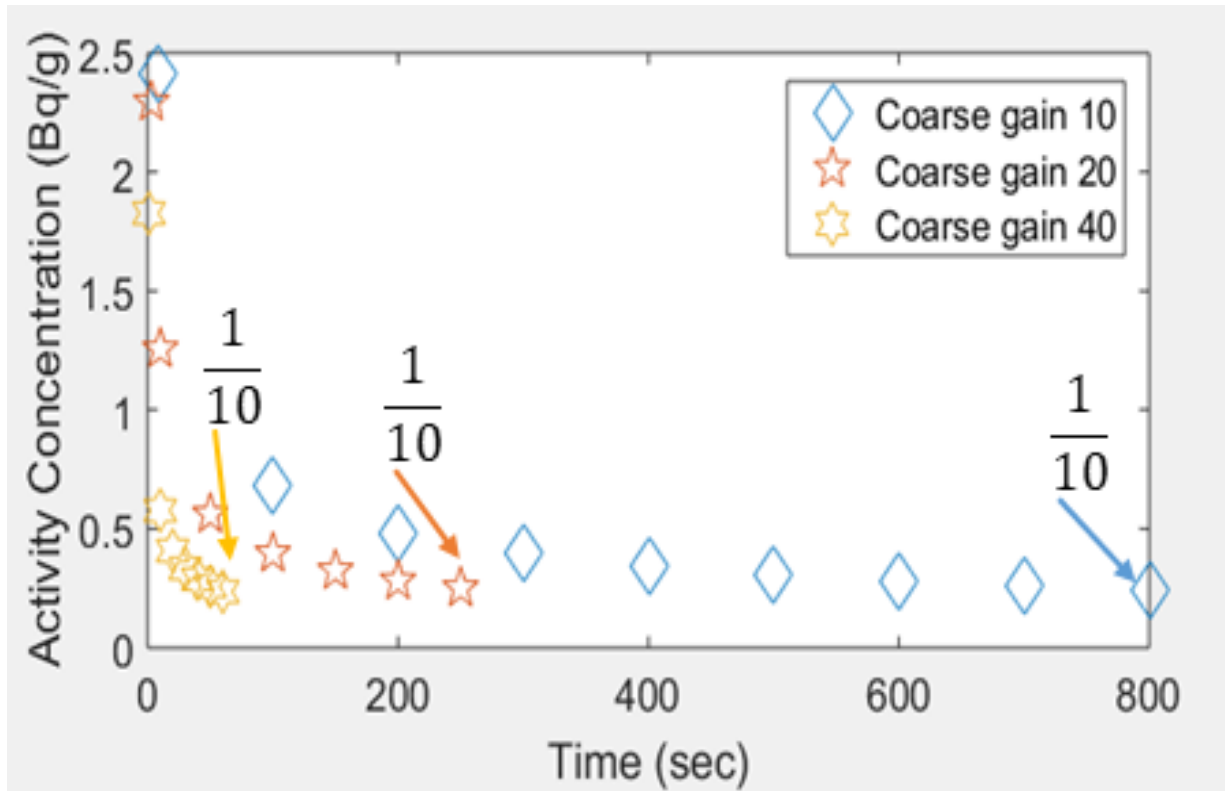
Figure 65 Trends about derived radioactivity concentration according to the change of coarse gain and detection time for ^{90}Sr 2.51 Bq/g

Table 41 shows the background and total count rate of ^{90}Sr 5.02 Bq/g at coarse gains 10, 20, and 40. The background level is similar, but the value of the total count rate is increased compared to the previous data.

Table 41 Background and total count rate of ^{90}Sr 5.02 Bq/g at coarse gain 10, 20 and 40

Radioactive source	^{90}Sr		
Radioactivity concentration (Bq/g)	5.02		
Coarse gain	10	20	40
Background count rate (cps)	7.41 ± 0.12	8.04 ± 0.15	14.97 ± 0.18
Total count rate (cps)	19.42 ± 0.21	30.89 ± 0.18	59.90 ± 0.17

Table 42 shows the MDA according to the measurement time derived by each gain using the measured background radioactivity and detection efficiency.

Table 42 Derived MDA according to measurement time per coarse gain for ^{90}Sr 5.02 Bq/g

Coarse gain 10		Coarse gain 20		Coarse gain 40	
Time (sec)	Radioactivity concentration (Bq/g)	Time (sec)	Radioactivity concentration (Bq/g)	Time (sec)	Radioactivity concentration (Bq/g)
2	**4.59 ± 0.090**	**1**	**3.43 ± 0.068**	**1**	**1.75 ± 0.022**
10	2.05 ± 0.040	10	1.09 ± 0.022	2	1.24 ± 0.016
30	1.18 ± 0.024	20	0.77 ± 0.016	4	0.87 ± 0.011
50	0.92 ± 0.018	25	0.69 ± 0.014	6	0.71 ± 0.009
70	0.78 ± 0.016	30	0.63 ± 0.013	8	0.62 ± 0.008
90	0.68 ± 0.014	35	0.58 ± 0.012	10	0.55 ± 0.007
110	0.62 ± 0.013	40	0.54 ± 0.011	**12**	**0.50 ± 0.007**
130	0.57 ± 0.012	45	0.51 ± 0.011		
150	**0.53 ± 0.011**	**50**	**0.49 ± 0.010**		

The time required to derive the MDA of the injected source intensity level and that of 1/10th the intensity of the injected source is 2 and 150 s for coarse gain 10, 1 and 50 s for coarse gain 20, and 1 and 12 s for coarse gain 40, respectively. Figure 66 shows the trend of the measurement result. The higher the radioactivity concentration and the higher the coarse gain, the lower is the MDA obtained. When the radioactivity concentration is 5.02 Bq/g and the coarse gain is 20 or more, it is confirmed that the MDA of the injected radioactivity concentration level can be derived with only one second of measurement time.

Figure 66 Trends about derived radioactivity concentration according to the change of coarse gain and detection time for ^{90}Sr 5.02 Bq/g

Table 43 shows the background and total count rates of ^{90}Sr 7.53 Bq/g at coarse gains 10, 20, and 40. The background level is similar, but the value of the total count rate is increased compared to the previous data. In addition, the largest change in count rate is obtained at coarse gain 40.

Table 43 Background and total count rate of ^{90}Sr 7.53 Bq/g at coarse gain 10, 20 and 40

Radioactive source	^{90}Sr		
Radioactivity concentration (Bq/g)	7.53		
Coarse gain	10	20	40
Background count rate (cps)	7.48 ± 0.11	8.28 ± 0.11	15.15 ± 0.17
Total count rate (cps)	26.32 ± 0.18	44.63 ± 0.13	87.78 ± 0.19

Table 44 shows the MDA according to the measurement time derived at each gain by using the measured background radioactivity and detection efficiency.

Table 44 Derived MDA according to measurement time per coarse gain for ^{90}Sr 7.53 Bq/g

Coarse gain 10		Coarse gain 20		Coarse gain 40	
Time (sec)	Radioactivity concentration (Bq/g)	Time (sec)	Radioactivity concentration (Bq/g)	Time (sec)	Radioactivity concentration (Bq/g)
1	**6.21 ± 0.101**	**1**	**3.24 ± 0.045**	**1**	**1.62 ± 0.019**
10	1.96 ± 0.032	4	1.62 ± 0.023	2	1.15 ± 0.014
20	1.39 ± 0.023	7	1.22 ± 0.017	3	0.94 ± 0.011
30	1.13 ± 0.019	10	1.02 ± 0.014	4	0.81 ± 0.010
40	0.98 ± 0.016	13	0.90 ± 0.013	**5**	**0.72 ± 0.009**
50	0.88 ± 0.015	16	0.81 ± 0.012		
60	0.80 ± 0.013	**19**	**0.74 ± 0.011**		
70	**0.74 ± 0.013**				

The time required to derive the MDA of the injected source intensity level and that of 1/10th the intensity of the injected source is 1 and 70 s for coarse gain 10, 1 and 19 s for coarse gain 20, and 1 and 5 s for coarse gain 40, respectively. Figure 67 shows the trend for the measurement result. The higher the radioactivity concentration and the higher the coarse gain, the lower is the MDA obtained. When the radioactivity concentration is 7.53 Bq/g, in all cases of coarse gain, it is confirmed that the MDA of the injected radioactivity concentration level can be derived with only one second of measurement time. In addition, in the case of coarse gain 40, the time required to derive an MDA of 1/10th the intensity of the injected source is confirmed to be only 5 s.
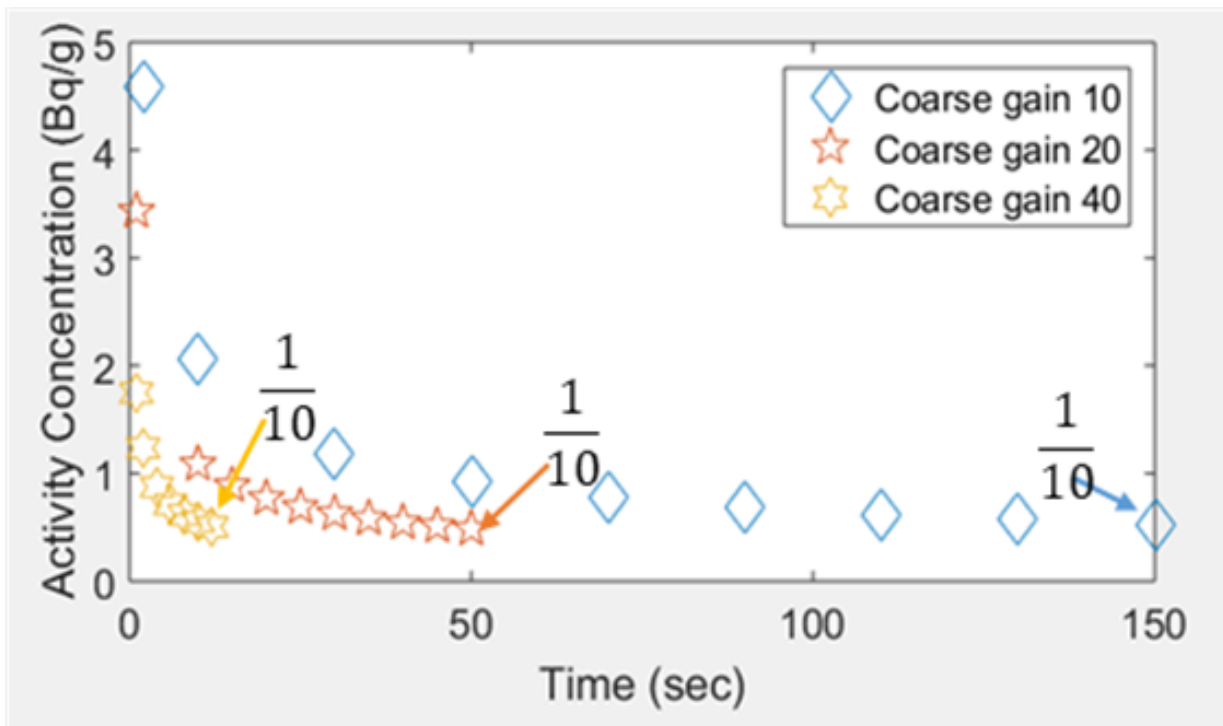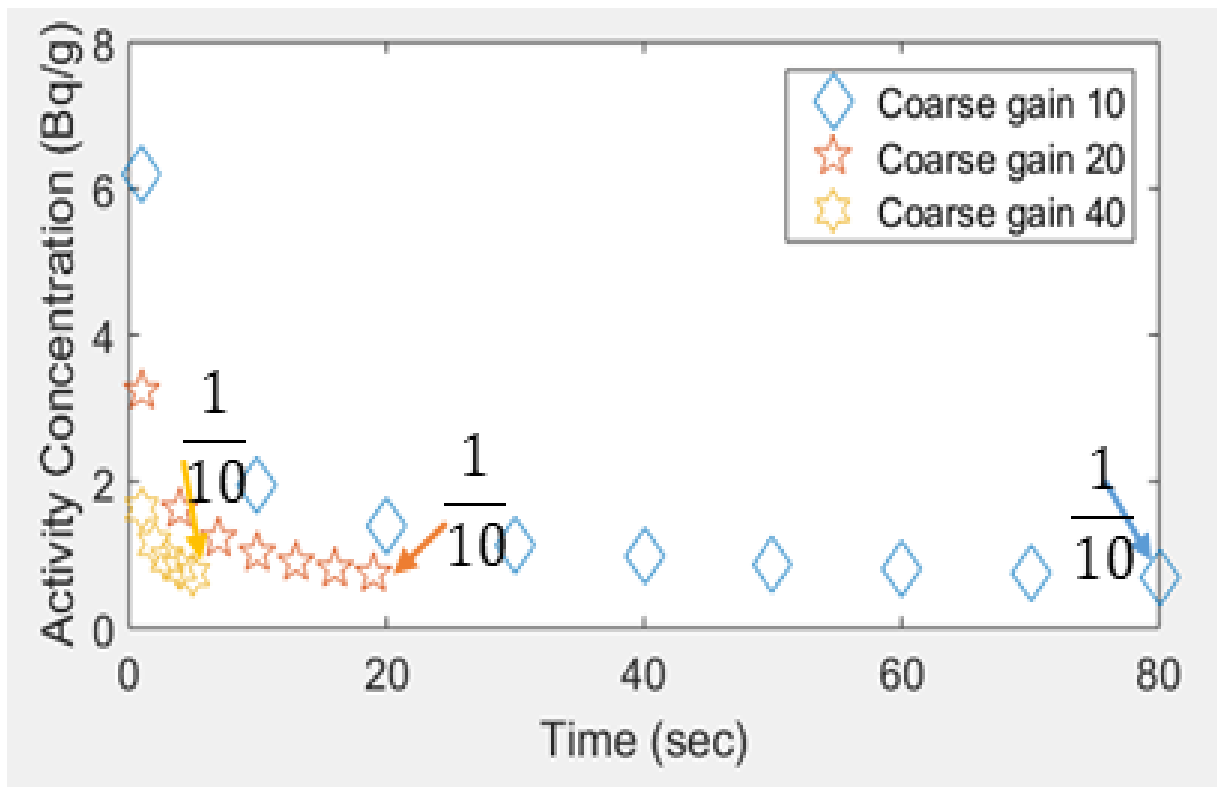

Figure 67 Trends about derived radioactivity concentration according to the change of coarse gain and detection time for ^{90}Sr 7.53 Bq/g

Table 45 shows the background and total count rates of ^{90}Sr 10.04 Bq/g at coarse gains 10, 20, and 40. The background level is also similar, but the value of the total count rate is increased compared to the previous data.

Table 45 Background and total count rate of ^{90}Sr 10.04 Bq/g at coarse gain 10, 20 and 40

Radioactive source	^{90}Sr		
Radioactivity concentration (Bq/g)	10.04		
Coarse gain	10	20	40
Background count rate (cps)	7.60 ± 0.23	7.97 ± 0.19	15.26 ± 0.19
Total count rate (cps)	33.05 ± 0.12	58.75 ± 0.10	106.94 ± 0.19

Table 46 shows the MDA according to the measurement time derived by each gain using the measured background radioactivity and detection efficiency.

Table 46 Derived MDA according to measurement time per coarse gain for ^{90}Sr 10.04 Bq/g

Coarse gain 10		Coarse gain 20		Coarse gain 40	
Time (sec)	Radioactivity concentration (Bq/g)	Time (sec)	Radioactivity concentration (Bq/g)	Time (sec)	Radioactivity concentration (Bq/g)
1	**6.12 ± 0.187**	**1**	**3.09 ± 0.074**	**1**	**1.71 ± 0.022**
10	1.94 ± 0.060	3	1.78 ± 0.043	2	1.21 ± 0.016
20	1.37 ± 0.042	5	1.38 ± 0.034	**3**	**0.99 ± 0.013**
30	1.12 ± 0.035	7	1.17 ± 0.028		
35	**1.04 ± 0.032**	**9**	**1.03 ± 0.025**		

The time required to derive the MDA of the injected source's intensity level and the MDA of 1/10th the intensity of the injected source is 1 and 35 s for coarse gain 10, 1 and 9 s for coarse gain 20, and 1

and 3 s for coarse gain 40, respectively. Figure 68 shows the trend for the measurement result. The higher the radioactivity concentration and the higher the coarse gain, the lower is the MDA obtained. When the radioactivity concentration is 10.04 Bq/g, in all cases of coarse gain, the MDA of the injected radioactivity concentration level can be derived with only one second of measurement time. In addition, in all cases of coarse gain, the time required to derive an MDA of 1/10th the intensity of the injected source is confirmed to be less than 35 s.

Figure 68 Trends about derived radioactivity concentration according to the change of coarse gain and detection time for ^{90}Sr 10.04 Bq/g

Linearity tests are performed to evaluate the experimental results with changes in radioactivity concentration and coarse gain of the main amplifier. The detection result changes according to each amplification degree and the source concentration are confirmed. The measured results are graphed and R^2 values are derived. A linearity test for coarse gains 10, 20, and 40 are shown in Figure 69–Figure 71. In the case of coarse gain 10, the R^2 value is derived as 0.9998. In case of coarse gain 20, the R^2 value is 0.9992, and at coarse gain 40, it is 0.9954. In case of ^{90}Sr, the experiment is performed according to

the amplification degree and the radioactivity concentration. The measurement characteristics obtained according to the amplification degree are used for the radioactivity analysis.
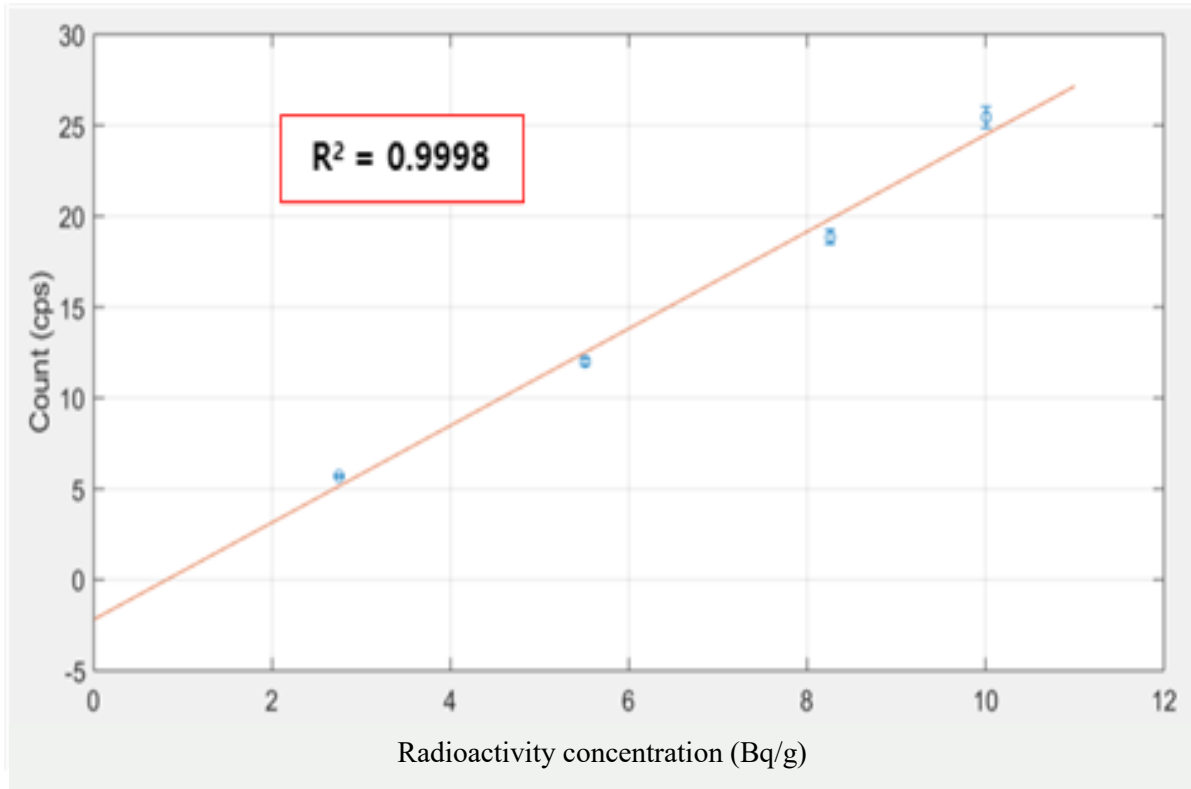
Figure 69 Linearity test for ^{90}Sr source of coarse gain 10
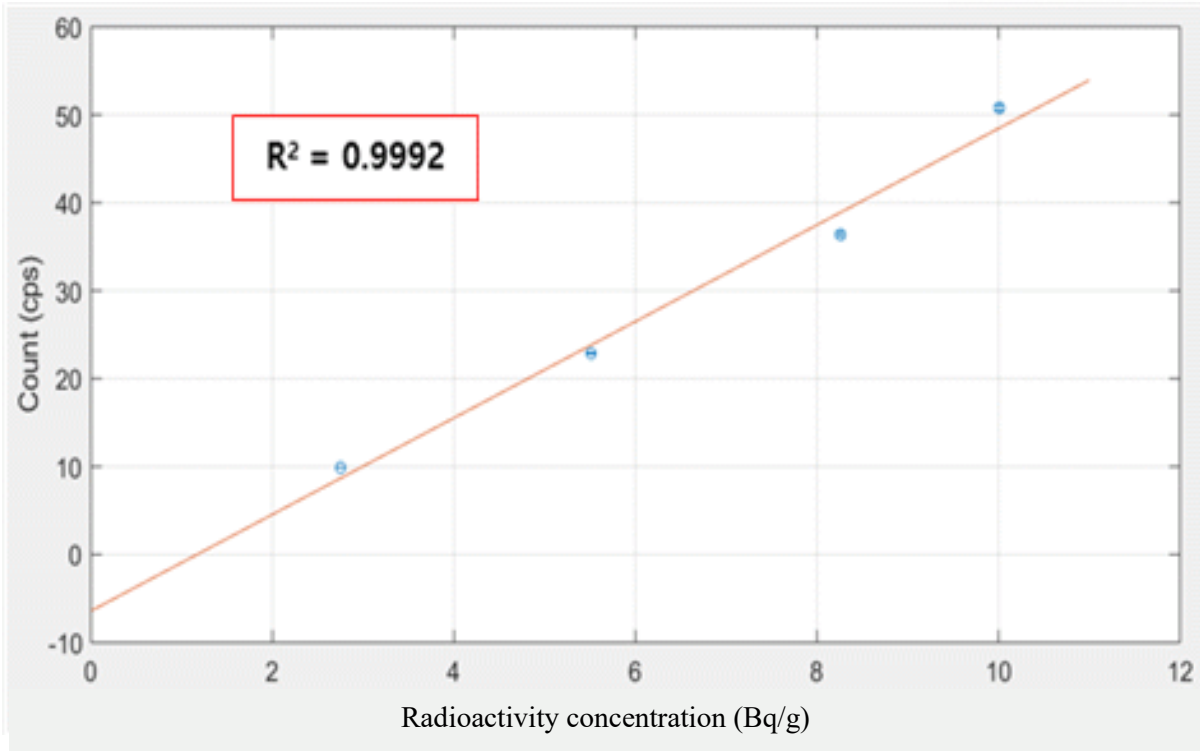
Figure 70 Linearity test for ^{90}Sr source of coarse gain 20
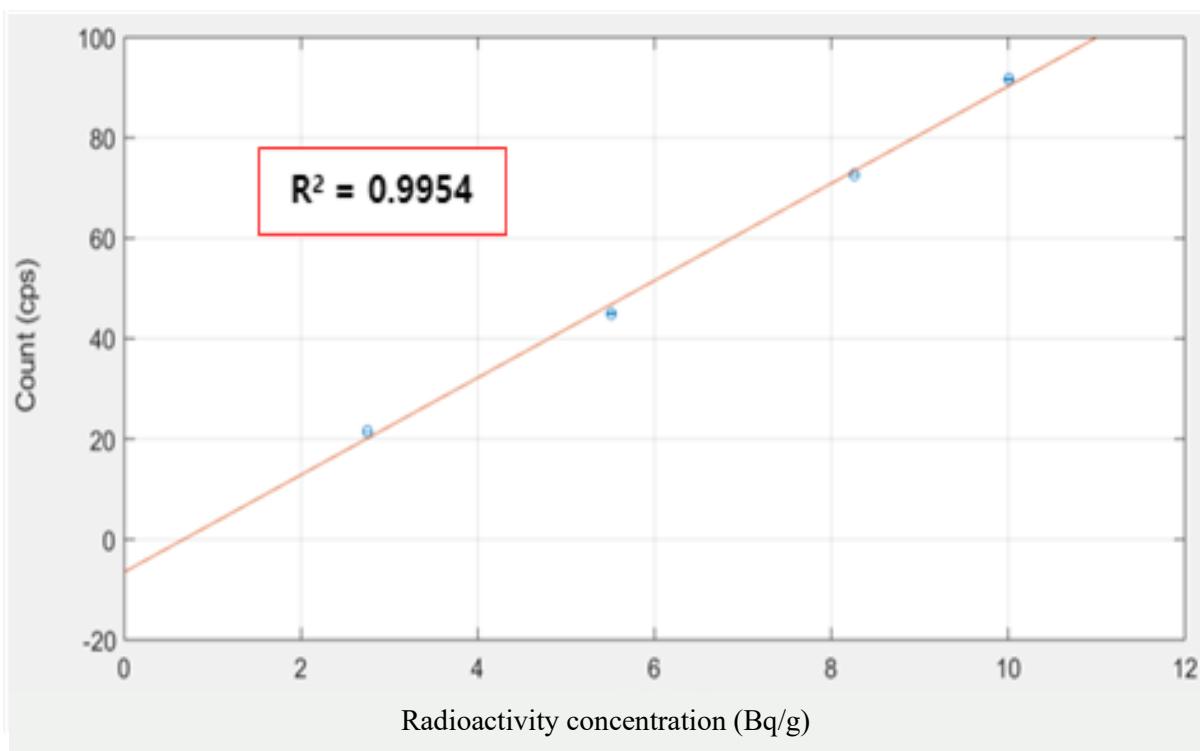
Figure 71 Linearity test for ^{90}Sr source of coarse gain 40

In case of ^{3}H, experiments are performed for concentrations of 253,206 Bq/g, 506,413 Bq/g, 759,620Bq/g, and 1,012,827 Bq/g. Table 47 shows the background and total count rates of ^{3}H 253,206 Bq/g at coarse gains 10, 20, and 40.

Table 47 Background and total count rate of ^{3}H 253,206 Bq/g at coarse gain 10, 20 and 40

Radioactive source	^{3}H		
Radioactivity concentration (Bq/g)	253,206		
Coarse gain	10	20	40
Background count rate (cps)	7.19 ± 0.12	9.59 ± 0.19	15.36 ± 0.17
Total count rate (cps)	8.83 ± 0.10	11.58 ± 0.11	50.6 ± 0.18

Table 48 shows the MDA according to the measurement time derived by each gain using the measured background radioactivity and detection efficiency in case of 253,206 Bq/g of ^{3}H.

Table 48 Derived MDA according to measurement time per coarse gain for ^{3}H 253,206 Bq/g

Coarse gain 10		Coarse gain 20		Coarse gain 40	
Time (sec)	Radioactivity concentration (Bq/g)	Time (sec)	Radioactivity concentration (Bq/g)	Time (sec)	Radioactivity concentration (Bq/g)
90	**252,730 ± 5,098**	**61**	**252,991 ± 5,559**	**20**	**24,950 ± 291**
3000	43,774 ± 883	1000	62,484 ± 1,373	100	11,158 ± 130
4000	37,909 ± 765	2000	44,183 ± 971	1000	3,528 ± 42
5000	33,907 ± 684	3000	36,075 ± 793	1200	3,221 ± 38
6000	30,953 ± 625	4000	31,242 ± 687	1400	2,982 ± 35
7000	28,656 ± 578	5000	27,943 ± 614	1600	2,789 ± 33
8000	26,806 ± 541	6000	25,509 ± 561	1800	2,629 ± 31
9000	**25,273 ± 510**	**6100**	**25,299 ± 556**	**2000**	**2,495 ± 30**

The time required to derive the MDA of the injected source intensity level and that of 1/10th the intensity of the injected source is 90 and 9,000 s for coarse gain 10, 61 and 6,100 s for coarse gain 20, and 20 and 2,000 s for coarse gain 40, respectively.

The radioactivity concentration of tritium is much higher than that of ^{90}Sr, but the time required to reach the MDA is much longer. In the case of tritium, the detection efficiency is lower than that of ^{90}Sr. The Figure 72 shows the trend for the measurement result: the higher the radioactivity concentration and the higher the coarse gain, the lower is the MDA obtained.
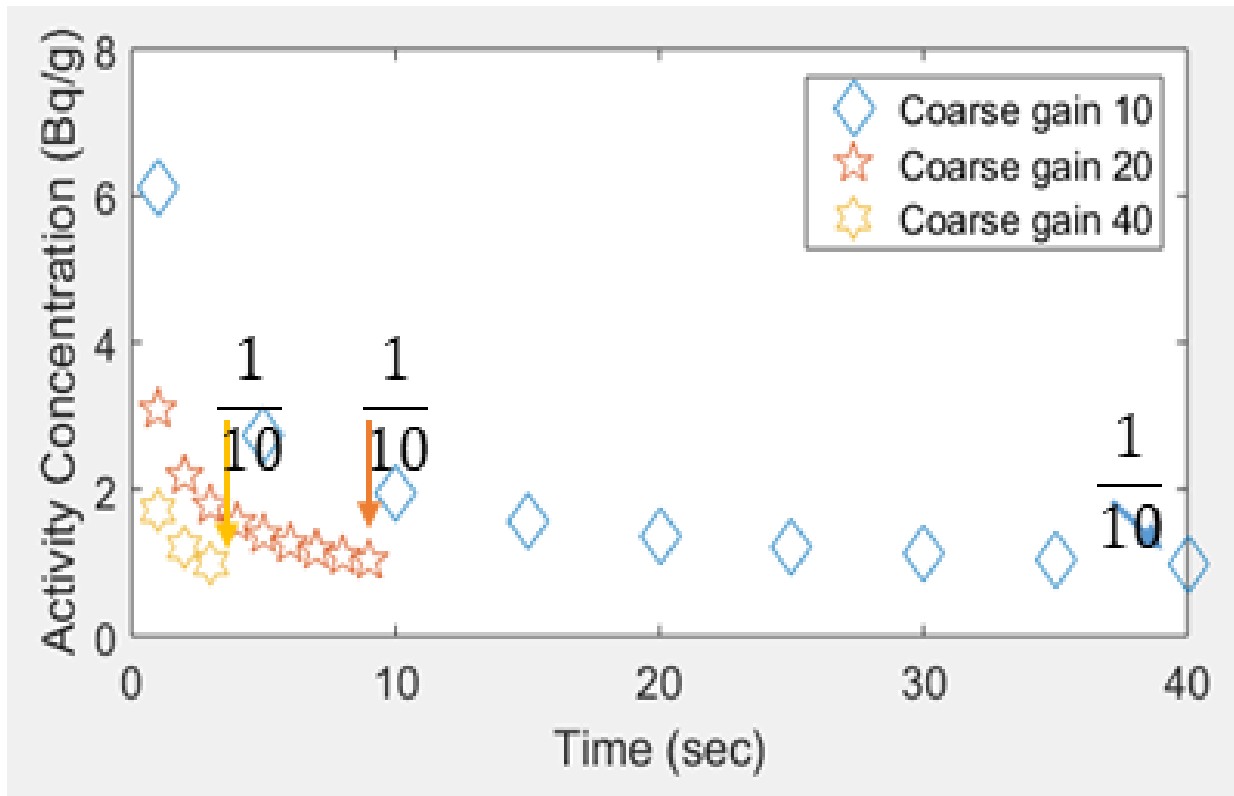

Figure 72 Trends about derived radioactivity concentration according to the change of coarse gain and detection time for ^{3}H 253,206 Bq/g

Table 49 shows the background and total count rates of ^{3}H 506,413 Bq/g at coarse gains 10, 20, and 40. The background level is similar to that in the previous experiment, but the value of the total count rate is increased.

Table 49 Background and total count rate of ^{3}H 506,413Bq/g at coarse gain 10, 20 and 40

Radioactive source	^{3}H		
Radioactivity concentration (Bq/g)	506,413		
Coarse gain	10	20	40
Background count rate (cps)	7.40 ± 0.15	9.80 ± 0.18	15.26 ± 0.14
Total count rate (cps)	11.09 ± 0.12	16.32 ± 0.16	111.50 ± 0.26

Table 50 shows the MDA according to the measurement time derived by each gain using the measured background radioactivity and detection efficiency.

Table 50 Derived MDA according to measurement time per coarse gain for ^{3}H 506,413 Bq/g

Coarse gain 10		Coarse gain 20		Coarse gain 40	
Time (sec)	Radioactivity concentration (Bq/g)	Time (sec)	Radioactivity concentration (Bq/g)	Time (sec)	Radioactivity concentration (Bq/g)
18	**$502,332 \pm 11,543$**	**6**	**$492,413 \pm 10,253$**	**1**	**$81,714 \pm 950$**
1000	$67,394 \pm 1,549$	10	$381,422 \pm 7,942$	2	$57,780 \pm 672$
1200	$61,522 \pm 1,414$	100	$120,616 \pm 2,512$	**3**	**$47,177 \pm 549$**
1400	$56,959 \pm 1,309$	300	$69,637 \pm 1,450$		
1600	$53,280 \pm 1,225$	500	$53,941 \pm 1,124$		
1800	**$50,233 \pm 1,155$**	**600**	**$49,241 \pm 1,026$**		

The time required to derive the MDA of the injected source's intensity level and the MDA of 1/10th the intensity of the injected source is 18 and 1,800 s for coarse gain 10, 6 and 600 s for coarse gain 20, and 1 and 3 s for coarse gain 40, respectively. Figure 73 shows the trend for the measurement result. The

116

higher the concentration of radioactivity concentration and the higher the coarse gain, the lower is the MDA obtained. When the radioactivity concentration is 506,413 Bq/g and the coarse gain is 40, the MDA of the injected radioactivity concentration level can be derived with only one second of measurement time.

Figure 73 Trends about derived radioactivity concentration according to the change of coarse gain and detection time for ^{3}H 506,413 Bq/g

Table 51 shows the background and total count rates of ^{3}H 759,620 Bq/g at coarse gains 10, 20, and 40. The background level is similar, but the value of the total count rate is increased compared to the previous data.

Table 51 Background and total count rate of ^{3}H 759,620 Bq/g at coarse gain 10, 20 and 40

Radioactive source	^{3}H		
Radioactivity concentration (Bq/g)	759,620		
Coarse gain	10	20	40
Background count rate (cps)	7.19 ± 0.14	10.07 ± 0.15	14.99 ± 0.22
Total count rate (cps)	13.22 ± 0.14	25.28 ± 0.18	154.01 ± 0.28

Table 52 shows the MDA according to the measurement time derived by each gain using the measured background radioactivity and detection efficiency.

Table 52 Derived MDA according to measurement time per coarse gain for ^{3}H 759,620 Bq/g

Coarse gain 10		Coarse gain 20		Coarse gain 40	
Time (sec)	Radioactivity concentration (Bq/g)	Time (sec)	Radioactivity concentration (Bq/g)	Time (sec)	Radioactivity concentration (Bq/g)
7	**739,398 ± 16,389**	**1**	**775,560 ± 12,805**	**1**	**84,853 ± 987**
100	195,626 ± 4,337	10	245,253 ± 4,050	**2**	**60,000 ± 698**
250	123,724 ± 2,743	100	77,556 ± 1,281		
400	97,813 ± 2,169	102	76,791 ± 1,268		
550	83,415 ± 1,849	104	76,049 ± 1,256		
700	**73,939 ± 1,639**	**106**	**75,329 ± 1,244**		

The time required to derive the MDA of the injected source's intensity level and the MDA of 1/10th the intensity of the injected source is 7 and 700 s for coarse gain 10, 1 and 106 s for coarse gain 20, and 1 and 2 s for coarse gain 40, respectively. Figure 74 shows the trend for the measurement result. The

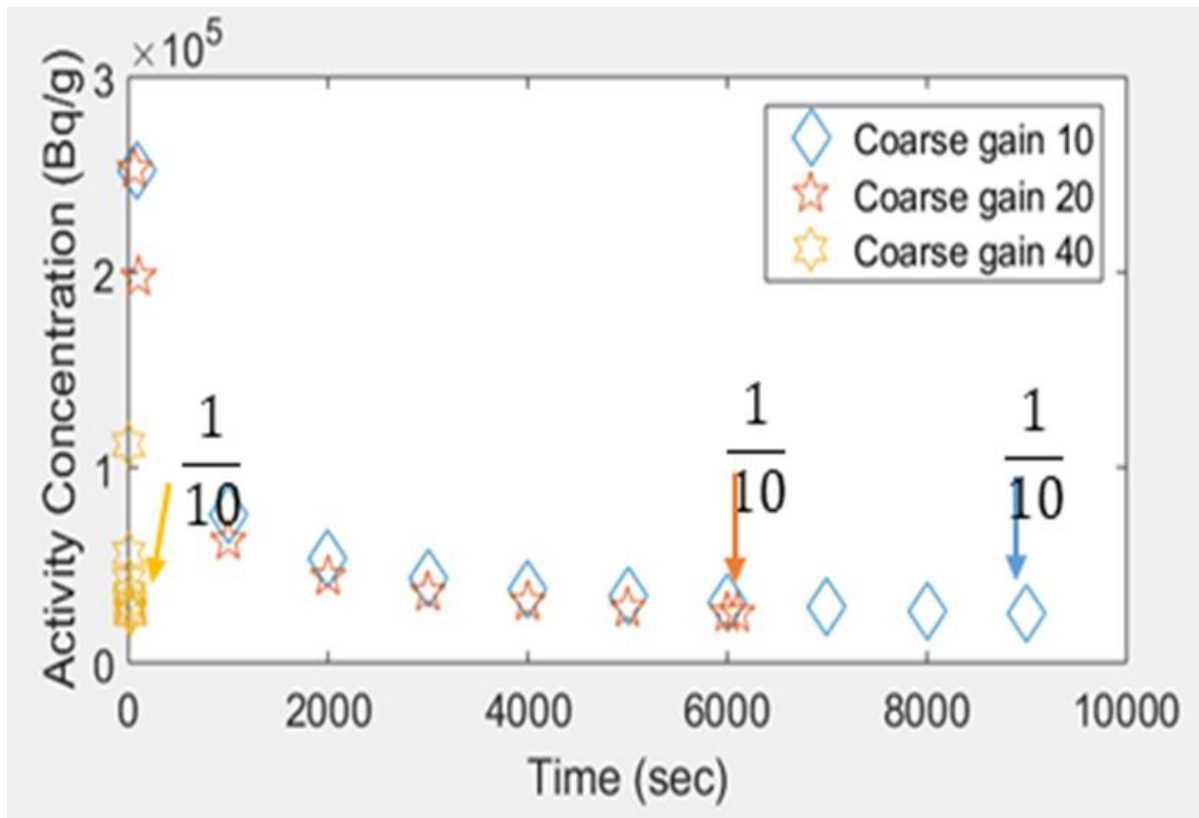higher the radioactivity concentration and the higher the coarse gain, the lower is the MDA obtained. In the case of tritium, the time required for obtaining the MDA is very low at coarse gain 40 because the radioactivity concentration is high enough. In the case of coarse gain 20, the MDA can be derived in ~100 s. In the case of coarse gain 10, the MDA derivation requires much more time.

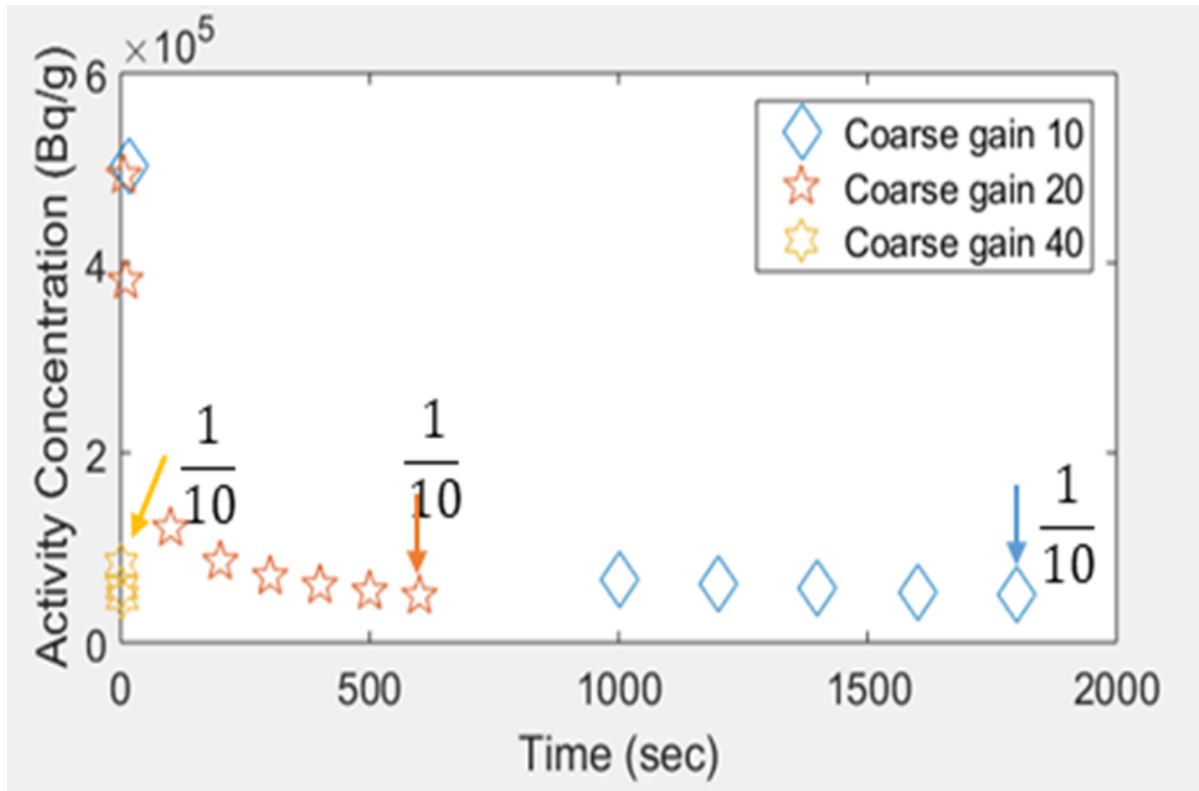**Figure 74** Trends about derived radioactivity concentration according to the change of coarse gain and detection time for ^{3}H 759,620 Bq/g

Table 53 shows the background and total count rates of ^{3}H 1,012,827 Bq/g at coarse gains 10, 20, and 40. The background level is also similar, but the value of the total count rate is increased compared to the previous data.

Table 53 Background and total count rate of ^{3}H 1,012,827 Bq/g at coarse gain 10, 20 and 40

Radioactive source	^{3}H		
Radioactivity concentration (Bq/g)	1,012,827		
Coarse gain	10	20	40
Background count rate (cps)	7.13 ± 0.14	10.09 ± 0.21	14.33 ± 0.18
Total count rate (cps)	15.18 ± 0.18	35.95 ± 0.23	199.12 ± 0.19

Table 54 shows the MDA according to the measurement time derived by each gain using the measured background radioactivity and detection efficiency in case of 1,012,827 Bq/g of ^{3}H.

Table 54 Derived MDA according to measurement time per coarse gain for ^{3}H 1,012,827 Bq/g

Coarse gain 10		Coarse gain 20		Coarse gain 40	
Time (sec)	Radioactivity concentration (Bq/g)	Time (sec)	Radioactivity concentration (Bq/g)	Time (sec)	Radioactivity concentration (Bq/g)
4	**976,916 ± 22,409**	**1**	**608,211 ± 13,244**	**1**	**85,117 ± 990**
100	195,383 ± 4,482	10	192,333 ± 4,188	**2**	**60,186 ± 700**
150	159,529 ± 3,660	20	136,000 ± 2,962		
200	138,156 ± 3,170	30	111,043 ± 2,418		
300	112,804 ± 2,588	**40**	**96,166 ± 2,094**		
350	104,436 ± 2,396				
400	**97,691 ± 2,241**				

The time required to derive the MDA of the injected source's intensity level and that of 1/10th the intensity of the injected source is 4 and 400 s for coarse gain 10, 1 and 40 s for coarse gain 20, and 1 and 2 s for coarse gain 40, respectively. Figure 75 shows the trend for the measurement result. The higher

120

the radioactivity concentration and the higher the coarse gain, the lower is the MDA obtained. In the case of tritium, the time to reach the target MDA still take 400 s or more at coarse gain 10. In addition, it is confirmed that amplifying the output signal sufficiently affects the measurement. It has been found that there is much benefit in terms of measurement time at coarse gain above 40.
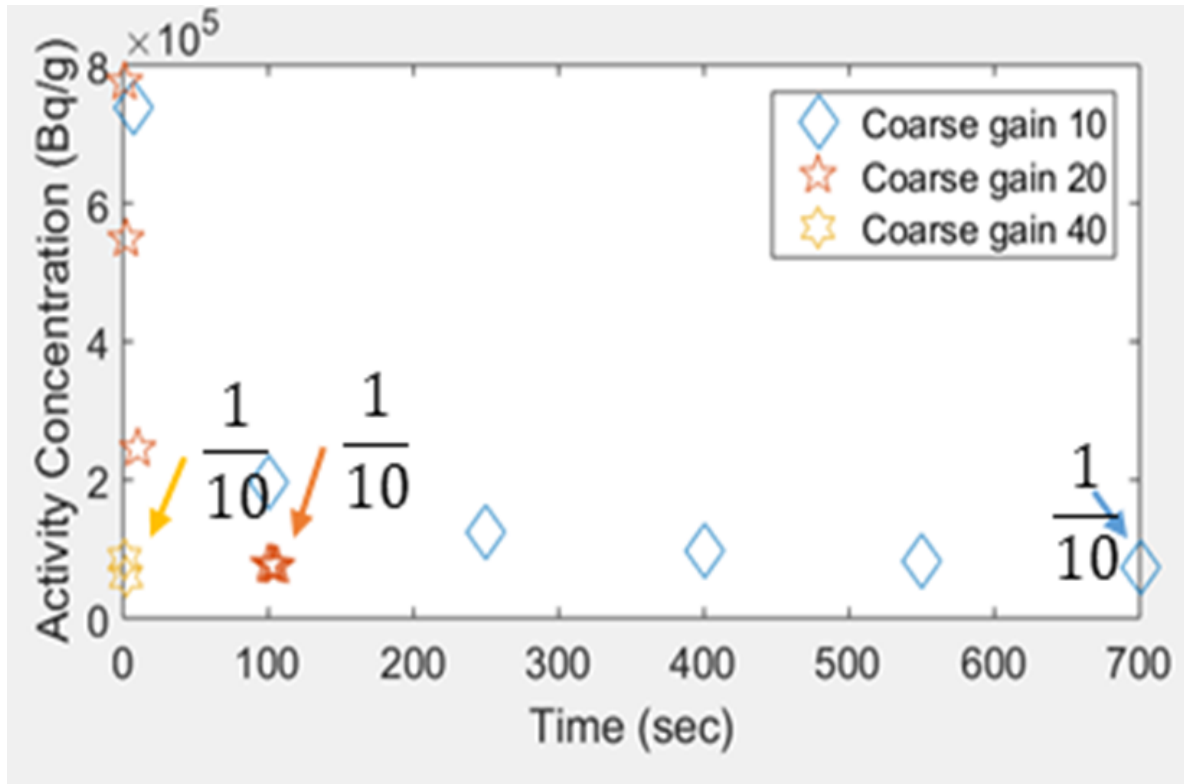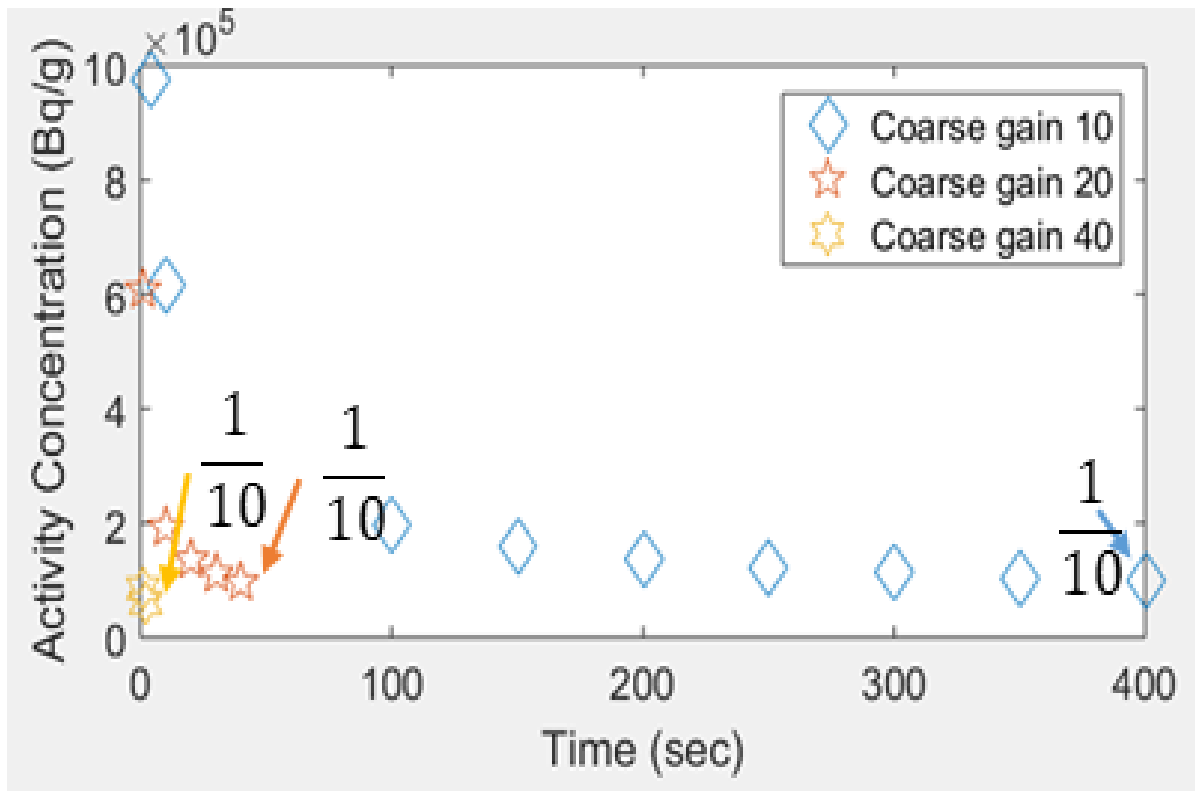

Figure 75 Trends about derived radioactivity concentration according to the change of coarse gain and detection time for ^{3}H 1,012,827 Bq/g

Linearity tests are performed to evaluate the experimental results with changes in radioactivity concentration and coarse gain of the main amplifier. The detection result changes according to each amplification degree and source concentration are confirmed. The measured results are graphed and R^2 values are derived. The linearity test for coarse gains 10, 20, and 40 are shown in Figure 76–Figure 78. In the case of coarse gain 10, it is confirmed that the R^2 value is derived as 0.9992. In case of coarse gain 20, the R^2 value is 0.9711, and at coarse gain 40, the value is 0.9934. In case of ^{3}H, the experiment is performed according to the amplification degree and the radioactivity concentration. The measurement characteristics according to the amplification degree are used for the radioactivity analysis.
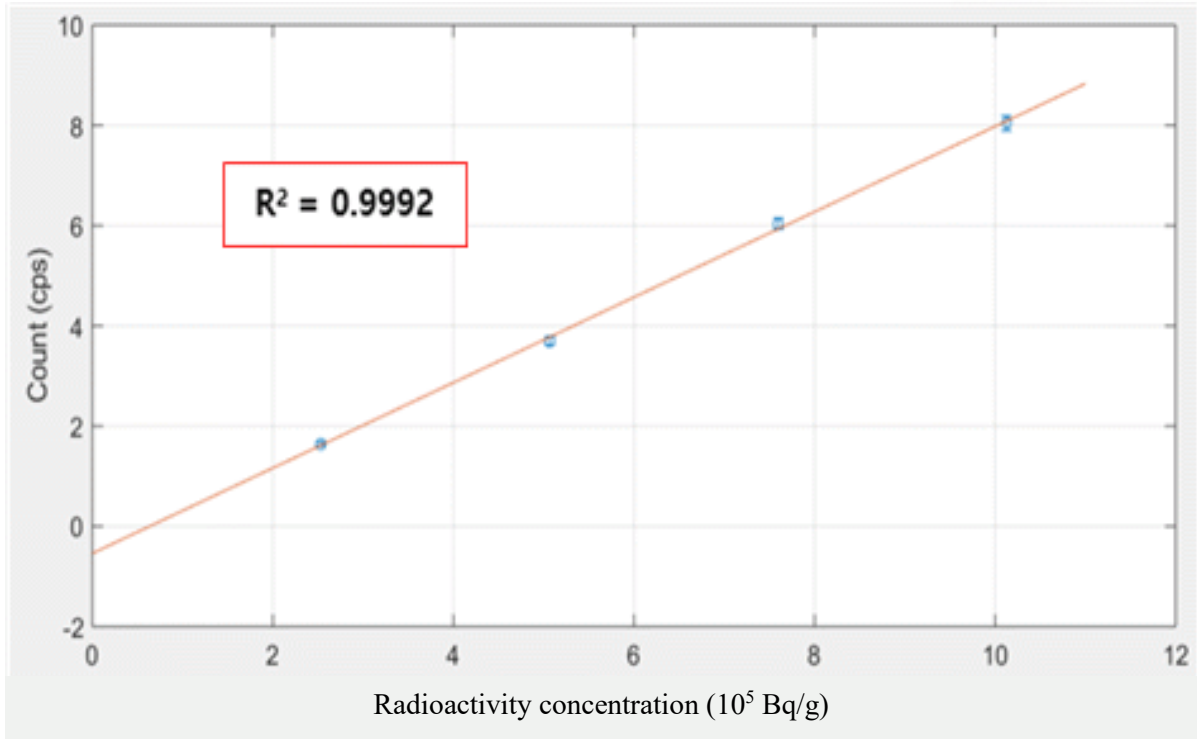
Figure 76 Linearity test for ^{3}H source of coarse gain 10
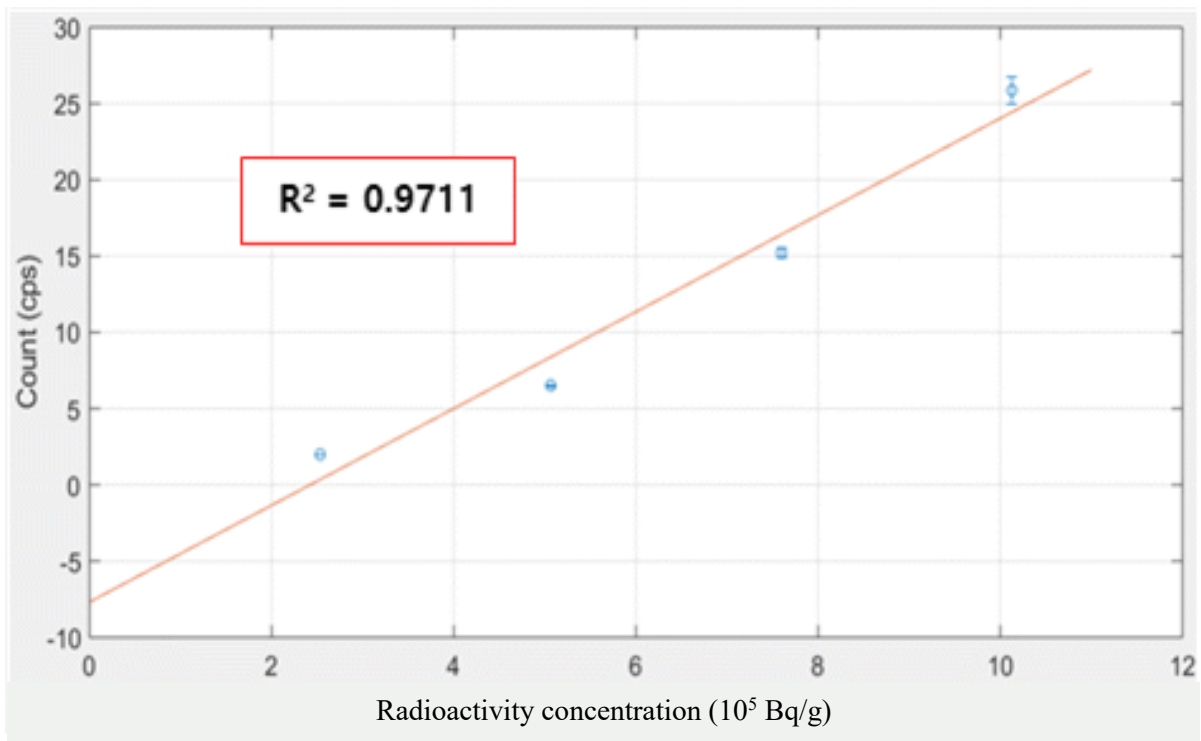
Figure 77 Linearity test for ^{3}H source of coarse gain 20
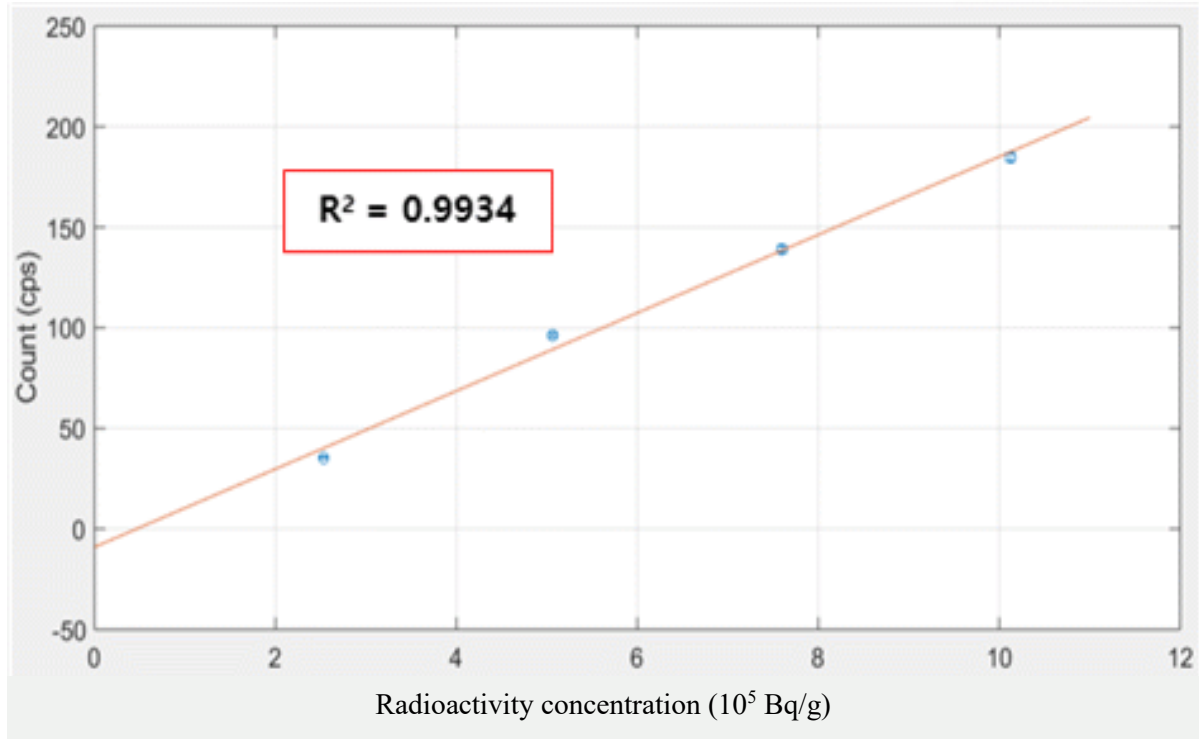
Figure 78 Linearity test for ^{3}H source of coarse gain 40

4.4 Optimization for detection condition for each radionuclide

The pretreated samples are analyzed considering beta energy. To select the amplification degree and number of scintillators suitable for tritium and strontium, the measurements according to the amplification degree of the main amplifier and 7 and 13 scintillators are performed. The MDA criteria for tritium and strontium are established and the detection conditions for the analysis that can be measured in the field are derived. The information of the source used in the experiment is shown in Table 55. Experiments are proceeded in the shield box, as shown in Figure 79.

Table 55 Source information used in efficiency calculation experiment

	^{3}H	^{90}Sr
Density (g/cm^3)	1.004E+00	1.002E+00
Radioactivity concentration (Bq/g)	3.575E+05	3.777E+00
Volume of input source (ml)	1.800E+01	7.000E+00
Mass of input source (g)	1.807E+01	7.013E+00
Radioactivity (Bq)	6.460E+06	2.649E+01
Mass of prepared sample (kg)	1.800E+00	1.800E+00
Volume of prepared sample (L)	1.805E+00	1.805E+00
Radioactivity concentration of sample (Bq/L)	3.579E+06	1.467E+01

Figure 79 Detection preparation with detection chamber, light guide, and PMT in lead shield

The detection chamber uses 7 and 13 scintillators. The used amplifications are 10, 20, 40, and 100 for coarse gain and 2.5, 6.5, 10.5, and 12.5 for fine gain.

For tritium and strontium, the trend of the measurement efficiency according to the amplification degree of the main amplifier with cases of 7 and 13 scintillators is determined. The product of fine gain and coarse gain is defined as total amplification, and the measurement efficiency according to the total amplification is defined. In the cases of tritium and strontium, the measurement efficiency is determined. The results are shown in the table and the trend is shown in the figure.

In both cases of tritium and strontium, the point where the measurement efficiency increases drastically is checked. All measured values increase rapidly at the maximum fine gain of 12.5. The values of fine gain 12.5 are excluded in both cases. Appropriate amplification of each radionuclide should be derived based on the efficiency changes according to the total amplification. Negative values or values greater than 1 are not applicable as efficiency values are excluded. In addition, the MDA derivation is not related to efficiency alone, so the amplification degree and the number of scintillators for tritium and strontium are also derived considering the background radiation level.
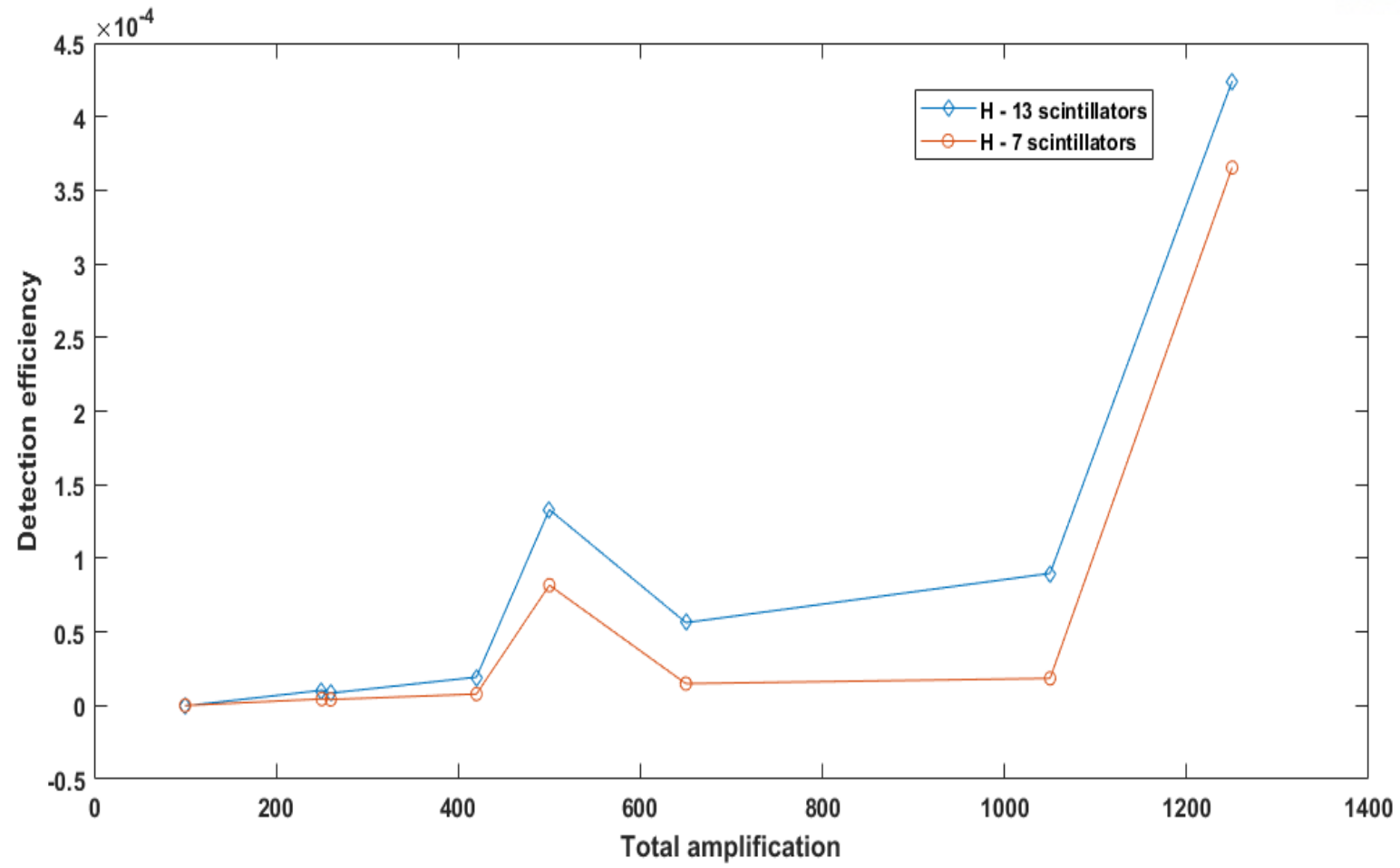
Figure 80 Detection efficiency trend with total amplification in case of tritium sample
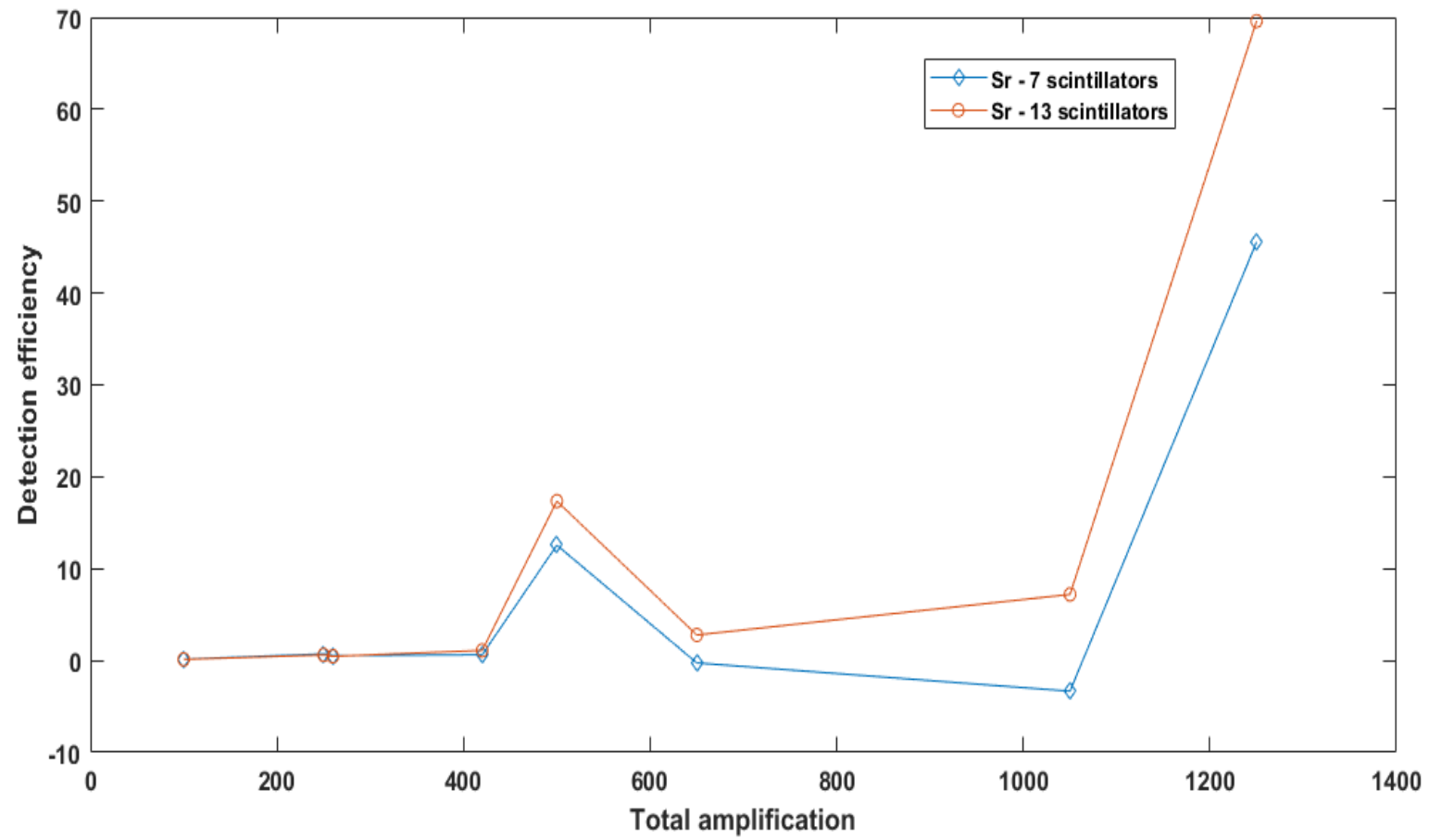
Figure 81 Detection efficiency trend with total amplification in case of strontium sample

Table 56 Detection efficiency of tritium and strontium with 7 scintillators

Detection efficiency of 7 scintillators							
Coarse gain	40				100			
Fine gain	2.5	6.5	10.5	12.5	2.5	6.5	10.5	12.5
^{3}H	5.83E-08	4.12E-06	7.82E-06	8.17E-05	4.45E-06	1.49E-05	1.85E-05	3.65E-04
^{90}Sr	1.51E-01	5.34E-01	6.28E-01	1.26E+01	7.22E-01	-2.59E-01	-3.33E+00	4.55E+01

Table 57 Detection efficiency of tritium and strontium with 13 scintillators

Detection efficiency of 13 scintillators							
Coarse gain	40				100			
Fine gain	2.5	6.5	10.5	12.5	2.5	6.5	10.5	12.5
^{3}H	-2.26E-07	8.46E-06	1.93E-05	1.33E-04	1.03E-05	5.63E-05	8.98E-05	4.24E-04
^{90}Sr	1.29E-01	4.61E-01	1.11E+00	1.74E+01	6.12E-01	2.78E+00	7.19E+00	6.96E+01

4.4.1 Considerations for ^{3}H

In order to derive measurement conditions suitable for tritium, a detection chambers using 7 scintillators and 13 scintillators are used. Various gains are applied. Simply high detection efficiency cannot be considered appropriate in the aspect of MDA. The measurement conditions of tritium were selected by deriving MDA for each measurement condition. The measured background radiation and count rate of tritium source are shown in the Table 58 and Table 59.

Table 58 Measured count rate for background radation and ^{3}H with 7 scintillators and various amplifications

Count rate of 7 scintillators (cps)							
Coarse	40				100		
Fine	2.5	6.5	10.5	12.5	2.5	6.5	10.5	12.5
BKG	14.388	20.976	28.942	40.798	21.188	116.594	219.97	250.068
^{3}H	14.45	25.356	37.262	127.736	25.924	132.43	239.616	638.878

Table 59 Measured count rate for background radation and ^{3}H with 13 scintillators and various amplifications

Count rate of 13 scintillators (cps)							
Coarse	40				100		
Fine	2.5	6.5	10.5	12.5	2.5	6.5	10.5	12.5
BKG	23.268	29.218	37.412	51.204	29.3	125.546	236.556	326.684
^{3}H	23.044	37.614	56.568	183.3	39.558	181.416	325.662	747.52

The MDA is derived based on the measured values except for the fine gain 12.5 value and the negative efficiency for tritium, and the values are shown in the Table 60. In the case of tritium, the lower MDA is obtained under the higher the number of scintillators with same gain condition and the lower MDA is obtained under the higher gain condition with same the number of scintillators. In the case of tritium, high amplification and high number of scintillators are found to be advantageous for deriving low MDA. Therefore, tritium measurement is conducted with applying 13 scintillators, coarse gain 100 and fine gain 10.5.

Table 60 Derived MDA with different gain and the number of scintillators

MDA (Bq/g)						
Coarse gain	40			100		
Fine gain	2.5	6.5	10.5	2.5	6.5	10.5
7 scintillators	8.74E+04	1.38E+03	8.23E+02	1.28E+03	7.89E+02	8.72E+02
13 scintillators	-	7.22E+02	3.58E+02	5.92E+02	2.24E+02	1.92E+02

Linearity evaluation is performed to confirm the stability of the tritium application of the measurement system. In the case of tritium, the measurement is carried out according to five concentrations and the measurement results according to the source used are shown in the Table 61. The results of linearity test are also shown in Figure 82 and its R square values is 0.998. In both cases of tritium and ^{90}Sr, it is confirmed that the results of linearity test (R square vale) are nearly 1, and the analysis is performed according to the radioactivity concentration.

Table 61 Detection efficiency and source information of ^{3}H

^{3}H	5 ml	10 ml	15 ml	20 ml	25 ml
Volume of sample (L)	4.240E-01	4.240E-01	4.240E-01	4.240E-01	4.240E-01
Radioactivity (Bq)	8.430E+05	1.686E+06	2.529E+06	3.372E+06	4.215E+06
Net count rate (cps)	1.799E+01	3.723E+01	5.904E+01	8.159E+01	1.024E+02
Detection efficiency (%)	2.134E-03	2.208E-03	2.335E-03	2.420E-03	2.429E-03
Standard deviation (%)	6.028E-01	1.564E+00	1.495E+00	1.716E+00	1.938E+00
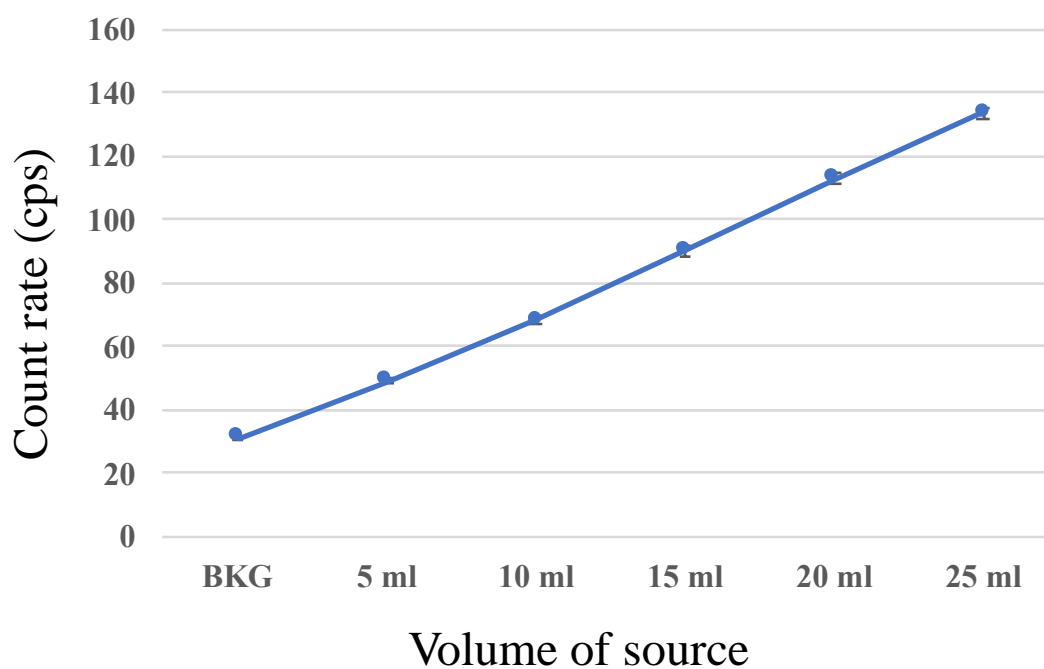
Figure 82 Linearity test about count rate and radioactivity concertation of ^{3}H

The time required to derive a MDA that satisfies the tritium-related standards under conditions of 13 scintillators, coarse gain 100 and fine gain 10.5 is calculated and the results are shown in the Table 62. 2,300 seconds are needed to satisfy 40 Bq/g of the effluent concentration level, and it is confirmed that tritium can be quickly monitored with a value within an hour.

Table 62 Required time for satisfying target standards of tritium

MDA	Required time	Standard
740 Bq/g	7 sec	Derived annual intake limit of drinking water
74 Bq/g	680 sec	1/10 of derived annual intake limit of drinking water
40 Bq/g	2,300 sec	Effluent concentration level

4.4.2 Considerations for ^{90}Sr

^{90}Sr is also measured by applying 7 and 13 scintillator-based detection chamber and various fine and coarse gains. The measured values of efficiency are shown in the Table 63. Negative values, greater than 1 value that could not be defined by the efficiency and the value at fine gain 12.5 are excluded. In the case of coarse gain 40, 7 scintillators show higher efficiency than 13 scintillators. In coarse gain 100, only fine 2.5 is applicable, and the efficiency of 7 scintillators is higher.

Table 63 Measured efficiency of ^{90}Sr with 7 and 13 scintillators

Coarse gain	40			
Fine gain	2.5	6.5	10.5	12.5
7 scintillators	1.51E-01	5.34E-01	6.28E-01	1.26E+01
13 scintillators	1.29E-01	4.61E-01	1.11E+00	1.74E+01
Coarse gain	100			
Fine gain	2.5	6.5	10.5	12.5
7 scintillators	7.22E-01	-2.59E-01	-3.33E+00	4.55E+01
13 scintillators	6.12E-01	2.78E+00	7.19E+00	6.96E+01

In order to determine the detection environment of strontium, the time and efficiency of deriving the MDA of 0.1 Bq/g is confirmed. The Table 64 shows the results for 7 scintillators and the Table 65 shows the results for 13 scintillators.

Table 64 Required efficiency for satisfying 0.1 Bq/g of MDA with 7 scintillators

7 scintillators				
Coarse	40			100
Fine	2.5	6.5	10.5	2.5
1 sec	4.80E+01	5.66E+01	6.54E+01	**5.69E+01**
2 sec	3.26E+01	**3.87E+01**	**4.49E+01**	3.89E+01
3 sec	2.61E+01	3.11E+01	3.62E+01	3.13E+01
4 sec	2.24E+01	2.67E+01	3.11E+01	2.68E+01
5 sec	1.99E+01	2.37E+01	2.77E+01	2.39E+01
6 sec	1.80E+01	2.16E+01	2.52E+01	2.17E+01
7 sec	1.66E+01	1.99E+01	2.32E+01	2.00E+01
8 sec	1.55E+01	1.86E+01	2.17E+01	1.86E+01
9 sec	**1.46E+01**	1.75E+01	2.04E+01	1.75E+01
10 sec	1.38E+01	1.65E+01	1.93E+01	1.66E+01
Efficiency	1.51E+01	5.34E+01	6.28E+01	7.22E+01

Seven scintillators are found to be able to derive an MDA of less than 0.1 Bq/g in one or two seconds except for coarse gain 40 and fine gain 2.5. It is also confirmed that the target MDA can be reached within 1 second under the conditions of coarse gain 100 with fine gain 2.5.

Table 65 Required efficiency for satisfying 0.1 Bq/g of MDA with 13 scintillators

13 scintillators			
coarse	40		100
Fine	2.5	6.5	2.5
1	5.93E+01	**6.57E+01**	6.58E+01
2	4.06E+01	4.51E+01	**4.52E+01**
3	3.27E+01	3.64E+01	3.64E+01
4	2.80E+01	3.12E+01	3.13E+01
5	2.49E+01	2.78E+01	2.78E+01
14	1.46E+01	1.63E+01	1.63E+01
15	1.41E+01	1.57E+01	1.58E+01
16	1.36E+01	1.52E+01	1.52E+01
17	1.32E+01	1.48E+01	1.48E+01
18	**1.28E+01**	1.43E+01	1.43E+01
Efficiency	1.29E+01	4.61E+01	6.12E+01

Detection chamber with 13 scintillators is found to be able to derive an MDA of less than 0.1 Bq/g in one or two seconds except for coarse gain 40 with fine gain 2.5. 13 In the case of measurement using 13 scintillators, all possible amplification degrees can be applied to 7 scintillator-based detection chamber, and when the same amplification degrees, the seven detection chamber has higher efficiency and less time to reach the target MDA. Therefore, in case of ^{90}Sr, 7 scintillator-based detection chamber are used, and the values of coarse gain 100 and fine gain 2.5 that have the highest efficiency are applied.

In order to analyze the ^{90}Sr using the constructed system, a linearity test between source concentration and counting rate is conducted to evaluate the quantification of the system. In the case of ^{90}Sr, the measurement is carried out according to three concentrations and the measurement results according to the source used are shown in the Table 66. The results of linearity test are also shown in Figure 83 and its R square values is 0.991.

Table 66 Detection efficiency and source information of ^{90}Sr

^{90}Sr	6 ml	12 ml	18 ml
Volume of sample (L)	4.240E-01	4.240E-01	4.240E-01
Radioactivity (Bq)	5.348E+00	1.070E+01	1.604E+01
Net count rate (cps)	1.769E+00	3.193E+00	5.485E+00
Detection efficiency (%)	3.309E+01	2.985E+01	3.419E+01
Standard deviation (%)	2.789E-01	3.771E-01	2.578E-01
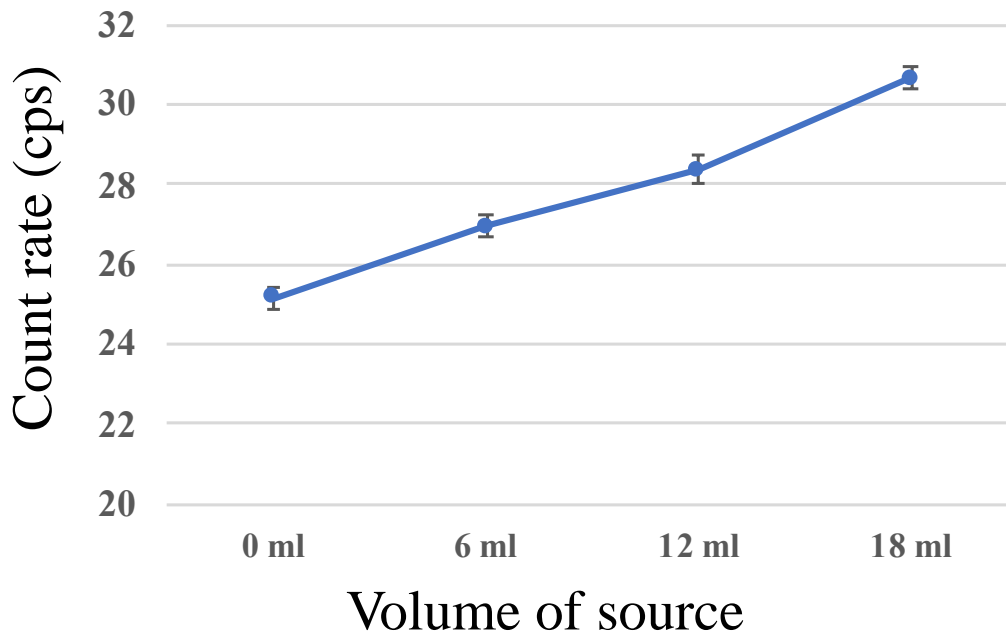
Figure 83 Linearity test about count rate and radioactivity concertation of ^{90}Sr

The time required to derive a MDA that satisfies the ^{90}Sr-related standards under conditions of 7 scintillators, coarse gain 100 and fine gain 2.5 is calculated and the results are shown in the Table 67. 18 seconds are needed to satisfy 0.02 Bq/g of the effluent concentration level. Furthermore, 1,750 seconds are needed to satisfy 1/10 of effluent concentration level MDA. This system can be applied rapid monitoring for ^{90}Sr in water.

Table 67 Required time for satisfying target standards of ^{90}Sr

MDA	Required time	Standard
0.1 Bq/g	1 sec	1/10 of clearance level
0.02 Bq/g	18 sec	Effluent concentration level
0.002 Bq/g	1,750 sec	1/10 of effluent concentration level

5. Conclusions

A study is conducted to establish a system for detecting beta nuclides in water samples, such as groundwater and seawater, around nuclear facilities. To detect short beta nuclides in the water samples, a detection part, where the water sample and scintillator directly contact each other, is designed. An efficient detection system is constructed using a plastic scintillator-based coincidence circuit. To construct the measurement system, a simulation of the amount of water sample, thickness of the scintillator, and the reaction cross-sectional area is performed to optimize the measurement system.

In addition, to secure the field applicability of the established measurement system, a pretreatment system is installed to remove components such as floating thongs and ions in the water sample. A system for extracting pure water using an ion-exchange resin and a membrane filter is constructed.

Using the constructed system, ^{3}H and ^{90}Sr nuclides are used to evaluate the measurement effects of flow rate, amplification degree of main amplifier, and radioactivity concentration. In addition, analytical methods have been applied, especially for the analysis of tritium with extremely low energy. The characteristics of ^{3}H and ^{90}Sr according to the amplification degree of the main amplifier are analyzed so that effective measurement could be performed by applying the measurement conditions for each radionuclide. The detection condition for ^{3}H and ^{90}Sr is applied criteria that could satisfy effluent concentration level. Using the constructed system, ^{90}Sr and ^{3}H can be monitored with the MDA of effluent concentration level with the measurement time of 18 and 2,300 sec.

The system is expected to be used for monitoring beta nuclides, including tritium, in seawater and groundwater near nuclear decommissioning sites and nuclear facilities. In addition, it is expected to be used for tritium monitoring with improved efficiency, using additional pretreatments such as electrolysis, because the monitoring system is linked with the equipment for producing pure water.

References

[1] Coltman, J. W., &Marshall, F. H.. Photomultiplier radiation detector. Nucleonics , 1 (3), 58-64. (1947)

[2] 고성진, et al. 방사선 계측학. 2001.

[3] 서범경, et al. 알파 및 베타선 동시측정용 ZnS (Ag)/플라스틱 이중섬광체 검출센서 개발. 분석과학, 21.2: 117-122, (2008)

[4] 한국표준과학연구원, 측정불확도 표현 지침, (2010)

[5] Ortec Inc. "Model 556H High Voltage Power Supply Operating and Service Manual"

[6] Matsuyama, Masao. "Development of a new detection system for monitoring high-level tritiated water." Fusion Engineering and Design 83.10-12: 1438-1441, (2008)

[7] Kawano, T., T. Uda, T. Yamamoto, and H. Ohashi. "Tritium water monitoring system based on CaF2 flow-cell detector." Fusion Science and Technology 60, no. 3: 952-955, (2011)

[8] Tarancón, A., J. F. Garcıa, and G. Rauret. "Determination of beta emitters (90Sr, 14C and 3H) in routine measurements using plastic scintillation beads." Nuclear Instruments and Methods in Physics Research Section A: Accelerators, Spectrometers, Detectors and Associated Equipment 516, no. 2-3 : 602-609, (2004)

[9] Tkachuk, R. "A continuous flow beta scintillation detector for aqueous solutions." Canadian Journal of Chemistry 40, no. 12 : 2348-2356, (1962)

[10] HAMAMATSU, "Photomultiplier tube R878" www.hamamatsu.com

[11] Ortec Inc. "Model 855 Dual Spectroscopy Amplifier Operating and Service Manual"

[12] Ortec Inc. "Model 551 Timing Single-Channel Analyzer Operating and Service Manual"

[13] Ortec Inc. "EASY-MCA-8KTM EASY-MCA-2KTM Digital Gamma-Ray Spectrometer User's Manual"

[14] Ortec Inc. "Experiment 13, Gamma-Gamma Coincidence with Angular Correlation" www.ortec-online.com

[15] PASTERNACK, RF Adapters Technical Data Sheet (PE9336)

[16] PASTERNACK, RF Adapters Technical Data Sheet (PE9363)

[17] http://rarecomponents.com/store/1017, Search: 19-March-2018

[18] Saint-Gobain Crystals. "Organic Scintillation Materials", 2014

[19] ALAEI, Parham. Introduction to health physics. Medical Physics, 2008, 35.12: 5959-5959.

[20] CROFT, Stephen, et al. The Estimation of the Minimum Detectable Activity from Measured Passive Neutron Coincidence Counter Data. In: Proc. 46th Int. Symp. on Nuclear Material Management (INMM). 2005.

[21] O. Kuras, P. B. Wilkinson, P. I. Meldrum, et al. Sci. Total Environ. 566, 350 (2016).

[22] L. M. Robredo, T. Navarro, and I. Sierra. Appl. Radiation Isotopes 53, 345 (2000).

[23] G. Hemic. Journal Office de la Republique Française 4, 88 (1988).

[24] K. S. Jeong, K. W. Lee, and H. K. Lim. Annals Nuclear Energy 37, 1751 (2010).

[25] L. El-Guebaly. Nuclear Fusion 47, S485 (2007).

[26] K. Jeong, D. Lee, K. Lee, and H. Lim. Annals Nuclear Energy 35, 1954 (2008).

[27] H. El-Ghonemy, L. Watts, and L. Fowler. Environ Int. 31, 89 (2005).

[28] C. Bayliss, and K. Langley. Elsevier (2003).

[29] W. E. Lee, M. I. Ojovan, and C. M. Jantzen (Eds.). Elsevier (2013).

[30] K. S. Jeong, and H. K. Lim. Annals Nuclear Energy 36, 1639 (2009).

[31] P. D. Meyer, and G. W. Gee. Division of Risk Analysis and Applications, Office of Nuclear Regulatory Research, US Nuclear Regulatory Commission (1999).

[32] H. A. Berry. Reynolds Electrical and Engineering Co (1981).

[33] C. F. Holoway, J. P. Witherspoon, H. W. Dickson, P. M. Lantz, and T. Wright. Oak Ridge National Lab (1981).

[34] M. J. Hartman, W. D. Webber, and L. F. Morasch. United States Department of Energy (2006).

[35] L. M. Chirovsky, W. P. Lee, A. M. Sabbas, A. J. Becker, J. L. Groves, and C. S. Wu. Nuclear Instruments Methods Physics Res. 219, 103 (1984).

[36] B. F. Myasoedov, and E. G. Drozhko. J. Alloys Compounds 271, 216 (1998).

[37] T. Davinson, W. Bradfield-Smith, S. Cherubini, et al. Nuclear Instruments Methods Physics Res. Section A: Accelerators, Spectrometers, Detectors Associated Equipment 454, 350 (2000).

[38] X. Hou. Appl. Radiation Isotopes 62, 871 (2005).

[39] T. W. Burrows, and C. L. Dunford. In AIP Conference Proceedings 768, 582 (2005).

[40] M. Schubert, W. Buerkin, P. Pena, A. E. Lopez, and M. Balcázar. Radiation Meas. 41, 492 (2006).

[41] T. W. Bowyer, C. Schlosser, K. H. Abel, et al. J. Environ. Radioactivity 59, 139 (2002).

[42] G. Stephan, S. Pressl, G. Koshpessova, and B. I. Gusev. Radiation Res. 155, 796 (2001).

[43] G. Thoma, N. Esser, C. Sonntag, W. Weiss, J. Rudolph, and P. Leveque. In Isotope Hydrology (1978).

[44] A. Cremers, A. Elsen, P. De Preter, and A. Maes. Nature 335, 247 (1988).

[45] D. Beals, B. Crandall, and P. Fledderman. J. Radioanalytical Nuclear Chem. 243, 495 (2000).

[46] W. Deng, D. P. Morrison, K. L. Gale, and J. N. Lucas. Radiation Res. 150, 400 (1998).

[47] S. Krishnaswami, W. C. Graustein, K. K. Turekian, and J. F. Dowd. Water Resources Res. 18, 1663 (1982).

[48] S. Luo, T. L. Ku, R. Roback, M. Murrell, and T. L. McLing. Geochimica et Cosmochimica Acta 64, 867 (2000).

[49] N. A. Wogman, R. L. Brodzinski, and D. P. Brown. IEEE Trans. Nuclear Sci. 27, 733 (1980).

[50] O. Reistad, M. Dowdall, Ø. G. Selnaes, W. J. F. Standring, S. Hustveit, F. Steenhuisen, and A. Sørlie. J. Environ. Radioactivity 99, 1045 (2008).

[51] A. S. Beddar, T. R. Mackie, and F. H. Attix. Phys. Medicine Biology 37, 1883 (1992).

[52] N. R. Stanton. Ohio State Univ. Research Foundation (1971).

[53] L. Ovechkina, K. Riley, S. Miller, Z. Bell, and V. Nagarkar. Phys. Procedia 2, 161 (2009).

[54] S. I. Imai, S. Soramoto, K. I. Mochiki, T. Iguchi, and M. Nakazawa. Review Scientific Instruments 62, 1093 (1991).

[55] G. F. Knoll. John Wiley & Sons (2010).

[56] L. Archambault, T. M. Briere, F. Pönisch, L. Beaulieu, D. A. Kuban, A. Lee, and S. Beddar. Int. J. Radiation Oncology* Biology* Phys. 78, 280 (2010).

[57] W. G. Cross, C. G. Soares, S. Vynckier, and K. Weaver. J ICRU 4, (2004).

[58] M. H. Agnew. Phys. Rev. 77, 655 (1950).

[59] L. Li. Natick (2002).

Acknowledgement (감사의 글)

2010 년 시작한 UNIST 에서의 4 년간의 학부 생활과 6 년간의 대학원 생활이 이 짧은 글로 정리가 된다고 생각하니 시원 섭섭한 마음이 가득합니다. 강산도 변한다는 10 년의 시간동안 저라는 사람이 변할 수 있도록 저에게 도움을 주신 많은 분들께 이 글을 통하여 감사의 말씀을 전하려 합니다.

가장 먼저 김희령 교수님께 무한한 감사의 말씀을 드립니다. 의욕만 넘치던 학부생 시절부터 차근차근 적응할 수 있도록 진심 어린 관심과 조언으로 6 년간의 대학원 생활을 무탈하게 마무리할 수 있었습니다. 한편으로는 교수님의 기대만큼 좋은 성과를 이루지 못한 것 같아 죄송한 마음도 함께합니다. 교수님의 가르침을 항상 기억하며 성실하고 정직하게 연구하는 사람이 되도록 노력하겠습니다. 감사하고 존경합니다 교수님.

바쁘신 와중에 귀한 시간을 내주시고 저의 연구에 대하여 아끼지 않는 조언을 주신 이승준 교수님과 박재영 교수님께도 감사의 말씀을 드립니다. 또한 외부에서 울산이라는 먼 곳까지 오셔서 저의 연구에 대한 코멘트 주신 이근우 교수님과 홍상범 박사님께도 진심으로 감사의 말씀을 드립니다.

람다 랩 구성원 여러분들께도 감사의 말씀을 드립니다. 동생이고 후배지만 항상 배울 점이 있는 준우, 내 더러운 성격 받아주는 내 친구 충위, 랩장 일 넘겨 받아 고생하는 시형이랑 기준, 내 밑에서 일 배운다고 고생 많이 한 우년, 자기일 열심히 하는 찬기, 고생하는 신입생들 세원, 민지, 재훈 마지막으로 MHD 녀석들까지 고맙습니다.

졸업 준비하면서 가장 도움을 많이 주신 관윤이형 고맙습니다. 항상 두서없이 물어봐도 척하고 알아들으시고 도움 주셔서 정말 많은 도움이 되었습니다. 놀리는듯 그래도 항상 관심 주시는 한이형도 감사합니다. 저와 같은 아픔을 나눈 재선이형, 우린 행복해질거에요. 그리고 철민, 태원, 경찬, 오훈 사랑방 식구들도 고맙습니다.

저의 홈메이트 진수, 바리, 벼리에게도 감사의 말씀드립니다. 특히 진수는 최고의 홈메이트였어 덕분에 대학원생활 마무리 잘 할 수 있었다.

아들이 하는 선택에 대하여 무한히 존중해주시고 뒷바라지해주신 부모님께 감사의 말씀 올립니다. 그리고 자기일 묵묵히 잘하는 동생에게도 고맙습니다.

마지막으로 퍽퍽한 대학원 생활 비타민, 활력소, 윤활유 등등 여러 역할을 수행해주신 절세미녀 여자친구님께도 감사의 말을 올립니다.

다시 한번 저의 졸업을 위하여 관심과 정성을 베풀어 주신 모든 분들께 진심을 담아 말씀드립니다.

감사합니다.

2019.12.27 이욱제 올림